The Design of Daylight-Transporting Systems For Deep Space Illumination

Indhava Kunjaranaayudhya

Thesis submitted to the faculty of the Virginia Polytechnic Institute and State University in partial fulfillment of the requirements for the degree

Master of Science
in
Architecture

James R. Jones, Chair
Robert J. Dunay, Committee
Robert P. Schubert, Committee

February 11, 2005
Blacksburg, Virginia

Keywords: Daylight penetration, Anidolic ceiling, Light tube

The Design of Daylight-Transporting Systems For Deep Space Illumination

Indhava Kunjaranaayudhya

Abstract

Daylight penetration into a deep interior space can be achieved by using a light tube strategy. This research investigates how effective a room's ceiling cavity can be as a daylight transporting system. The design, therefore, tries to answer the question "What is the optimal geometry for a ceiling cavity and inlet aperture to bring deeper daylight penetration and achieve a higher illumination level, measured at the back of a room, than that achieved by a typical high window opening?"

Corporate affiliate 3M assisted this project by providing a prismatic and highly specular surface to cover the underlying geometry of the ceiling cavity.

A 16' deep room section with a high window opening on one side was constructed as a test cell. Inside, sensors were set up to allow light measurement at task level along the depth of the room. Light rays were deflected by the geometry of the ceiling cavity, through a number of internal reflections on the highly reflective film surface, to a diffuser at the back. The three most promising geometric designs from scaled model tests were selected, installed and tested for efficiency in the full-scale test cell.

Acknowledgement

The author would like to thank the advisor, Prof. James Jones, who gave valuable advices and provided science equipment for conducting the experiment, Prof. Robert Schubert who saved the six scaffolding wheels for the test cell, as well as the 3M Company that donated prismatic sheets for testing in this research. Additional thanks are extended to the following individuals of my friends who have supported the labor part of this research by giving a hand to construct the test cell and geometric mockups. The author is grateful to the following individuals for their contributions to this study:

1. Prof. James Jones, Advisor, Committee Chairman, Associate Professor of the Department of Architecture
2. Prof. Robert Schubert, Committee member, Dean of the Department of Architecture
3. Prof. Robert Dunay, Committee member, Dean of the Department of Industrial Design
4. Bill, Tim, John, and Buddy, technicians in the wood/ metal shop- Burchard Hall
5. Amit Khanna, student in the Department of Architecture
6. Jeremy Garret, student, Teaching Assistant, in the Department of Physics
7. Mischa Kim, student in the Department of Aerospace Engineering
8. Adam Shumaker, student in the Department of Geological Engineering
9. Paul Sweetman, student in the Department of Electrical Engineering
10. Pathom Rakfuekfon, student in the Department of Business Administration
11. Wattanasak Kamonpornpaisan, student in the Department of Business Administration
12. Ross Marks, student in the Department of Building Construction
13. Bernard Raj Louisnathan, student in the Department of Architecture
14. Hur, Hae-Kyu, student in the Department of Aerospace Engineering
15. An-chi Tai, student in the Department of Architecture
16. Li-wen Sung, student in the Department of Architecture
17. Noah Antisdel, student in the Department of Business Administration
18. Adebisi Oyedeji, student in the Department of Architecture
19. Jung-Rae, student in the Department of Architecture
20. Kun-Lin Hsieh, student in the Department of Mechanical Engineering

Table of Contents

List of Figures

Appendix

List of Equations

Appendix

List of Tables

Appendix

Chapter 1. Introduction

1.1 Inspiration for Daylight Research

Buildings are human-occupying units that are among the largest fossil-energy consuming sectors. Due to rising oil prices and a concern for the environment, people from all walks of life, including architects are now being conscious of energy consumption. Energy conservation is a responsibility for a new generation of architects. As a decision-maker, the architect's solution impacts energy consumption both directly and indirectly. The energy needs in a building relates to what type of environmental design strategies (system integrations such as passive solar) the architect is able to apply.

The author is an architecture student in Thailand who graduated in a period of energy shortage in the U.S. and was interested in pursuing a Master of Science in Building Science at Virginia Tech. During the program, the author had a chance to participate in a student solar house design competition "Solar Decathlon 2003". As a member of the design team, the author made a lighting-effect simulation model to visualize applications of several optical materials including a new prismatic film, from the 3M Company, to help the team make a decision on material for a luminescent ceiling in the house.

The unique internal reflection characteristics of the film caught the author's interest to test the film under daylight conditions. The challenge came to the design of a new set of light tubes which are based on a geometric concept; the internal surface of the tubes are lined with such a film that daylight will transfer through the length of the tube by means of internal reflections. This "Daylight transporting system" will illuminate the rear space of a room and can be fit in a ceiling cavity of any existing room after a special arrangement for space sharing with all existing ductwork.

1.2 Background

Since the availability of daylight is abundant during both overcast and clear sky periods, bringing daylight into buildings is desirable. For single-story buildings, the daylight zone can be extended to the interior through skylights. This option is limited for multi-story buildings. The challenge in this case is to maximize the daylight collected at the perimeter and efficiently transport it deep into the interior. This is addressed through this research.

Regarding the benefits from daylighting on the horizontal workplane, typical top or side lighting has the characteristics as shown below:

Top lighting

Pro:
- Suitable for horizontal workplane.
- Easy to control glare.

Con:
- Typically can illuminate only the top floor of a building.

Side lighting

Pro:
- Can illuminate every floor of a building.

Con:
- Needs to be installed as high as Possible
- Difficult to control glare.

The proposed daylight transporting system has the advantages of both the top and side light sources. It performs like the horizontal task light, requires little glare control, and can be used to illuminate every floor of a high-rise building.

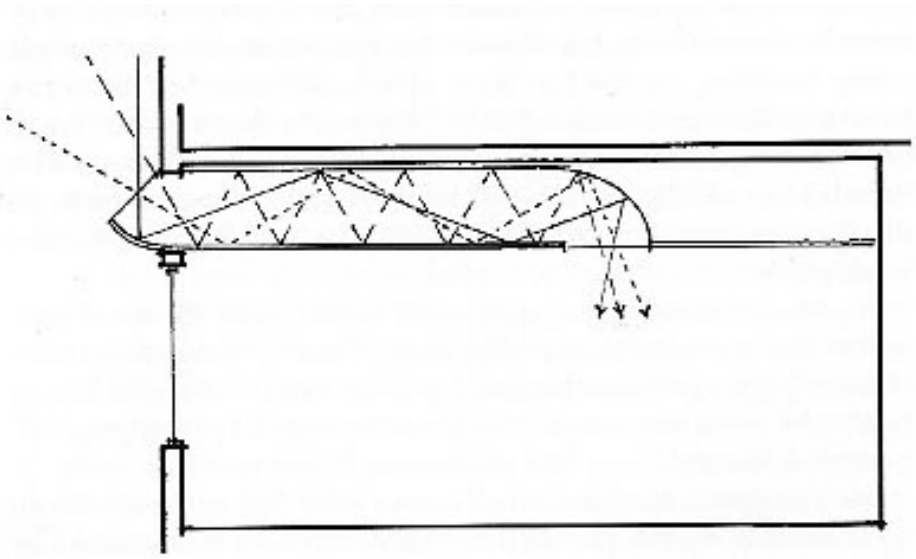

Figure 1.1: A section of a daylight transporting system, Anidolic ceiling (Szokolay and Steven, 2004)

A daylight transporting system takes advantage of ray bouncing on a highly-reflective material *(See Figure 1.1).*

There are two types of highly reflective materials, each of which has differences in characteristics.

1. *Prismatic sheets:*

- The reflectivity is a total reflection resulting from a series of triangular grooving textures of a transparent material whose refraction index is very high.
- Rays lying within the acceptable angles will reflect parallel to the grooves.
- Rays lying beyond the acceptable angles will transmit through.

Note that the range of acceptable angles depends on the refraction index of each material (*See Figure 1.2).*

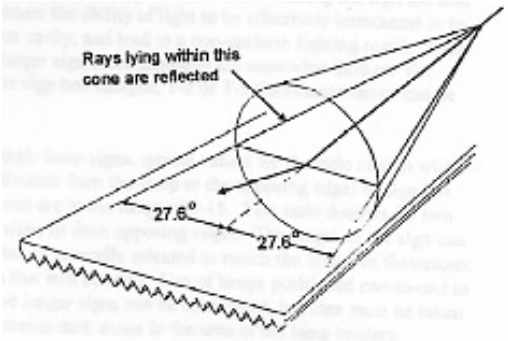

Figure 1.2: A sample of prismatic sheet (3M Bulletin: Optical Lighting Film, 2001)

2. *Specular sheets:*

- The reflectivity follows the basic reflection rule which states that the incidence ray angle equals the reflected ray angle.
- They yield the absorbance and transmittance coefficient of the material (*See Figure 1.3).*

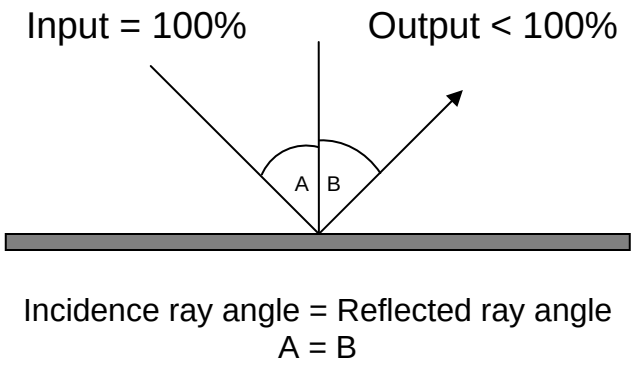

Figure 1.3: A sample of specular sheet

1.3 Problem Statement 1

Some techniques have been found to achieve a greater daylight penetration into buildings such as narrow plan building forms. This theory states that in comparison between any two buildings with the same volume, the one that has more light transmitting surface area will have greater daylight penetration and a higher percentage of the building floor area within the daylight zone, all else being equal. To apply such theory, building shape such as that from the floor plan B is recommended (*See Figure 1.4)*. This means cored buildings with large floor areas, such as of floor plan A, will have small daylight zones with corresponding larger electric lighted zones.

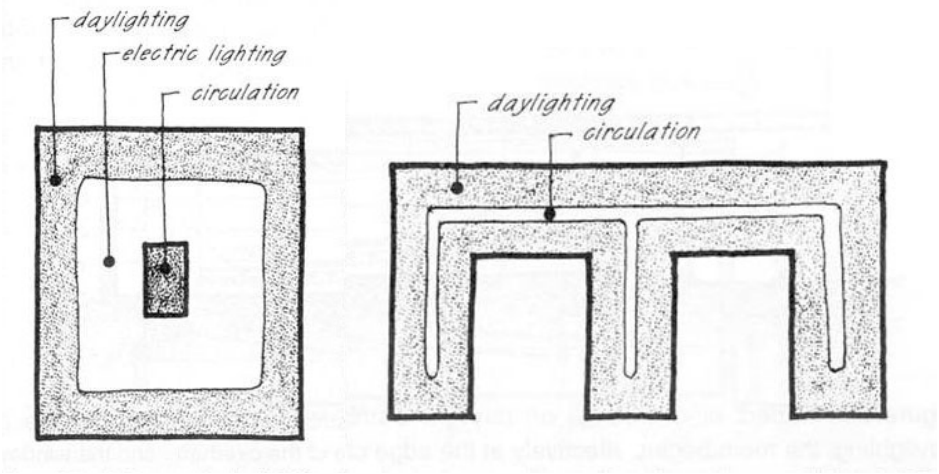

Figure 1.4: Access to daylight increases as the surface-to-volume ratio increases (Moore, 1997)

However, by means of an integrated daylight transporting system, buildings that have large floor areas will have extended daylight zones at a further distance from the parameter *(See Figure 1.5).*

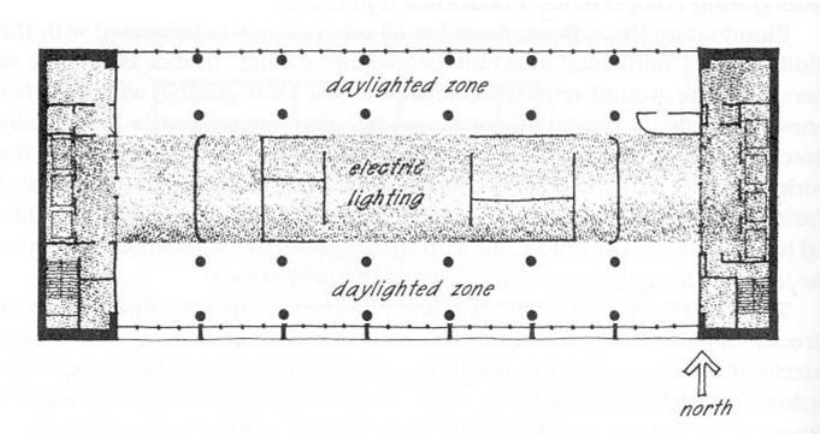

Without a daylight system

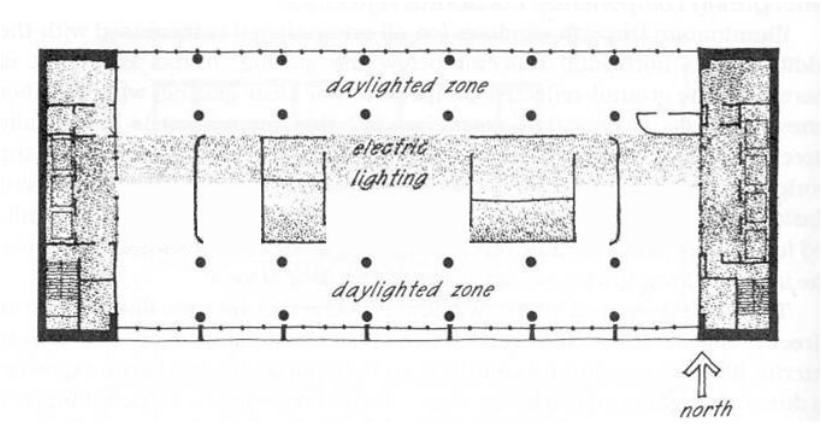

With a daylight system

Figure 1.5: Farm Credit Bank Building: Typical floor plan (Moore, 1997)

Moreover, traditional window daylighting can provide adequate daylight up to about 15 ft. from the window. The use of a larger window to achieve an additional illumination level can result in increased cooling loads and visual discomfort *(See Figure 1.6)*, as recommended by Fuller Moore in his book, Environmental Control Systems: heating, cooling, lighting.

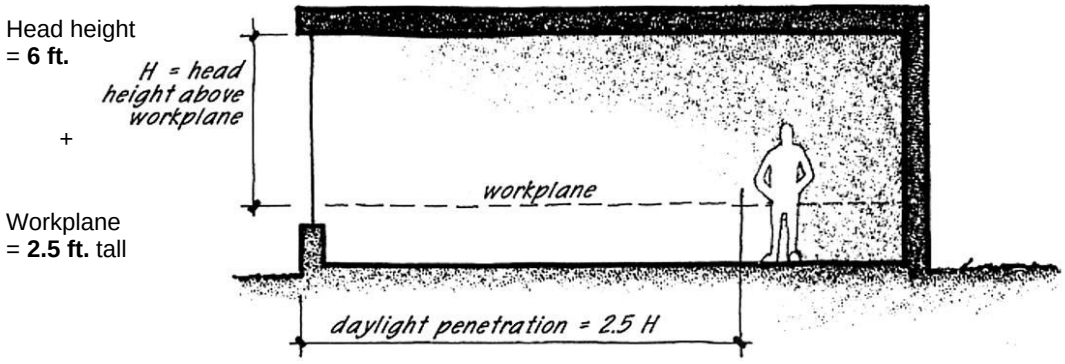

Daylight penetration = 2.5 x H = 2.5 x 6 = 15ft.

Figure 1.6: The height to depth room ratio of daylight penetration through a clear glass window (Moore, 1993)

1.4 Test Hypothesis

Using a geometric optimized ceiling cavity as a daylight transporting system, the illumination level will be greater at the rear part of a room when compared to without the transporting system. *(See Figure 1.7).*

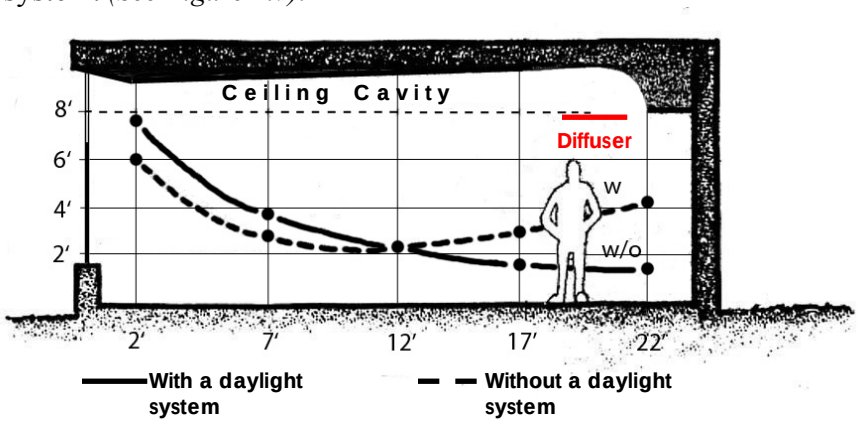

Figure 1.7: Interior daylight distribution comparison between with (w) and without (w/o) a geometric optimized daylight transporting system

Testing the system's efficacy requires time and resources to professionally construct and test each system in full scale under real sky conditions. Therefore, experimentation with scale models is mainly used to evaluate the performance of each design. The research tests the following three hypotheses.

1.5 Hypothesis One

Scale model tests with simple sky-simulating equipment will represent full-scale experimental results.

1.6 Hypothesis Two

Illumination levels measured in the scale models will be proportional to those measured in the full-scale experiments. The proportionality ratio will be estimated.

$$Ill_{sm} \times P = Ill_{fs}$$

Where Ill_{sm} = Illumination level for scale model
Ill_{fs} = Illumination level for full scale experiment
P = proportional constant

1.7 Hypothesis Three

The daylight transport system with the multi-curvature design will result in the highest light levels in the rear of the space when compared to the other light transport configurations.

$$M_{mc} > M_n$$

Where M_{mc} = average illumination level for the multi-curvature geometry
M_n = average illumination level for the other alternative transport systems (n).

1.8 Goals and Objectives

Goals

- To provide a higher and deeper atmospheric illuminance on the horizontal workplane at the rear part of a room.
- To find an economical yet effective way to enhance daylight penetration to interior spaces.
- To promote the concept for commercial use, such as in schools or office buildings where a large floor area is needed.

Objectives

- To optimize the design of the daylight transporting system .

1.9 Contributions to the Body of Knowledge

A typical prism light guide design uses a light injector, as an input light source, to inject light into a hollow tube cavity. As introduced above, by means of a high refraction index prismatic surface material, light rays are allowed to travel reflectively from the injector along the internal cavity to the ending mirror back and forth *(See Figure 1.8)*. To extract light rays down to the space below, the upper prismatic material uses a printed white dot pattern as a light extractor to spread the ray angles out for the acceptable angular range.

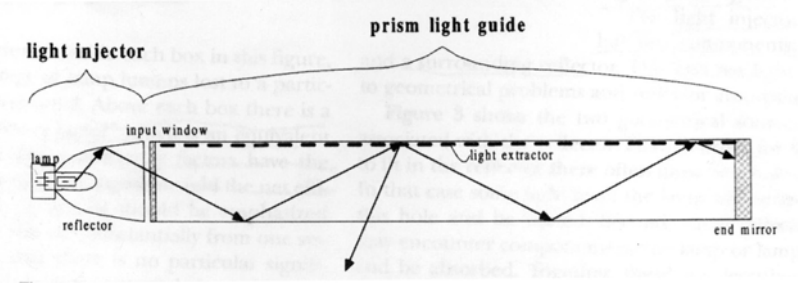

Figure 1.8: Longitudinal section of a typical prism light guide system (Whitehead and Hoffmann, 1998)

However, there are loss mechanisms in this prismatic light guide. These losses come from material absorptions in the system, including that from the reflector, the end mirror, and the cover *(See Figure 1.9)*. Subsequent loss of light in the prismatic light guide results in an inferior net system efficiency.

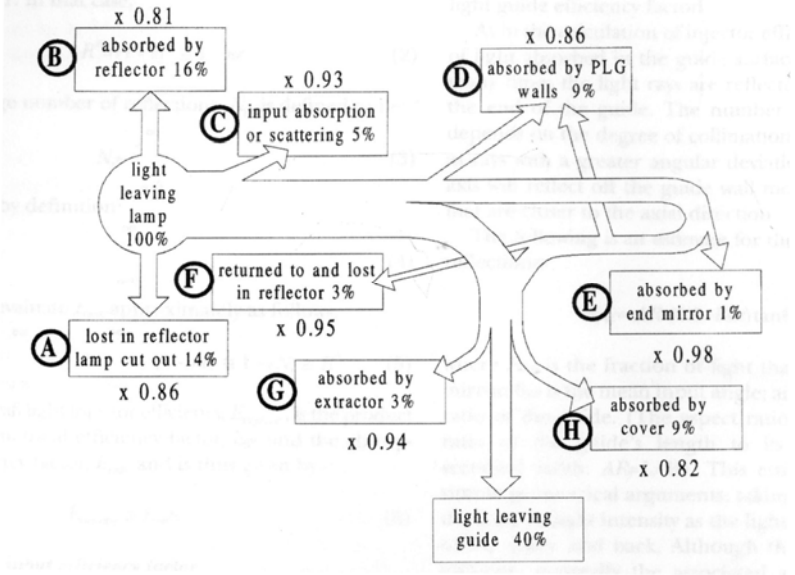

Figure 1.9: Losses in a typical light guide system (Whitehead and Hoffmann, 1998)

As a result, the idea of concentrating and diffusing light by means of geometrically optimization design is highly anticipated that it can be used to generate an efficient system when compared with that generated by a typical light guide system. The rays can be deflected in such a way that the final ray angles will be almost perpendicular to the diffuser surface, thereby, allowing a better transmission into the room.

Combining the two types of reflective materials, prismatic and specular, together is a desirable way for light tube designers whose design goal is geometric optimization. This is because the specular sheet can be used for directional control whereas the prismatic sheet can be used for collimating the ray paths and reducing the energy loss.

1.10 Important Assumptions and Limitations

The most important assumptions and limitations to this research include:

Assumptions

- The scale models approximate the characteristics for the full-scale transport system.
- The experimental setup approximates the characteristics of as-built rooms.

Limitations

- The prototypes are only extended for 16ft. deep due to the construction limits.
- This is the work for limited sky conditions including summer clear/ overcast skies, and fall clear/ overcast skies.
- The prototypes are tested at the location of 36º North Latitude.
- Due to the limited available number of sensors, the full-scale model measurements need to be conducted as a point measurement; instead of a uniform measurement that generates more reliable results.

Chapter2. Literature Review

2.1 Lighting Design Introduction

Since the energy crisis of the 1970's, there have been many research activities whose efforts have been to continue developing higher efficiency systems with minimal energy use. Lighting design is one of the leading disciplines that have considerable benefits on reducing global energy consumption. In 2002, estimated energy consumption for electricity in the United States was $10.45 trillion, according to a statistics report from www.nationmaster.com. Lighting accounts for 20% to 25% of the annual electricity usage in the United States, based on a statistics record from www.energizeamerica.org. Efficient daylighting can reduce this consumption.

Lighting design has two approaches which fall under the category of either art or science. The former group is more phenomenological and contemplates their design on the expression of architectural lighting elements, the relationship between shadow and rhythm or pattern and color, and so forth. The latter group is more concerned with the physics of light and considers their design based on illumination level satisfaction, and is able to test their hypotheses using experimental methods (MEEB, p.1049). In this group, a lighting design project can be categorized by its attributes which are either quantitative or qualitative. The quantitative projects are concentrated on the measurable aspects of *luminous intensity, luminous flux* (flow of light), *illuminance*, and *luminance*. The qualitative projects deal with wave energy components, *frequency* and *wavelength*. These technical terms in italic can be found in physics of light which is fundamental to all lighting design. Such background knowledge is provided in the Appendix chapter of this paper.

Some recent lighting research were studied and are introduced throughout this chapter.

2.2.1 Advanced Optical Daylighting Systems: Light Shelves and Light Pipes

(L.O. Beltrán, E.S. Lee, and S.E. Selkowitz)

Summary

In their paper titled "Advanced Optical Daylighting Systems: Light Shelves and Light Pipes" L.O. Beltrán, E.S. Lee, and S.E. Selkowitz propose two advanced daylighting systems, light shelves and light pipes. There systems were designed to produce higher illumination levels on the workplane at 30ft depth room over a period of daylight hours, throughout the year. The two types of light-collecting systems take advantage of the highly reflective property (88-95%) of coated thin-films to transmit sunlight more effectively. Each type of film produces a different characteristic of reflection, which are specular and narrow spread. The designs were assisted by computer ray-tracing calculations to configure optical elements.

All systems are assumed to:

- Achieve deeper light penetration and give uniformity to the visual atmosphere, by redirecting sunlight to the ceiling plane.
- Reduce heat gain and attain light-energy saving, by having a small inlet glazing area with directional daylight control.
- Decrease the amount of heat and excessive luminance, by avoiding direct sun beam.

Light Shelves

South-facing light shelves were created to fit within a 1.5-3.75ft. deep articulated building façade. They were applied in conjunction with a low window. Each designed component was carefully calculated for optimal angle, shape, curve, and size to suit for the window orientation and the site latitude (34˚N latitude). The following variations were studied.

1. Base case light shelf

This design is the reference performance for other systems. The base case was a horizontal flat rectangular plane with white matte surface *(See Figure 2.1)*.

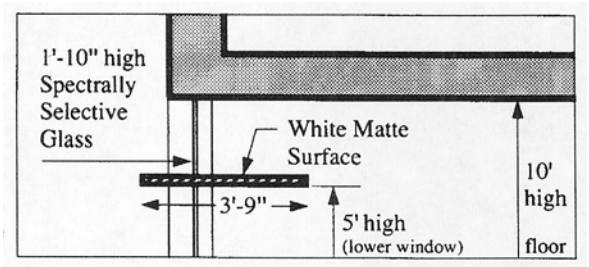

Figure 2.1: Base case light shelf (Beltrán, Lee, and Selkowitz, 1997)

2. Single level light shelf

This design has a tilted small inlet window and side reflectors. Sunlight is reflected along specular reflective film mounted on the top and bottom of geometric surfaces, as well as the side reflectors *(See Figure 2.2)*.

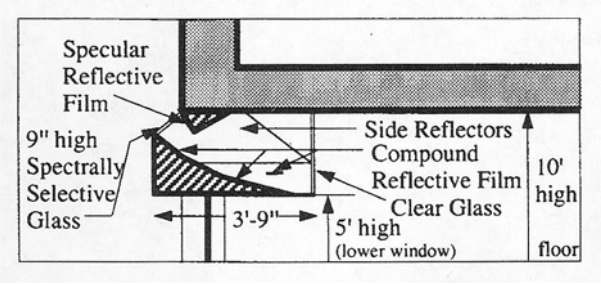

Figure 2.2: Single level light shelf, with &without side reflectors (Beltrán, Lee, and Selkowitz, 1997)

3. Bi-level light shelf

In this design, the size of glazing aperture was increased, with a lower viewing window, for the benefit of capturing more sunlight through the system, whereas reducing the depth of the light shelf *(See Figure 2.3)*.

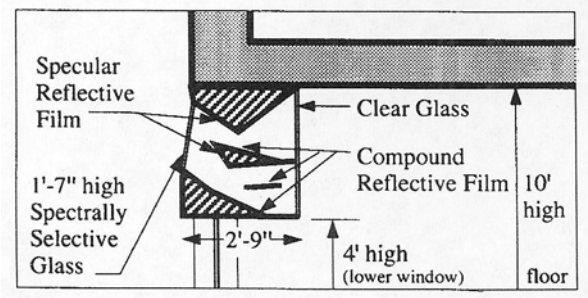

Figure 2.3: Bi-level light shelf (Beltrán, Lee, and Selkowitz, 1997)

4. Multi-level light shelf

This design maximizes the light capturing surface area, more than previous designs, and minimizes the depth of the light shelf. The system has the biggest size of glazing aperture and reflector area *(See Figure 2.4)*.

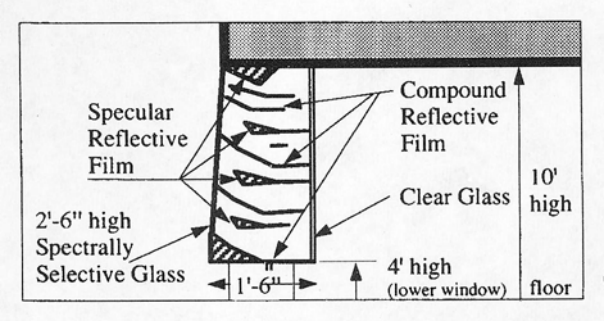

Figure 2.4: Multi-level light shelf (Beltrán, Lee, and Selkowitz, 1997)

Light Pipes

To retrofit some existing buildings, light pipes were invented to fit in the ceiling cavity. The designs were applied in conjunction with a lower window. Due to its enclosed configuration, light pipe designs do not need to have elements that deal with glare control which makes the designs simpler.

The additional strategies for a design development are as follows:

- Optimizing the size of the system.
- Comparing the efficiency among different cross sections.
- Minimizing inter-reflections to maximize the efficiency.
- Varying the shape of the pipe's cross section and using different reflector designs

Four light pipe designs were constructed with various cross sections. All internal surfaces of 30ft. depth were covered with 95% specular reflective film to reflect sunlight. The diffusing area of these designs was located at the second half of the bottom ceiling plane, at 15ft. from the back. Rays are transported along the first half of the tube then they are diffused downward through a diffusing film area placed on the second half of the tube *(See Figure 2.5)*.

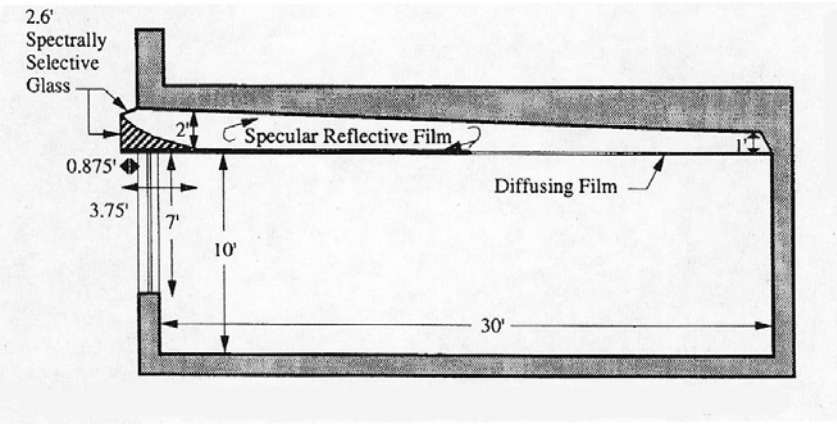

Figure 2.5: Section of trapezoidal light pipe C design (Beltrán, Lee, and Selkowitz, 1997)

A configuration of the four light pipe designs is described below:

1. Base case light pipe

This design has a rectangular section in plan but a trapezoidal section in elevation. From the elevation, the height is lower toward the innermost of the tube. It has a single central reflector at the front aperture; 2ft. wide in front view, to redirect the coming rays *(See Figure 2.6)*.

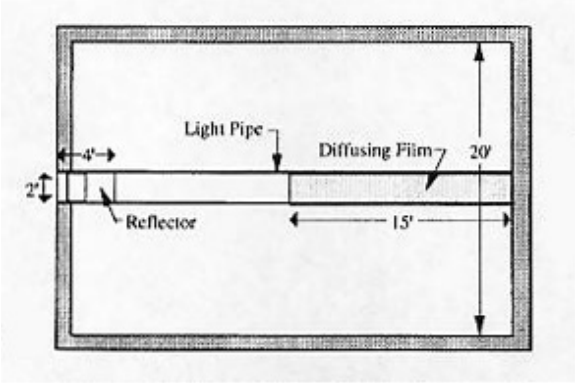

Figure 2.6: Base case light pipe (Beltrán, Lee, and Selkowitz, 1997)

2. Light pipe A

This design has 6ft. wide aperture looking from the front view, but maintains the 2ft. wide section at the back, generation a trapezoidal section in plan view. It has rectangular section in elevation, translated from its constant height *(See Figure 2.7)*.

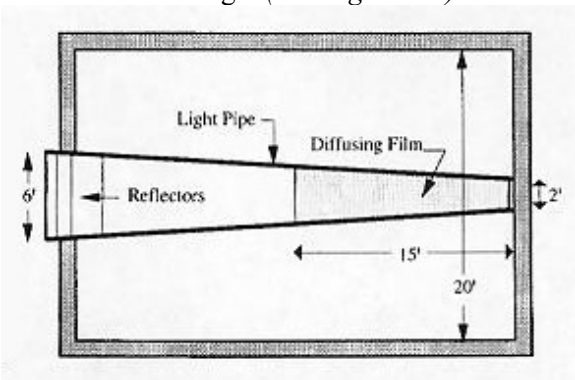

Figure 2.7: Light pipe A (Beltrán, Lee, and Selkowitz, 1997)

3. Light pipe B

This design is the modified version of the previous one (light pipe A). It has an extra element, which is the side reflector attached on each side of the central reflector. The reflectors were used to reduce the number of reflections from those of azimuth rays *(See Figure 2.8)*.

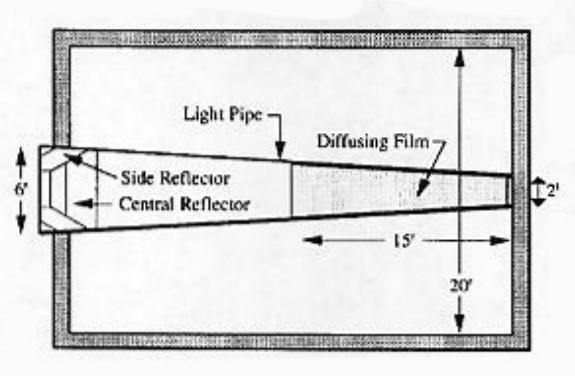

Figure 2.8: Light pipe B (Beltrán, Lee, and Selkowitz, 1997)

4. Light pipe C

This design uses a double unit of the light pipe B, but the width of the back end from this unit was increased to 3ft. and the section in elevation was switched to rectangular *(See Figure 2.9)*.

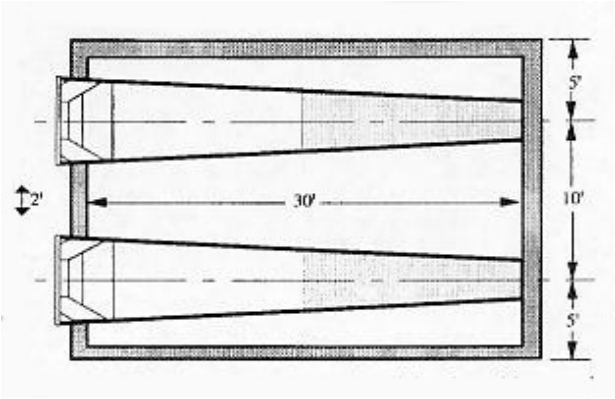

Figure 2.9: Light pipe C (Beltrán, Lee, and Selkowitz, 1997)

Evaluation Method

Types of light shelves and light pipes were evaluated through a two-step method. In the first step, scaled models at the ratio of 1:20 were constructed for outdoor testing. The evaluations were based on lighting penetration and glare control. Then, in the second step, all data measurements from the first step were used as the input condition to find a more accurate daylighting performance evaluation through computer-assisted experiments: the IDC method and DOE-2 energy simulation (*See the descriptions of these experiments in the original publication)*.

Daylight Performance

Light Shelf Results

IDC method shows that, under clear sky condition, at 27.5ft. away from the window wall, both single-level light shelves can produce over 200 lx (18.6fc.) at the workplane from 10:30am to 1:00pm throughout the year. At oblique sun angles (9:30am or 2:30pm), the single-level light shelf with side reflectors achieves up to 70% higher illumination levels than the other light shelves in the series. The bi-level light shelf produces almost the same amount of illuminance as the single light shelves. This occurs except in the midday hours of summer when illumination levels are as little as 48% lower than the single light shelves, despite having more glazing aperture and reflector areas. Between 10:00am and 2:00pm, all designed light shelves produce greater illumination levels than the base case light shelf throughout the year.

Light Pipe Results

All light pipe designs work better in terms of consistency, when compared to the light shelves. This is caused by the improvement of window size, geometry design, and internal reflective surface area. At 27.5ft. away from the window wall, light pipe C dominates the other designs by producing over 200lx (18.6fc), at the workplane level, from 8:30am to 3:30pm, throughout the year. Both light pipe A and B produce greater illumination levels than the base case light pipe. The success on workplane illuminance of light pipe designs results from the existence of side reflectors, larger distribution area, and the trapezoidal section.

Conclusion

Under most clear sky conditions, these two advanced light shelves and light pipes demonstrated sufficient ambient daylight on task level from 15 – 30ft. deep space, with small inlet area. The light pipe showed a better performance than did the light shelf overall. The best light shelf design used almost the same size of aperture area as that of the light pipe, but used less than half of the reflective surface area. The equipped side reflectors improved collimation of rays and generated illuminance levels over 200 lx for 7 hours a day in the light pipe version, and 4 hours a day in the light shelf version. A visual inspection of the physical scale model for the two designed versions demonstrated the improvement in level and uniformity of daylight, as light rays go parallel to the window.

The review of this research gives the author an opportunity to observe as a guideline through its experimental and design process, as well as its evaluating methods. The successful results in this paper have proven the concept of reflective duct to be a promising way for transporting daylight into a building. As a result, the author tried to redesign a new set of daylight transporting systems using such concept with an improved directional rays control by means of geometric optimization technique. With this technique, the author believes that the system efficacy will be higher, and thus results in a more commercial attraction.

2.2.2 New Simplified Design Procedures for Prism Light Guide Luminaires

(Lorne A. Whitehead)

Summary

In his paper titled "New Simplified Design Procedures for Prism Light Guide Luianires", Lorne A. Whitehead introduces the readers to the concept and initial design process of an illumination system, using prismatic light guide luminaries.

Background

The prism light guide is a hollow transparent pipe whose surface has longitudinal prismatic texture. From a cross section of the pipe, each prism has an isosceles right triangle shape running parallel to the axis of the length. Such shapes sit side by side to each other along the perimeter length of the cross section creating a tiny tooth texture to the outer pipe's surface. The longitudinal prisms cause the incident light rays in the hollow space to be reflected by internal reflection. This results from the refractive property of the pipe material *(See Figure 2.10).*

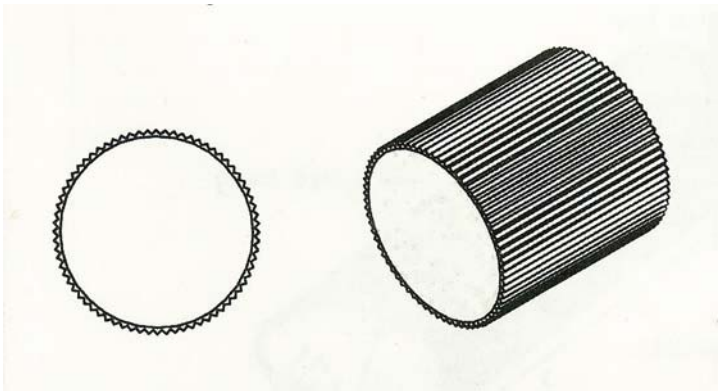

Figure 2.10: Prism light guide cross section and isometric view (Whitehead, 1998)

Prism light guides are available in various sizes and shapes. They can efficiently transport incident light rays whose angular deviation, θ, from the pipe axis is less than a value θ_c, where θ_c is a function of the refractive index *n*, of the pipe material, from the relationship below:

$$\theta_c = \arcsin\sqrt{(3-2\sqrt{2})(n^2-1)} \quad (1)$$

The concept of the prismatic light guide is a system that is able to collimate narrow spread light rays, whose angular deviation is within an acceptance angle, so that they are transferred through the cavity depth. A device called a light injector is used to produce such narrow spread beams from either end or both ends of the pipe. It then transfers the beams to another device called a light extractor. This device will scatter all the arriving beams to the outside range of acceptance angle that allows light to pass through the transparency. To achieve a uniform output, the extractor has to have a density of extraction increased as the distance from the light source increases, to compensate for the decreasing light intensity.

However, this idea can be achieved under a proper length as well as a certain amount of luminance and luminous flux per unit length.

General Characterization of the Prism Light Guide Luminaire Design Problem

There are two parameters that determine the performance of the prism light guide luminaire design. One is the luminous flux input from the light source (Φ_{in}). The other is the off axis angle at which the luminous intensity of the lamp output reduces to a half, measured against the pipe axis *(See Figure 2.11)*.

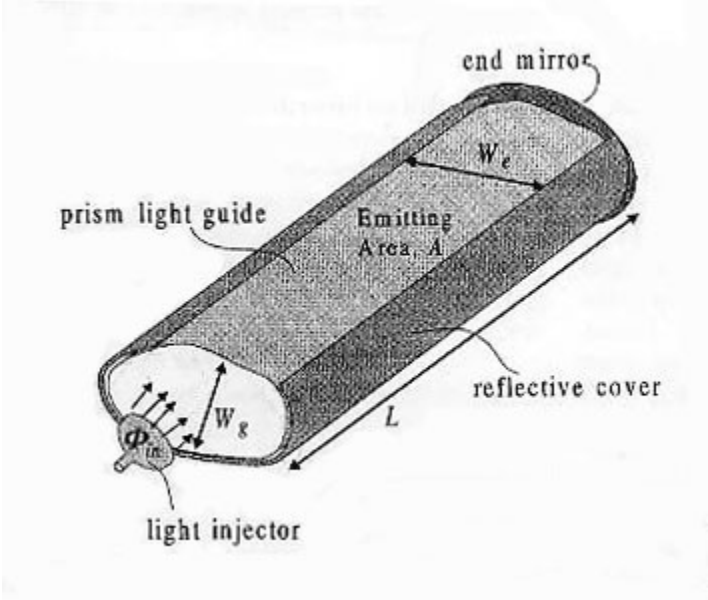

Figure 2.11: Prism light guide luminaire (Whitehead, 1998)

From Figure 2.11, the prism light guide has a specified length of "*L"*, along which the light can escape from an area "*A"* by the width of "W_e". The suggested area *A* is, at minimum, 25% of the entire guide surface area for an efficient light guide. The ratio of the length *L* to the minimum cross section width (the minor axis width, W_g) is called the aspect ratio, *AR*.

$$AR = \frac{L}{W_g} \quad (2)$$

These values, however, cannot be used to characterize the prismatic light guide. The parameter used to predict its efficiency is "N_g" defined as a number of internal reflections from the light injector to the opposite site, the end of the pipe, without any extraction.

The number of reflections per unit distance is

$$\frac{dn}{dx} \approx N_g \tag{3}$$

Where n = The refractive index
x = Distance

The optimal number in terms of the best design solution for the system is between 3 and 30; if N_g is smaller than about 3, the guiding performance of the prismatic material will not be different than that from typical reflective materials.

An appropriate estimation for these numbers is shown in equation 4:

$$N_g = \frac{\theta_{1/2}}{50}\frac{L}{W_g} \tag{4}$$

Where L = The length of prism light guide
W_g = The minor axis width
$\theta_{1/2}$ = The off axis angle at which the luminous intensity of the lamp has dropped to one half of its value in the axial direction

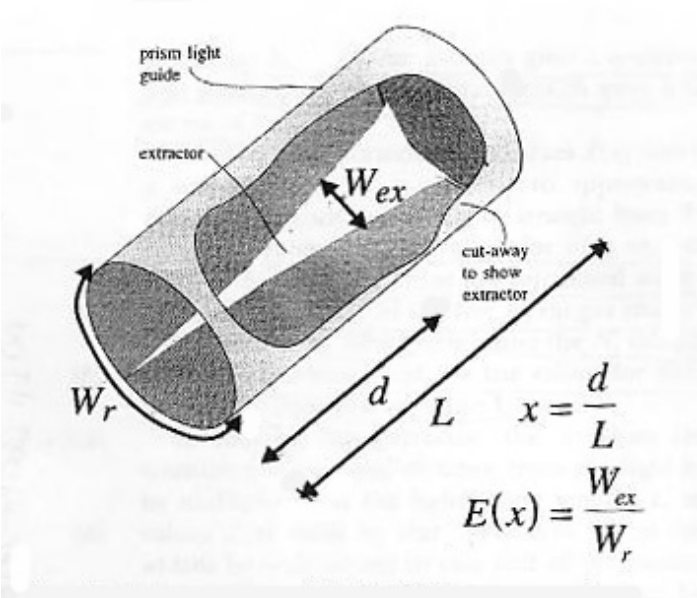

Figure 2.12: Fractional extractor width E(x) versus fractional length, x (Whitehead, 1998)

Figure 2.12 introduces a way to determine the dimensions of the extractor. The value "*x*" represents the fraction of the entire distance (light pipe length) light wanders in the prism light guide. If the injector is located at the middle of the guide, *x* will be 0 at the injector and it will be 1 at either end. If the injector is located at each end of the guide, *x* will be 0 at the either end and it will be 1 at the middle. Another function of length is also introduced here which is the extractor magnitude "*E(x)"*. *E(x)* is a ratio of the width of the extractor, at a specific point, to the perimeter length of the rear half of the guide. *E(x)* will be 1 if the extractor area covers all the rear half of the guide. Normally, *E(x)* is a fraction between 0 and 1.

Design of the Light Extractor

The paper shows an approximate calculation for defining the extraction value E as a function of x, for any given value of N_g. This calculation is based on the assumption that with a good extractor design, the relative amount of flux in the guide, $F(x)$, will be constantly reduced, at a uniform rate, from its maximum of 1, $F(0) = 1$, to its minimum of 0.25, $F(1) = 0.25$. The formula is shown below.

$$F(x) \cong 1 - (0.75)\,x \tag{5}$$

The minimum value indicates that no matter how arbitrary in dimensional design, at least 25% of the light will arrive at the opposite end of the guide, where most of them hit the end mirror and are direct back to the injector.

Table 2.1 – E(x) values for various ranges of N_g (Whitehead, 1998)

N_g range x values >>	0.00	0.25	0.50	0.75	1.00
3 to 6	0.27	0.35	0.48	0.71	1.00
6 to 12	0.11	0.15	0.21	0.32	0.61
12 to 18	0.04	0.06	0.10	0.17	0.34
18 to 24	0.01	0.03	0.05	0.10	0.23
24 to 30	0.00	0.01	0.03	0.07	0.16

Note that, the calculations are obtained by using the center value of N_g from its ranges.

Conclusion

This paper introduces an easy to follow procedure for creating an initial design for a prismatic light guide luminaire. This provision should be close to an ideal design for such a system and feasible to be used for its design performance and cost. This research gives confidence to the author on making decisions to optimize system dimensions. This procedure allows a system dimension to be in control while satisfying performance.

2.2.3 On Daylight Quality and Quantity and Its Application to Advanced Daylight Systems

(M. Moeck)

Summary

In his paper titled "On Daylight Quality and Quantity and Its Application to Advanced Daylight Systems", M. Moeck describes a new set of performance criteria to evaluate daylight quality and quantity for daylight systems. The five innovative vertical daylight systems were discussed and assessed based on the criteria. The performance of each system was simulated by using the RADIANCE visualization program.

The standard clear glass, with south-facing daylight aperture of 2 m^2, and the sun tracking Venetian blind (system 2) were used as a base case for stationary systems and sun tracking systems respectively. This allows comparison of efficiency among the six systems. The vertical window systems are introduced:

Daylight System 1: Standard clear glass

Daylight System 2: A sun tracking glossy white horizontal Venetian blinds was placed behind clear glass. Slats are perpendicular to direct sun under clear skies, and are horizontal under overcast skies. The altitude angle of slats at the surface normal is the same as the profile angle of the sun in the vertical section *(See Figure 2.13 and Figure 2.14).* This profile is also used in the other types of daylight systems.

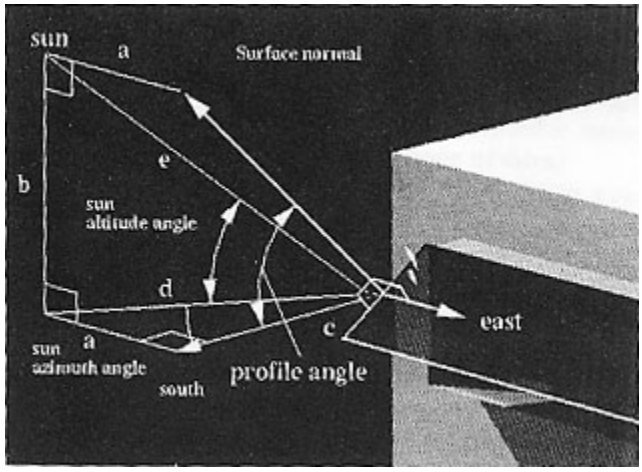

Figure 2.13: Definition of the profile angle for sun tracking daylight systems (Moeck, 1998)

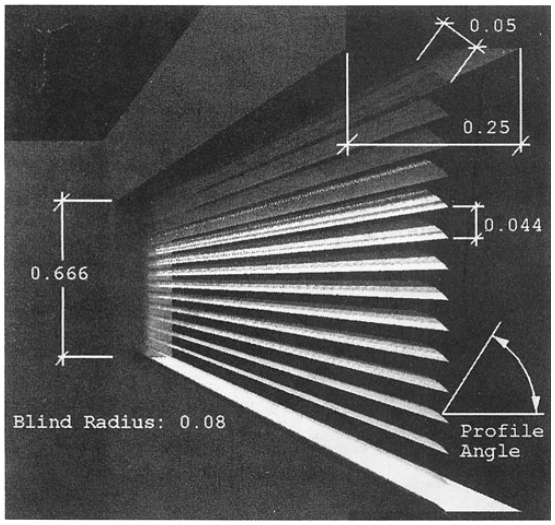

Figure 2.14: Sun tracking glossy white Venetian blinds (daylight system 2) (Moeck, 1998)

Daylight System 3: A stationary system utilizes partially silvered sun-rejecting prisms and partially silvered sun-redirecting prisms *(See Figure 2.15).*

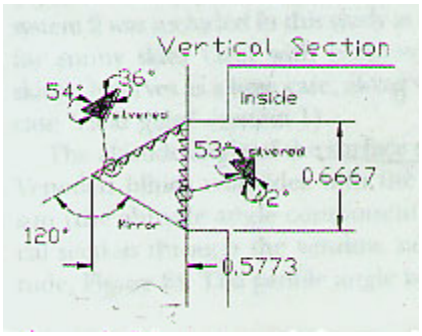

Figure 2.15: Stationary daylight system employing sun-rejecting prisms, a mirror, and light redirecting prisms (daylight system 3) (Moeck, 1998)

Daylight System 4: A stationary system utilizes an alignment of insulating glass panes, each of which is embedded with reflector stripes. The profile angles allow sunlight rejection at high angles and admission at low angles *(See Figure 2.16)*.

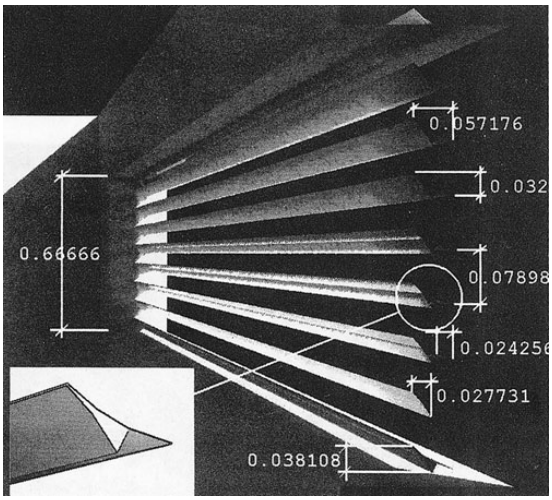

Figure 2.16: Stationary daylight system made out of reflector arrays (daylight system 4) (Moeck, 1998)

Daylight System 5: A sun tracking system is modified from system 3 by sandwiching the two prism types in a clear insulating glass pane. The glass pane rotates around the horizontal axis *(See Figure 2.17)*.

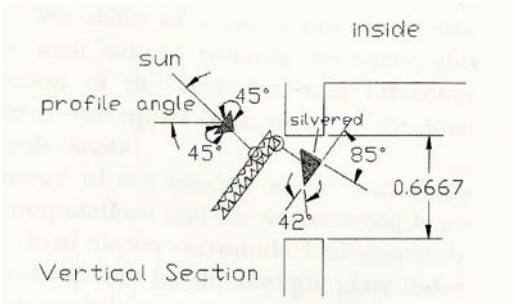

Figure 2.17: Sun tracking prisms sandwiched into an insulating glass pane (daylight system 5) (Moeck, 1998)

Daylight System 6: A sun tracking system contains a series of clear, vertical thin prism slats that rotate around their vertical axis to block direct sun throughout the day. The prism slats are installed on the interior side *(See Figure 2.18).*

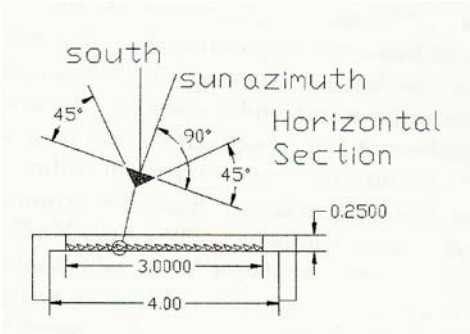

Figure 2.18: Sun tracking clear vertical prisms (daylight system 6) (Moeck, 1998)

The prisms have four selections of shapes, each of which is either clear or one side silvered. All prismatic materials are Polymethylmethacrylate (PMMA), whose surfaces are coated with the highest grade aluminum (Al 99.99).

2.2.3.1 Proposed Performance Criteria

The new performance criteria that M. Moeck proposed are based on daylight quality and quantity. The criteria were used to evaluate the performance of the five innovative daylight systems. These performance criteria are described as follow:

A: Luminous intensity distribution of the system for a specific time

This value indicates the prevalent direction and directional intensity of rays arriving at the space. The calculation was taken at noon for the entire month of December and June, as the two extreme periods of the year.

B: Illuminance on the workplane

The workplane illuminance is necessary for the computations of coefficients of utilization. This value also helps to approximate the minimum ratio of window to wall required to achieve a given annually average illumination level.

C: Illuminance distribution on the workplane (uniformity)

The light uniformity on the workplane can be found by either the gradient difference between any two points apart, or the difference between minimum and maximum illuminance on the workplane. Since the latter can be unknown for complicated daylight systems, the former approach is used.

D: Total lumens entering the space

This value designates the efficiency of daylight systems and derives the coefficients of utilization for any positioned workplane.

E: Total lumens in the upper back zone of the space

This value demonstrates the ability of systems to redirect daylight, which is the corresponding efficiency of those systems (total lumens in the upper back zone to total lumens entering the space)

F: Luminance of the window

The luminance of the window is instrumental for calculating glare and limits on the visual field surrounding luminance. However, since innovative daylight systems make use of

window aperture as an input entry, it becomes conflictive and therefore direct sunlight passing through the systems is not considered glare.

G: Total area in space that is overbright

This finding is useful for creating sun protection and adherence to luminance limits for visual field and visual comfort. Luminance value of 850 cd/m^2 is recommended by IESNA RP-1-1993 as the maximum luminance value in the visual field.

H: Spherical illuminance values

Spherical illuminance data are valuable to detect light directionality, as well as highlight and shadow effects, which can be a problem for visual tasks in small areas of high luminance. Minimum-to-maximum illuminance ratio on the matte sphere indicates the contrast between highlights and shadows. Diffusion can also be defined from this data, due to the dimensional spherical luminance that provides accuracy on ratio of vertical to horizontal illuminance.

2.2.3.2 Method of Analysis

Radiance is suitable for visualizing and simulating daylight. This program contains simulation code, developed by Compagnon, for various Siemens prism types. Its options include one prism side metalized, refraction indices, and mirrors of arbitrary specular reflectance. The innovative systems, therefore, were studied from the scene model generated by this program. A rectangular space of 3 m. in height, 4 m. in width, and 7 m. in depth, was built with a south window opening. The scene includes an exterior ground plane, as well as clear and overcast skies (CIE models) for three times a day, three days a year, and two latitudes. The code for prism simulation was assumed to have no dispersion of light and no absorption in the prism. A single refraction index was used for all wavelengths *(See Figure 2.19)*.

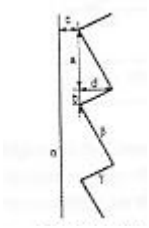

Figure 2.19 Definition of the geometrical parameters of the prism
Any face of the prism can be silvered. (Moeck, 1998)

Note that setups of the calculations for determining performance criteria and performance of all cases compared can be referred in the original article.

Conclusion

The daylight system comparisons were made to help customers choose from alternatives. A series of charts, referred to the results in the original publication, act as a catalog for daylight system selection. These provide information such as maximum window luminance, maximum throughput (efficiency orientation), the minimum window size for a yearly mean illuminance of 200 lx., and so forth.

The performance of daylight systems 2 and 5 are based on solar profile angle, and 6 is based on solar azimuth angles. The next development will focus on increasing daylight redirecting performance of the sun tracking system 2 by using specular metal rather than

white glossy paint. It also focuses on finding a good strategy to let the blinds admit more sunlight, instead of blocking it, without sacrificing glare.

In addition, for the future studies, they will consider performing an economic analysis. This idea includes a separate comparison between stationary and dynamic systems, according to their cost and performance difference.

The review of hi-tech reflector-based daylight system comparisons in this research helps the author to be up-to-dated of recently developed systems that utilize prismatic elements. The new performance criteria proposed in this paper are highly informative with sophisticated measurements. The achievement of these complicated designs was possible due to a high investment of professional manufacturing. The author's opinion is that the new criteria may not be all necessary to help contribute to practical use of these designs.

2.2.4 Method for Estimating the Efficiency of Prism Light Guide Luminaires

(Lorne A. Whitehead and Kristin Hoffmann)

Summary

In their paper titled "Method for Estimating the Efficiency of Prism Light Guide Luminaires", Lorne A. Whitehead and Kristin Hoffmann state that the prism light guide luminaire is well known as a light transporting technique that allows the input light source to be installed at a distance away from the output area. Light is injected along the length inside a cavity lined with a prismatic film. Rays travel back and forth reflectively on the film surface; meanwhile, partly being extracted to illuminate a space below *(See Figure 2.20)*. This technique becomes beneficial under sensitive situations when positioning or limiting a number of light sources contributes to an ease of handling. Those situations are present in lighting automotive tunnels, building exteriors, and road signs.

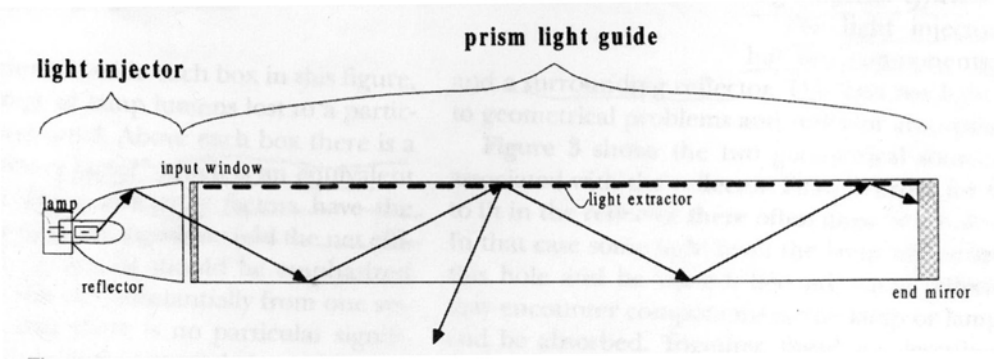

Figure 2.20: Longitudinal section of a typical prism light guide system
(Whitehead and Hoffmann, 1998)

Despite good performance, there are subsequent losses of light along the path of travel. These make the net system efficiency inferior to that of the typical luminary system *(See Figure 2.20)*. However, by using a more efficient luminous source as well as properly designed luminaire, better performance can be expected.

A simple calculation method is proposed to predict the efficiency of each redesign. The results are shown to correspond to that of photometric testing with a fair level of accuracy.

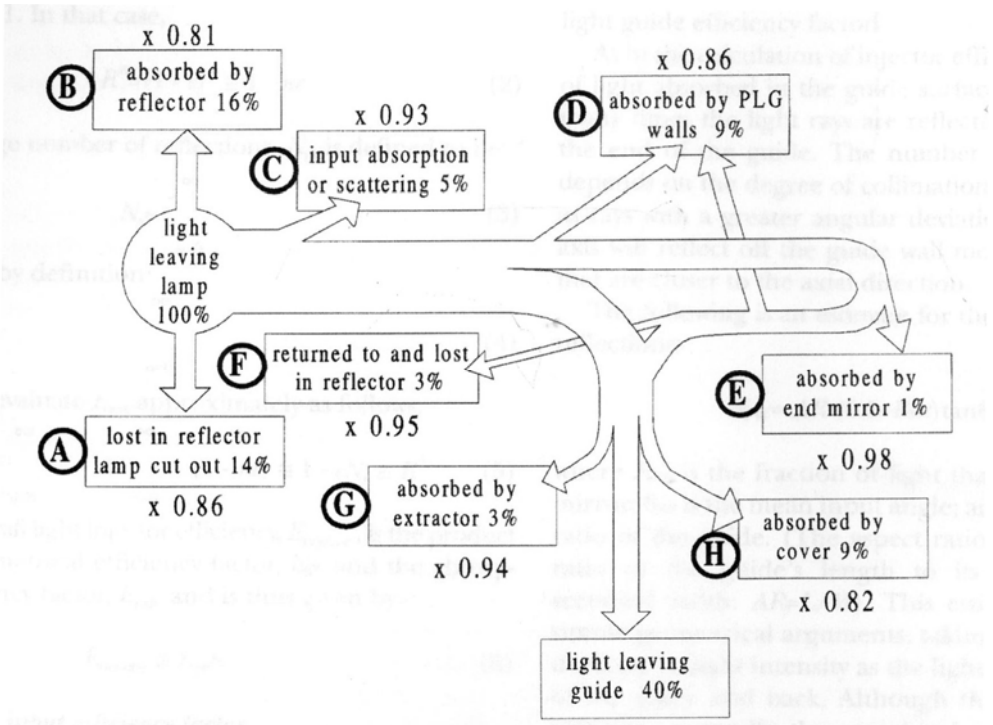

Figure 2.21: Losses in a typical light guide system (Whitehead and Hoffmann, 1998)

Conclusion

The proposed formulas could be used in the early stage of design when the calculation method is expected to predict every minor change of efficiency in each design. This provides a useful tool for the author to detect the effects on system efficiency after changing design elements. This will help the author to optimize the design combination to achieve cost-effectiveness.

Chapter Conclusion

Based on previous research, daylight transporting systems utilize two types of highly reflective films, specular and prismatic, as an internal finished surface to bounce daylight along the length of the cavity. Regarding the efficiency, the dimension of such cavity will derive from the relationship of N_g (referred to the equation 2 in "New Simplified Design Procedures for Prism Light Guide Luminaires"). Finally, to limit the number of subsequent losses of light along the path of travel, the designs should minimize the number of reflections by geometrical configuration to redirect daylight effectively to the diffuser target. Due to the required science equipment and professional manufacturing quality, the proposed performance criteria for advanced daylight systems can not be utilized. The daylight factor and luminance ratio will be the main methods for evaluating a design performance.

Chapter 3. Methodology

3.1 Background

The 3M Company has developed transparent prismatic grooved sheets called "Optical Lighting Film." They are applied as an internal finished surface of a hollow tube. Such application, when the tube is lit by a light injector at one end, light will be transported by means of refraction characteristics of the prismatic sheets. This creates internal reflections along the inner space through the length of the tube. Conceptually, the application can be used in combination with a new transparent light diffuser called a Radial Daylighting Lens. As installed on the lower horizontal ceiling plane at the end of the tube, this lens accepts collected rays and spreads them thus generating an ambient light to illuminate the interior space.

The evaluation of the efficacy of the optical lighting film could be performed by computer simulation, in-situ monitoring, scale model testing or full-scale experimentation. Computer simulation tools do not accurately model the complex reflection and refraction properties of the optical film, and therefore is not an appropriate methodology. In-situ monitoring also was not an option as there was not a room available that could be experimentally manipulated. Therefore, scale model testing and full-scale experimentation were applied as evaluation methods.

3.2 Experimental Process Check List

The experimental process follows the check list below:

- Designing systems using ray-tracing calculation in AutoCAD for three seasonal altitudes.
- Making a scale model of each designed system.
- Measuring each scale model system by using a light sensor and a ramp with an attached solar protractor to simulate the sun path effect of different altitudes and azimuths in each season.
- Selecting the three most efficient systems from the scale model test based on the illumination output level.
- Constructing a test cell, for the full-scale test, with a set of sensors positioning at the task level along the depth of the cell.
- Constructing and installing the first system.
- Collecting data from due South orientation for two weeks.
- Collecting data from East orientation for two weeks, for the winter sky effect.
- Constructing and installing the second system.
- Collecting data from due South orientation for two weeks.
- Constructing and installing the third system.
- Collecting data from due South orientation for two weeks.
- Performing data analysis and system evaluation.

3.3 Overview of Methodology

The research proceeds by using two experimental procedures; scale model tests and full-scale experiments. In the scale model test procedure, each prototype is conceptually described. Then the setup for prototype testing is shown and tests are performed to verify the hypotheses. In the full-scale experimental procedure, the construction process of each selected prototype is described. Then the setup for prototype testing is shown and tests are performed to verify the hypothesis. Finally, methods of analysis are described as an introduction to chapter four.

3.3.1 Scale Model Tests

3.3.1.1 Prototypes

Seven systems were designed to test in the scale models. All systems are stationary so that they can easily retrofit any existing office or classroom space, especially by installing into ceiling cavities of high-rise office buildings. In addition, the stationary system is likely more economical when compared to a dynamic system, such as a sun-tracking system. Out of these seven systems, the three most promising were selected based on performance to be built for the full-scale model experimentation.

Design strategies were applied to each prototype. The strategies are derived with respect to the average solar altitude angles of each season. Design and evaluation were made for solar altitude angles of 30 degrees for winter, 45 degrees for fall/spring and 60 degrees for summer. The seven prototypes are introduced:

1. Curvature Geometric System
2. Multi-Curvature Geometric System
3. Multi-Curvature Geometric System (Simplified Version)
4. Cylindrical Geometric System
5. Transforming Geometric System
6. Tapered Geometric System with seasonal louvers
7. Tapered Geometric System

1. Curvature Geometric System

The curvature geometric system was designed with the following strategies:

- Reduce the number of reflections by tapering the upper cavity plane from the back.
- Maximize reflective surface without sacrificing shading area.
- Design 30-degree reflectors for 60-degree incident rays.

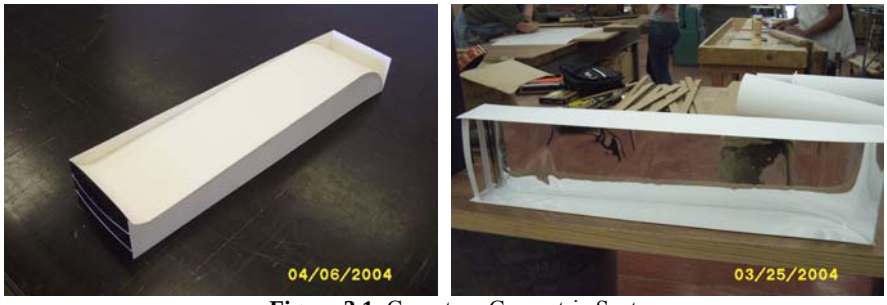

Figure 3.1: Curvature Geometric System

The first step was to manually ray-trace the reflective light path as shown in Figure 3.2. An upward slope of the upper surface from inlet to outlet was used to reduce the number of reflections along the entire length of the tube. The convex reflector at the upper inlet is treated to accept all 30, 45 and, 60-degree incident rays. The challenge was to bring the more oblique 60-degree rays deep inside an interior space. Thus, the 2 inch curved louvers, tilted at 30-degree, were designed to turn all 60-degree incident rays to the horizon at 0 degree. The concavity of the louvers is calculated to focus all striking rays to the center of the back reflector. The curved back reflector is treated in such a way that all horizontal rays moving toward the center of the back wall are reflected down to the diffuser area (*See Figure 3.1 and Figure 3.2).*

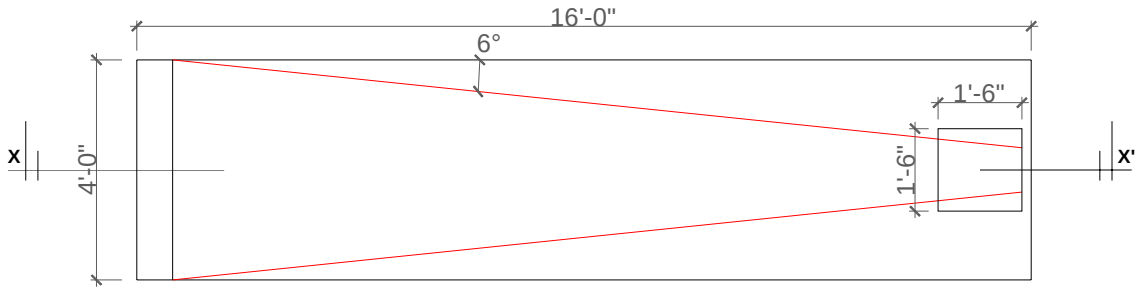

Top View

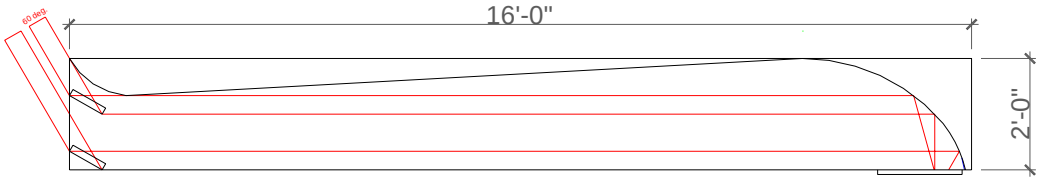

Sectional Diagram
(Reflective Bouncing in Curvature Geometric System for 60 Degree Incident Source Angle)

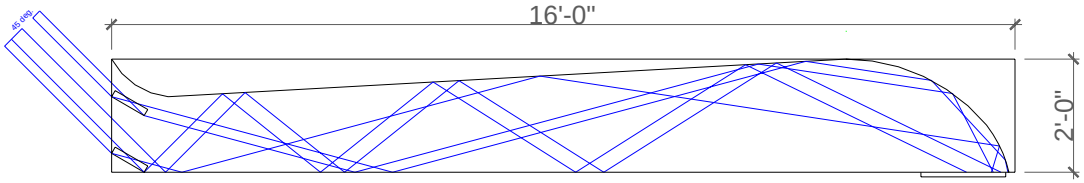

Sectional Diagram
(Reflective Bouncing in Curvature Geometric System for 45 Degree Incident Source Angle)

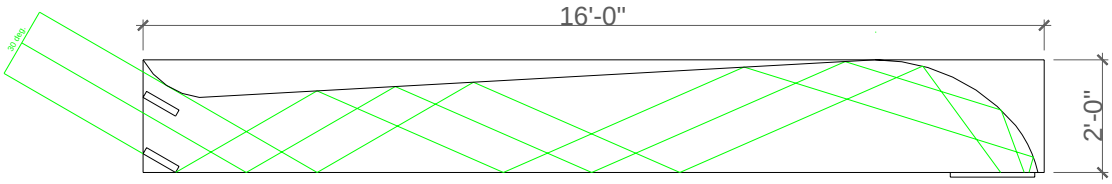

Sectional Diagram
(Reflective Bouncing in Curvature Geometric System for 60 Degree Incident Source Angle)

Figure 3.2: Drawings of the ceiling cavity showing ray-tracing in Curvature Geometric System for 30, 45, and 60-degree incident rays

From Figure 3.2, it is shown that all 60-degree incident rays that strike both louvers are successfully transferred to the diffuser area. All 30-degree incidence rays are successfully transferred to the diffuser area after reflecting along the internal surface without reflecting off of the louvers. Last, the 45-degree incident rays show the lowest amount of transported rays. The existence of louvers; however, makes it difficult and complicated when adding another element to deal with oblique sun angles in the early morning and late afternoon. Therefore, there is no special design for oblique sun angles in this prototype.

2. Multi-Curvature Geometric System

The multi-curvature geometric system was designed with the following strategies:

- Taper the upper cavity plane from the back to reduce the number of reflections.
- Use ceiling reflector to focus the rays and keep the inlet area free for side reflectors.
- Install 3-piece back reflectors for catching escaped rays.

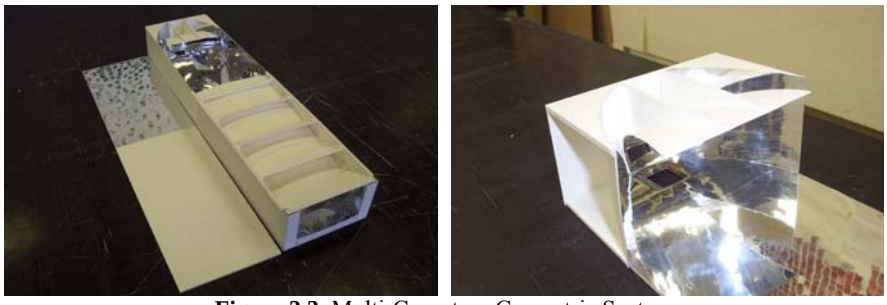

Figure 3.3: Multi-Curvature Geometric System

The design is inspired by a potential to redirect sunlight using carefully designed ceiling reflectors that can accommodate seasonal variation of incident sunrays. This idea is supported by the fact that, regardless of concavity, rays at 30-degree incidence will have the shortest travel path between the upper reflector and the target on the lower surface. Rays at a 45 and a 60-degree incidence will have longer travel paths, respectively. This is caused by the reflective geometry of the upper, concave reflector (*See Figure 3.4)*. In practice, a taller cavity is needed. Thus, the lower reflector at the inlet is used to correct the height discrepancy of a 2 ft. cavity. Finally, the 3-piece back reflectors are diagonally positioned and designed to work together with the inlet side reflectors catching most of the rays up to an azimuth angle of 45-degree source.

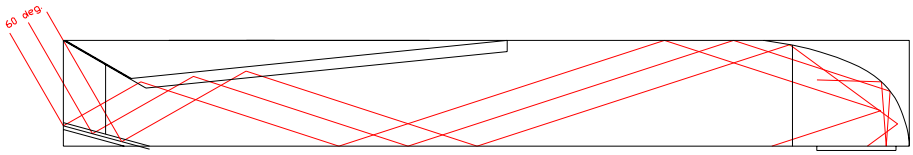

Sectional Diagram

(Reflective Bouncing in Multi-Curvature Geometric System for 60 Degree Incident Source Angle)

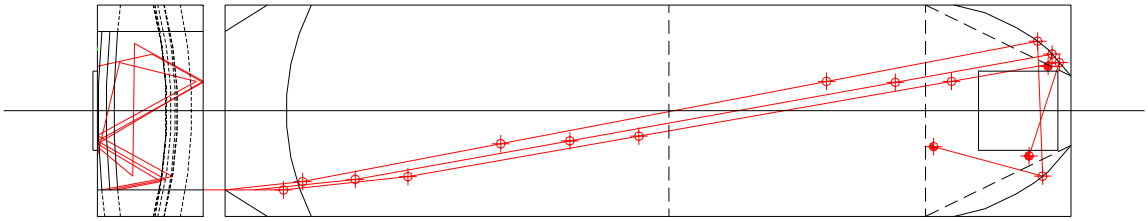

Front View **Top View**

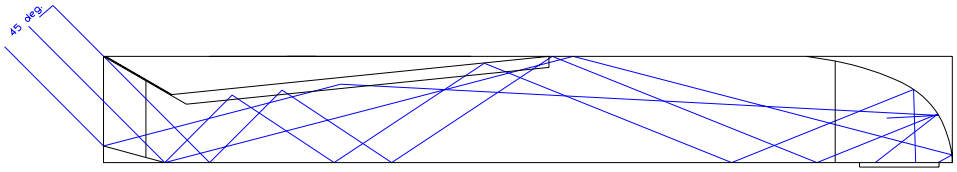

Sectional Diagram

(Reflective Bouncing in Multi-Curvature Geometric System for 45 Degree Incident Source Angle)

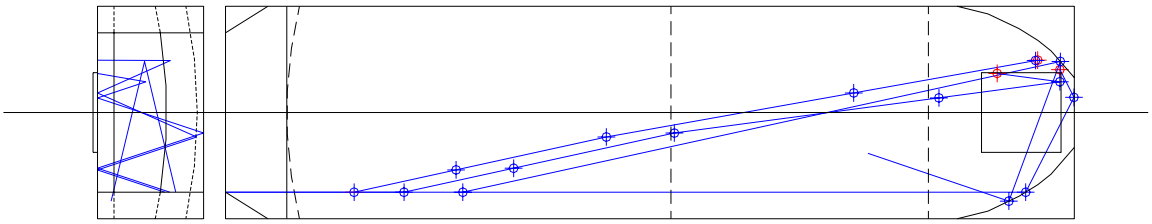

Front View **Top View**

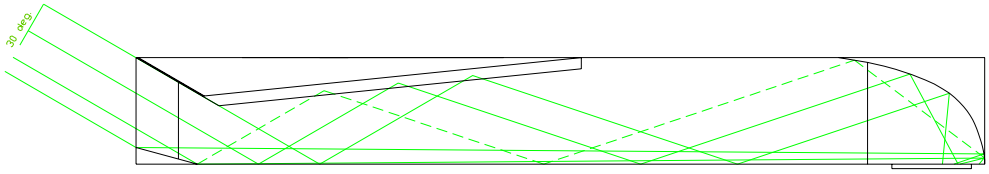

Sectional Diagram

(Reflective Bouncing in Multi-Curvature Geometric System for 30 Degree Incident Source Angle)

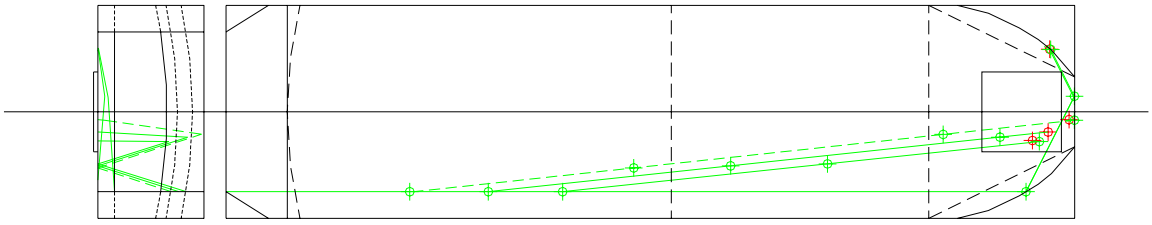

Front View **Top View**

Figure 3.4: Drawings of the ceiling cavity showing ray-tracing in Multi-Curvature Geometric System for 30, 45, and 60-degree incident rays

3. Multi-Curvature Geometric System (Simplified Version)

The multi-curvature geometric system (simplified version) was designed with the following strategies:

- Omit the side reflectors to increase the inlet area
- Maintain the lower reflector, the slanted ceiling reflector, and the 3-piece back reflector

The design is intended to use the main reflective elements of the successful multi-curvature geometric system with no side reflectors. This design variation is intended to reduce complexity and increase the effective inlet area. Thus, the geometry maintains the inlet lower reflector, slanted ceiling reflector, and the 3-piece back reflector. The degree of curvature for the slanted-ceiling reflector is increased to 2.5 inches to support a wider span. Incidence rays are expected to reflect toward the center of the ceiling width and hit the back reflector.

The test was conducted for the full-scale version as it is one of the most promising designs in the series.

4. Cylindrical Geometric System

The cylindrical geometric system was designed with the following strategies:

- Use a tubular form for easy integration with other architectural systems. The cylindrical form is easy to install and make connections from room to room above the ceiling.
- Equip it with a 45-degree back reflector; this is the best angle to redirect horizontal rays to strike perpendicularly on the diffuser.

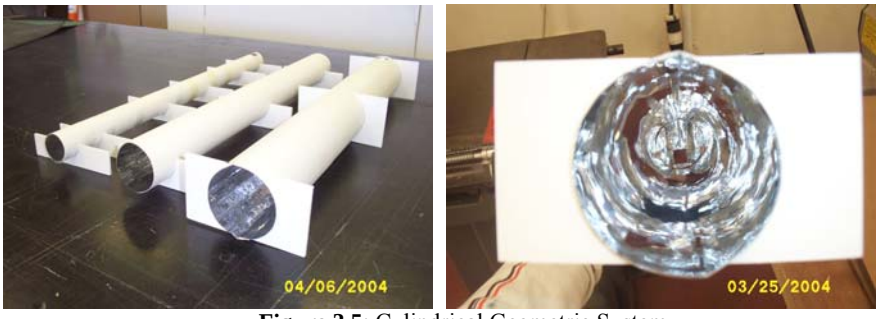

Figure 3.5: Cylindrical Geometric System

The design begins by finding the optimum diameter of a light tube to fit in a 2 ft. tall by 4 ft. wide by 16 ft. deep cavity space. Therefore, three orderly selected diameters for a hollow tube are chosen at 1 ft, 1.5 ft, and 2 ft. To reduce the likely condition of light bouncing away from the diffuser area, the 2 ft. diameter version has an elliptically shaped 45-degree back reflector attached to the inside end of the hollow tube.

5. Transforming Geometric System

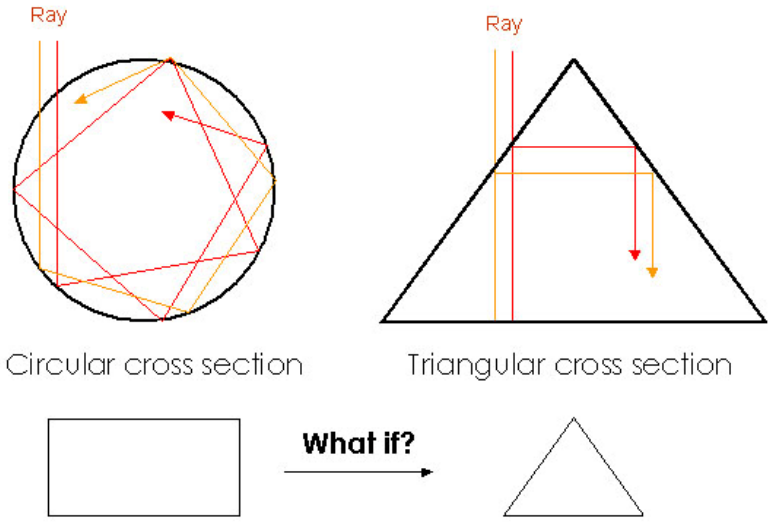

Figure 3.6: Cross-section diagram illustrating geometric transformation

The diagram in Figure 3.6 illustrates a comparison between the ray reflective characteristics inside the circular cross section and the triangular cross section. In the circular cross section, the rays reflect more often to complete the cycle than in the triangular cross section. This indicates that the cavity with a triangular cross section has a greater chance of directing the rays toward the diffuser at the back end with minimal reflective loss of light. With this concept, if a rectangular shape of 2 x 4 ft. is used for the inlet cross section and the triangular shape is used for the ending cross section, such configuration would maximize the inlet area and decrease the probability of rays missing the diffuser. This sets up the next geometric design; the transforming geometric system.

The transforming geometric system was designed with the following strategies:

- Take the whole inlet aperture area, a 2 x 4 ft. rectangular area, without any light obstructing elements to maximize the effective inlet area.
- Transform a rectangular cross section to an isosceles triangular cross section, with a 45-degree back reflector.

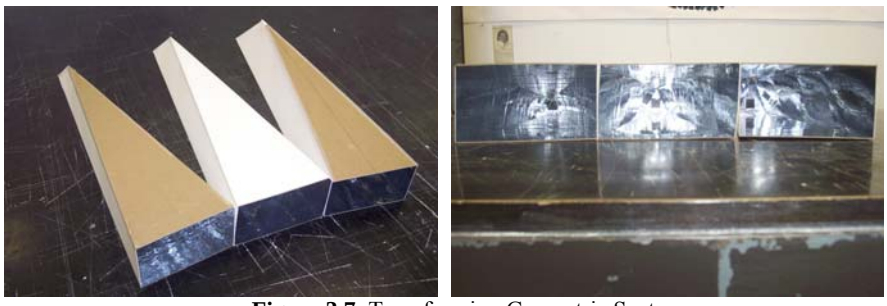

Figure 3.7: Transforming Geometric System

The design concept is intended to maximize the input source and minimize the number of output rays missing the diffuser target. Therefore, the whole rectangular sectional shape of 2 x 4 ft. is used for an inlet opening, from which in the section, transforms into an isosceles triangle shape, used as a 45-degree tilted back wall reflector. There are three sets of transformations based on three-selected triangle's base width of 1 ft., 1.5 ft., and 2 ft. The three Transforming Geometries are tested in comparison to find the most effective for daylight transportation.

6. Tapered Geometric System with seasonal louvers

The tapered geometric system with seasonal louvers was designed with the following strategies:

- Eliminate the triangular corner at the back of the ceiling by decreasing the tapered angle to provide a path for most parallel beams to strike in a better alignment.
- Replace the twisting side planes with vertical non-twisting side planes to make it simpler to construct.
- Installing two sets of seasonal louvers to deflect annual incident rays effectively to minimize reflections.

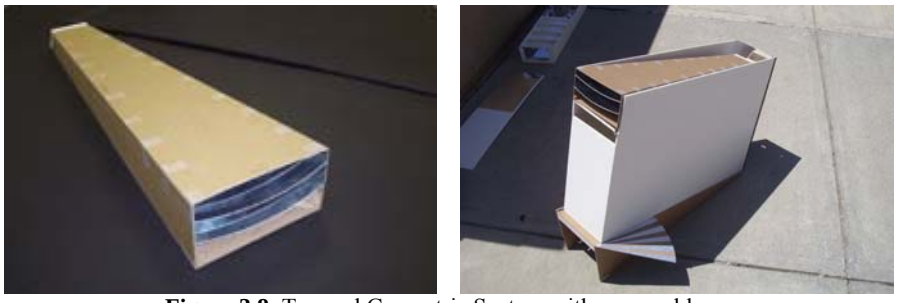

Figure 3.8: Tapered Geometric System with seasonal louvers

The idea with the Tapered Geometric design is to simplify the transforming geometric design. The tapered version uses a 1.5 ft. isosceles triangle for the base width of a 45-degree tilted rectangular back reflector. The seasonal louvers have two sets, each of which has three sectional curved planes to reflect incident rays of 30, 45, and 60- degrees. Each of the curved planes is calculated to have a maximum surface area for its annual incident ray to strike. Then they deflect the rays, to be almost horizontal, before striking to the 45-degree back reflector in order to finally reflect down almost perpendicularly to the diffuser area.

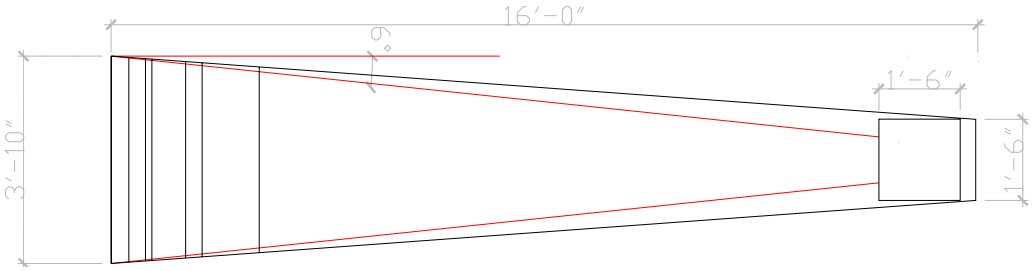

Top View

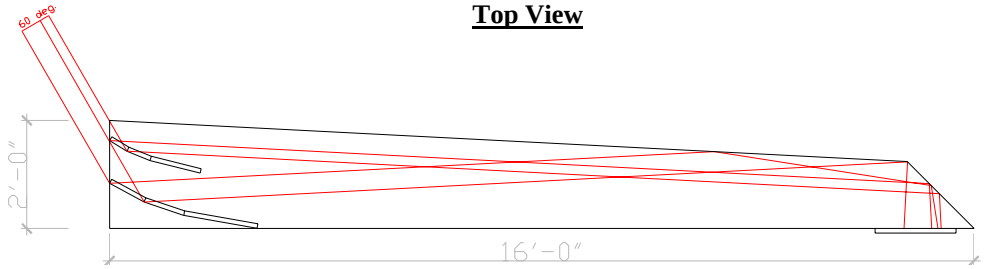

Sectional Diagram

(Reflective Bouncing in Tapered Geometric System for 60 Degree Incident Source Angle)

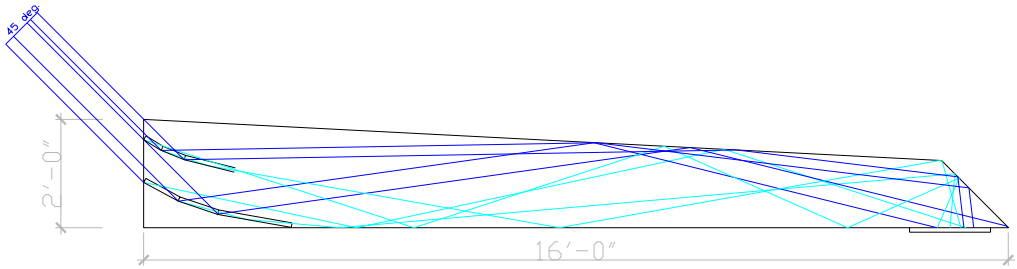

Sectional Diagram

(Reflective Bouncing in Tapered Geometric System for 45 Degree Incident Source Angle)

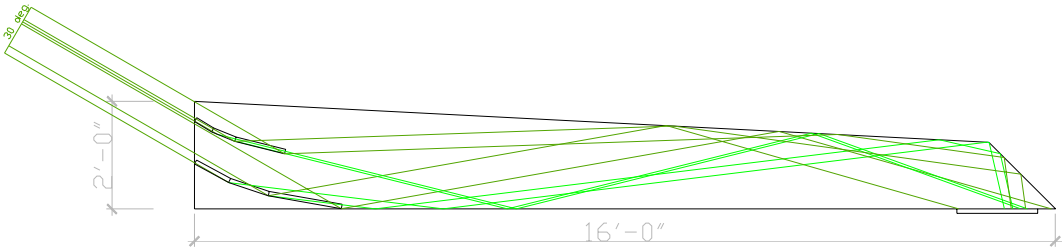

Sectional Diagram

(Reflective Bouncing in Tapered Geometric System for 30 Degree Incident Source Angle)

Figure 3.9: Drawings of the ceiling cavity showing ray-tracing in Tapered Geometric System (w/ louvers) for 30, 45, and 60-degree incident rays

7. Tapered Geometric System

The tapered geometric system was designed to meet the following objectives:

- Eliminate the triangular corner at the back of the ceiling by decreasing the tapered angle to provide a path for the most parallel beams to strike in a better alignment.
- Replace the twisting side planes with vertical non-twisting side planes to make it simpler to construct.
- Maximize the inlet area; the louvers are removed to maximize light penetration.

The existence of the seasonal louvers in the previous design reduces the effective inlet area. Therefore, this simplified version is proposed to compare the efficiency between the system with louvers and the system without louvers.

3.3.1.2 Experimental setup

A scale model of 1: 8 ratio (1.5 inch: 1 foot) was made to study the performance of each design. The scale model is divided into two sections. The first section is a room space with dimensions of 6 inches in width, 24 inches in depth, and 16.5 inches in height, with 1.5 inch high window opening on the front wall at 12 inches above the floor. The second section attaches to the top of the first section. This section is installed for testing the various light transporting systems above the ceiling cavity with dimensions of 6 inches in width, 24 inches in depth, and 3 inches in height *(See Figure 3.10)*. A photo sensor to measure the level of illuminance is inserted horizontally into the back wall of the scale model at task level and beneath the ceiling aperture (*See Figure 3.11*).

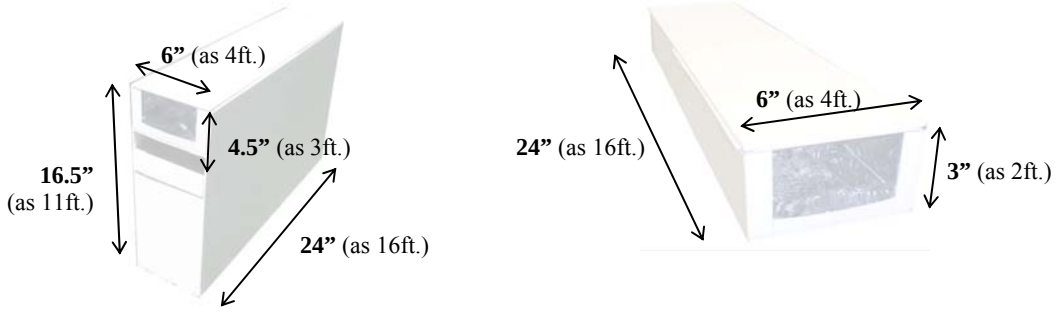

Figure 3.10: Scale model dimension of the room space (Left) with the geometric ceiling cavity (Right)

All internal geometric surfaces are mounted with silver Durallar, a high specular reflective film. Next, the completed geometric cavity is installed above the room section, with an 18 x 18 inch aperture, through the ceiling plane at 16 ft depth. The scale model is tested for its efficiency on daylight transporting performance under sunny and cloudy sky conditions between 11am and 1pm during the fall. A 15-degree ramp, with an equipped azimuth degree protractor (from 0 – 45 degree), is designed for the scale model to sit on as a means to simulate lower and higher incident sunrays for the other seasons (*See Figure 3.12*).

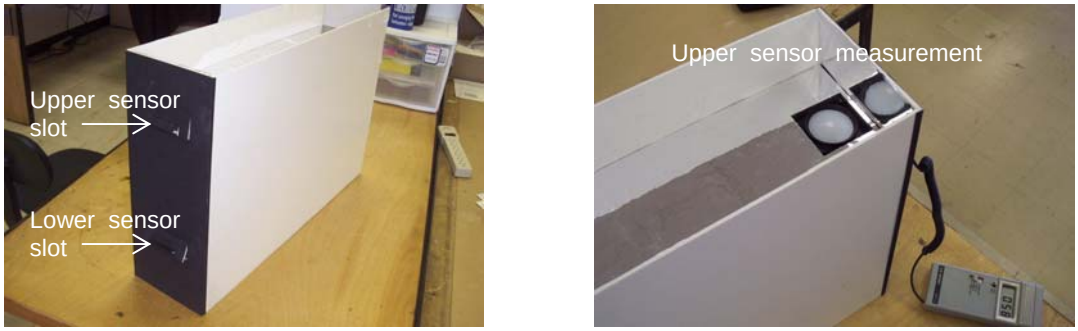

Figure 3.11: The sensor positions and diffuser area in the scale model test

Figure 3.12: The ramp used to simulate seasonal solar altitudes with an equipped solar protractor

Ten light level measurements were obtained from 0 - 45deg. incident angles total, at 5 degree increments. Each of the measurements was converted into time of a day by using the 36-degree North Latitude sundial, for Blacksburg's location (*See Figure 3.13*).

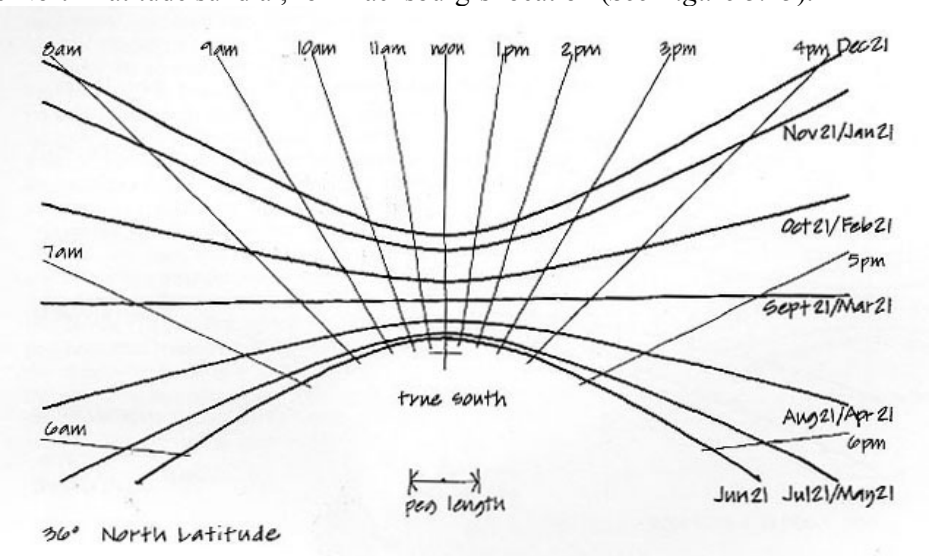

Figure 3.13: The sundial for 36 North Latitude (Brown, 1985)

3.3.1.3 Hypothesis Tests

Scale model tests are used to test the following hypotheses:

Hypothesis One

Scale model tests light levels with simple sky-simulating equipment will represent the full-scale experimental results.

Hypothesis Two

Illumination levels measured in the scale models will be proportional to those measured in the full-scale experiments. The proportionality ratio will be estimated.

The results are shown and discussed in chapter 4.

3.3.2 Full-scale Experimentation

3.3.2.1 Prototype

Based on the results discussed in chapter 4, the best three performing systems are the Curvature Geometric System, Tapered Geometric System, and Multi-Curvature Geometric System. These three systems were selected for full-scale analysis.

3.3.2.2 Experimental Setup

Because there was no full-scale room available with re-configurable systems, a full-scale experimental test apparatus was constructed.

A "slice" of space with dimensions of 4 ft. in width, 16 ft. in depth, and 11 ft. in height was constructed. The light-transporting systems were designed and installed above the ceiling of the experimental space. Reflective material, such as aluminum foil, was mounted on the inside walls of the test cell to simulate the luminance from side windows in a real room condition. Wheels were attached to allow mobility to a location where field tests were carried out. The cell was south-oriented to expose the sky conditions in summer, and then was rotated to the East to simulate low altitude sky conditions in winter.

At the test cell (a room space), seven photo cells were positioned to measure horizontal illuminance. Sensor 1 to sensor 6 were placed inside the cell, and sensor 7 was placed outside on the roof level of the cell. Sensor 1 was hung beneath the diffuser level, as an analog to the upper sensor in the scale model test *(See Figure 3.14)*, to measure horizontal illuminance received directly beneath the diffuser plane. At the task level (30 inches above the floor), sensor 2 to sensor 6 were placed along the centerline in width, at 3 ft. apart, running from the back to the front of the test cell. Sensor 2 in the test cell corresponds to the lower sensor in the scale model *(See Figure 3.11)*. Finally, the sensor 7 was attached on the top of the cell, outside the room space.

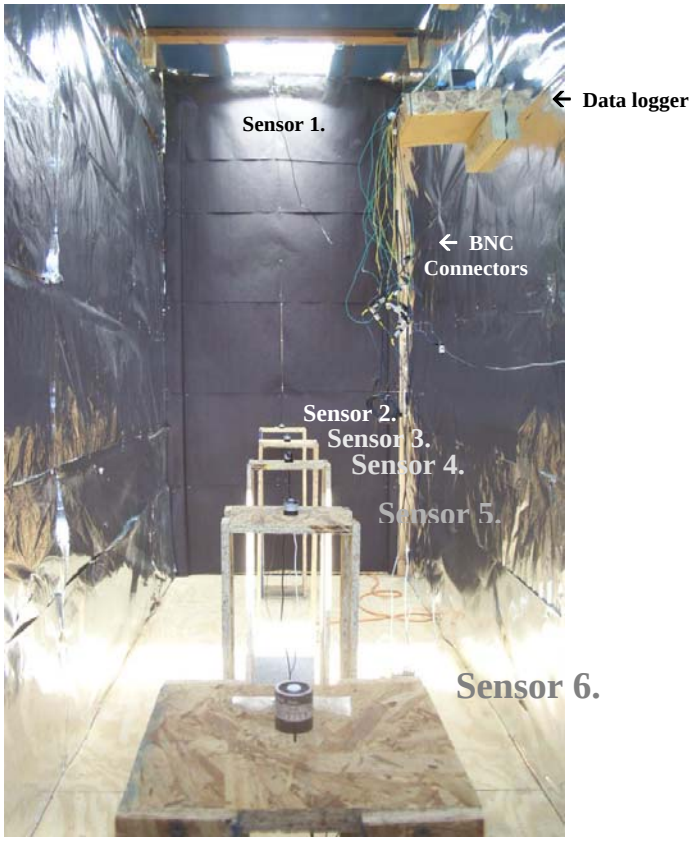

Figure 3.14: Science equipment positioning inside the test cell

Each sensor was wire-connected to a BNC connector before wiring to a channel of the Campbell Scientific 21X data logger. The BNC connector includes a resistor that allows a direct current signal to convert into a voltage signal. The data logger was set to record two values per input channel. The first is the average value of 60 one second measurements every minute. The other is the instantaneous value at one minute intervals.

Data collections proceeded for 24 hours. At approximately every two days, the data stored in the data logger was transferred to a storage module. The module then was connected to a PC computer through an isolator. This allows data to be displayed on the computer screen via database software *(See table 3.1)*.

Table 3.1: Sample data of the average value of 60 measurements, from each second, in every minute. Data was collected from the Multi-Curvature System between 8:00am and 8:30am

Time	Sensor 1	Sensor 2	Sensor3	Sensor 4	Sensor 5	Sensor 6	Sensor 7 (70%)	Sensor 7 (100%)
800	269.3	39.06	86.3	60.86	65.99	62.85	1099	1570
801	269.3	39.06	87	60.86	65.99	62.31	1096	1565.714
802	269.3	39.06	87	60.86	65.99	62.85	1099	1570
803	269.3	39.06	87	60.86	65.99	63.38	1099	1570
804	269.3	39.06	87	60.86	65.99	63.91	1099	1570
805	273.1	39.06	87	72.5	65.99	63.91	1099	1570
806	302	39.06	87	91.3	65.99	63.91	1099	1570
807	307.8	39.06	87	91.3	65.99	63.91	1099	1570
808	332.8	39.06	87	91.3	65.99	62.84	1110	1585.714
809	346.2	44.27	87	91.8	65.99	60.71	1235	1764.286
810	346.2	46.87	87	107.5	65.99	61.24	1308	1868.571
811	346.2	56.63	87	121.7	65.99	50.59	1319	1884.286
812	346.2	74.2	87	120.7	65.99	41.01	1349	1927.143
813	346.2	78.1	88.4	120.7	65.99	38.34	1458	2082.857
814	346.2	78.1	89.2	121.7	65.98	31.95	1539	2198.571
815	346.2	78.1	89.9	122.2	65.98	31.95	1539	2198.571
816	362.2	78.1	92.8	121.7	65.98	31.95	1539	2198.571
817	392.4	78.1	99.3	122.7	65.98	31.95	1539	2198.571
818	418.7	78.1	96.4	126.8	65.98	31.95	1539	2198.571
819	423.1	78.1	120.3	121.7	65.98	31.95	1539	2198.571
820	423.1	78.1	126.9	128.8	65.98	31.95	1539	2198.571
821	423.1	78.1	131.2	141.5	65.98	31.95	1539	2198.571
822	423.1	78.1	132.7	122.2	65.98	31.95	1539	2198.571
823	423.1	78.1	160.2	148.6	65.98	31.95	1539	2198.571
824	437.9	78.1	163.8	144.5	67.08	31.95	1539	2198.571
825	473.7	78.1	173.9	149.6	70.4	39.93	1539	2198.571
826	500	78.1	173.2	156.7	73.1	44.19	1539	2198.571
827	500	78.1	172.5	160.7	87.4	51.12	1539	2198.571
828	500	78.1	173.9	156.2	94	51.65	1542	2202.857
829	500	78.1	173.9	169.9	80.8	63.89	1638	2340
830	500	78.1	173.9	167.8	78.6	63.89	1857	2652.857

3.3.2.3 Test Cell Construction Process

The test cell is constructed by using a wood frame structure. The construction process starts with assembling a wood floor structure, of 4 x 16 ft.. Beneath the floor structure are ten rubber wheels that allow mobility to the test site. Then, pairs of 3 in. angled steel plates are bolted to the side beams to allow wood studs to stand vertically. Then, a 2 x 6 in. lumber beam is bolt connected to the tip of each cross stud, creating a frame for wall and ceiling attachments (*See Figure 3.15)*.

Figure 3.15: Wood studs are bolted to stand-vertically by being sandwiched with pairs of angled steel plates

Then the 4 x 8 ft. plywood sheets are screwed to the inside face of the studs to leave a smooth internal wall and ceiling surface (*See Figure 3.16)*. Inside the cell, aluminum foil is mounted on both of the internal side walls, and then the back wall surface is covered with black paper sheets. The room space is now ready for a daylight system to be installed, at the ceiling space. After a daylight system installation, a 3 x 4 ft. clear acrylic sheet is attached above the door level as an enclosure for a one foot high window and a two foot high inlet aperture of the system.

Figure 3.16: The finished primary rigid internal surface

Before being towed to the test site, the finished test cell is covered with heavy-duty construction plastic sheets for rain protection. An unsuccessful transport of the ten rubber wheels along the gravel dirt road of the test site resulted in the replacement of six scaffolding wheels. At the test site, spiral metal stakes are embedded into the ground to allow adjustable mechanic strips to tie down each corner, and therefore bracing the cell and creating moment resistance against wind force (*See Figure 3.17)*.

Figure 3.17: The arrangement for rain protection and wind force resistance

3.2.2.4 Geometric System Assembling Process

1. Curvature geometric system

Upper plane: Full-scale upper drawing lines of the longitudinal section are plotted and attached on the internal walls, at two sides of the ceiling cavity, as a marker for a geometric plane to tread. Then, screw-holes are drilled through the wall along the lines, on both sides, 1 foot apart for the straight-line part and 2 inches apart for the curve part (*See Figure 3.18).* Afterwards, the highly reflective silver Durallar film is mounted over the drawing layer. Then, a series of 1 x 2 x 47 in. lumber are cross-fixed by screwing from outside in at both ends of lumber, passing through the film surface, creating a geometric frame on which a surface material can be attached (*See Figure 3.19).* Then, corrugated cardboard sheets are the first layer attached on the lumber frame by stapling them through the frame, flushed along its surface. Next, the silver Durallar film is mounted on the first layer of corrugated cardboard sheets by spraying glue adhesive. Finally, the 3M prismatic sheets are stapled along the geometric plane to finish the surface for the upper plane of the ceiling (*See Figure 3.20)*.

Figure 3.18: Tracking the geometrical line

Figure 3.19: Framing the geometrical shape

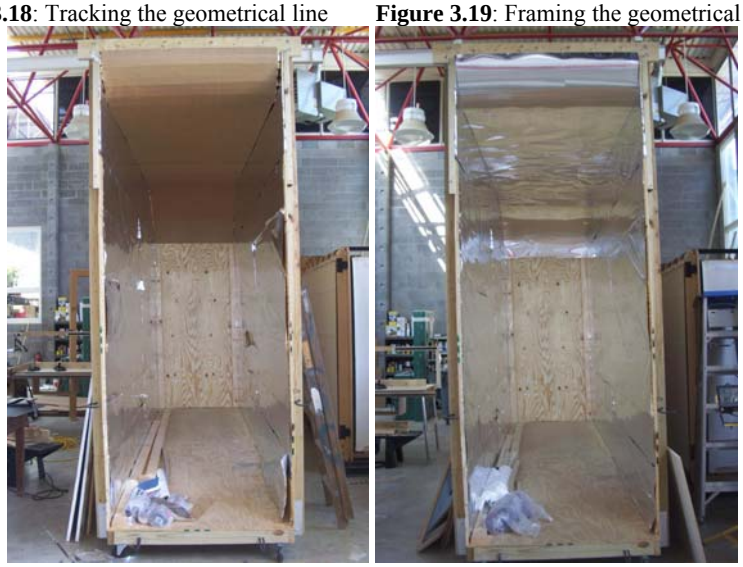

Figure 3.20: Attaching the corrugated cardboard layer, Durallar film, and the 3M prismatic sheets

Lower plane: Two sheets of 4 x 8 ft., one inch thick, insulation foam board are used to provide a lightweight rigid plane, for easy insertion along the room depth. Each of the boards is first taped by the silver Durallar film around the perimeter, followed by a layer of the prismatic sheets, as the top layer respectively. At the cross center, 4 inches away from the length edge of a board, a 1.5 x 1.5 ft. aperture is made for a diffuser area, where most of the rays are focused (*See Figure 3.21)*. On the ceiling level, aluminum angle bars are screwed running discontinuously toward the depth of both side walls, providing shoulder supports for the lower plane boards during installation (*See Figure 3.22)*.

(a)

(b)

Figure 3.21: The lower plane made out of an insulation board with specular film as the first layer (a) and prismatic sheet as the second layer (b).

Figure 3.22: The supporting shoulder for the lower planes to sit on.

Louver planes: Since the louvers are designed to be concave, a series of notches are made on a corrugated cardboard louver plane to allow bending. While bending the notched plane to a given curvature, the plane is glued to another rigid cardboard, forcing the whole piece to stay on the curved line. After the louver piece is formed, silver Durallar film is then glued to the louver followed by a prismatic layer sheet (*See Figure 3.23)*. Then, the next louver piece is made using the same procedure.

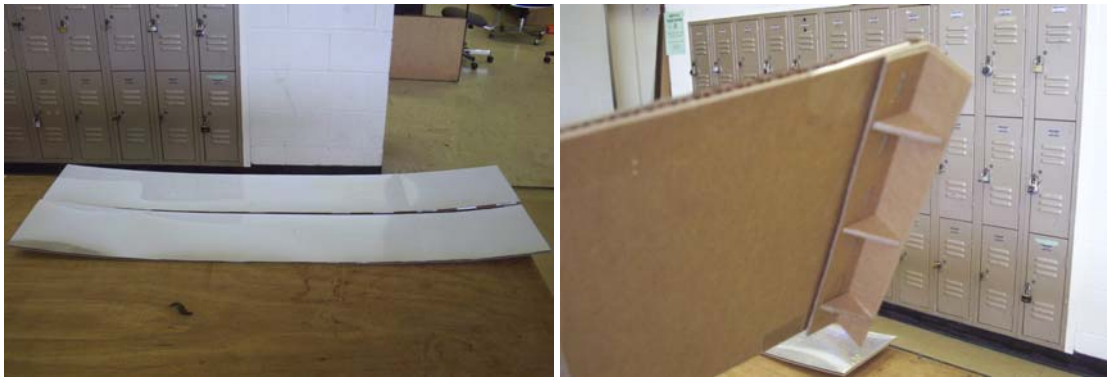

Figure 3.23: Louver planes with the side angle shoulders to allow attaching into the internal sidewalls

2. Tapered geometric system with seasonal louvers

This design version is planned to be preassembled outside the test cell and later inserted into the ceiling cavity. The enclosure is composed of two side planes, top and bottom planes, and a back plane. Each piece of the enclosure is constructed inside a workshop one by one. The assembling process starts from taping corrugated cardboards together to cover the length of a full-scale drawing line of its piece (16 ft. long). The continuing cardboards then were cut along the treading line. After getting the shape, the second corrugated cardboard layer is applied overlapping on the first layer by gluing over the surface and then cutting. Then, the process is repeated for the third layer. A corrugating pattern is also added from layer to layer, adding rigidity to the whole piece. Each piece of enclosure is then taped around the edge for further support (*See Figure 3.24*).

Figure 3.24: The first layer of the bottom piece in the Tapered Geometric System

During the next step, the silver Durallar film is applied on the top surface. To make a smooth covering surface, the film is fixed to one side of the enclosure's edge with a strip of clear tape at every inch along the side. Then the film is pulled tight and taped on the opposite side, resulting in a smooth top surface (*See Figure 3.25)*. The lower plane is the only one that has an extra layer of prismatic sheets applied on the top. The seasonal louvers are made in the same way as those of the first system without the prismatic sheet.

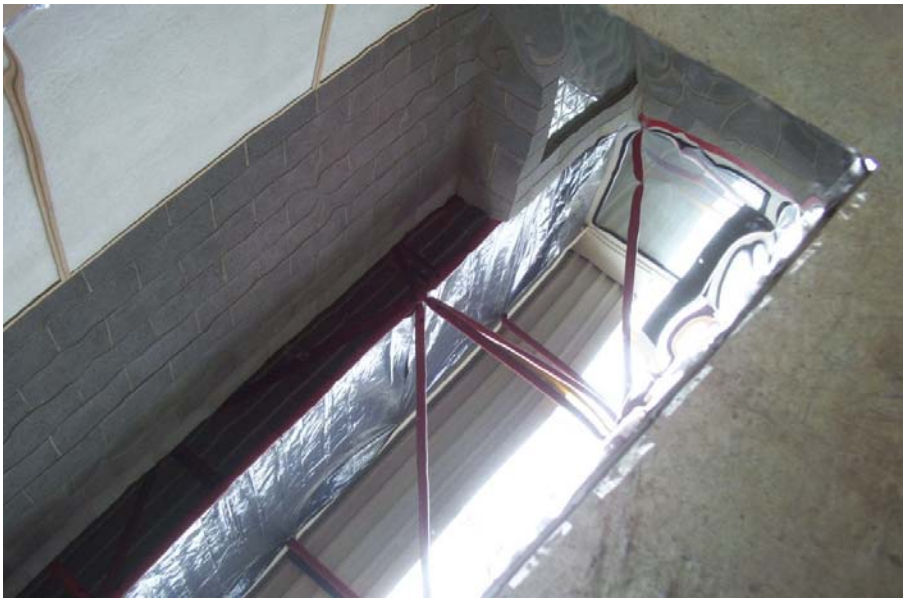

Figure 3.25: Tightening the specular film on the top cardboard layer by taping at both opposite sites along the length of the piece of enclosure

Figure 3.26: Brackets are screw fixed at a foot apart along the length of the piece of enclosure

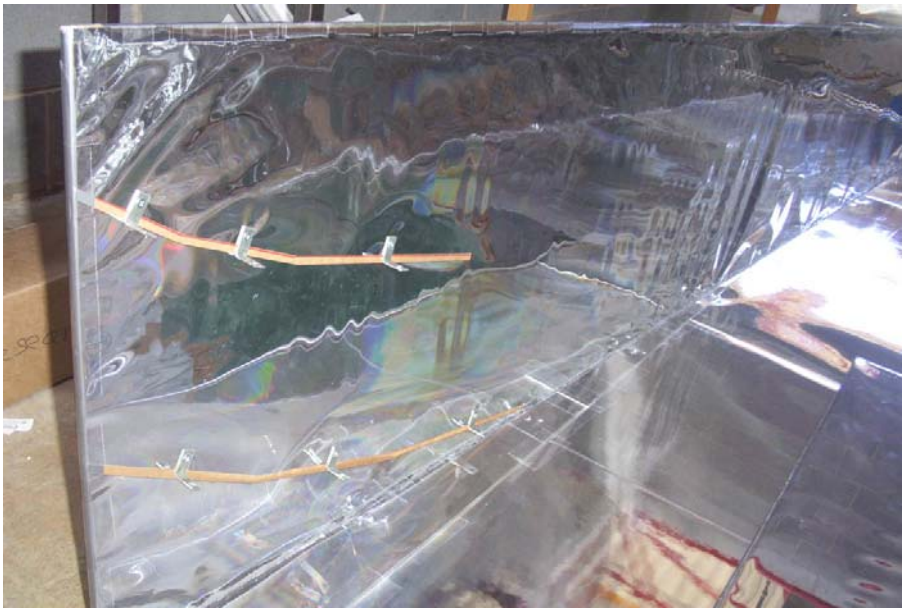

Figure 3.27: Smaller brackets are used as supporting points for the seasonal louver planes to sit on

After fabricating all geometric components of the system, assembly of the remaining parts is the final step in the process of construction. The 1-1/2 x 5/8 in. brackets are used to connect each plane together by screwing through the thickness of the plane at every foot apart (*See Figure 3.26).* The smaller brackets are used to attach the seasonal louver planes into their angle position (*See Figure 3.27).* The assembly is then carried to the test site and inserted into the ceiling cavity. A series of 1 in. x 2 in. cross lumber are prepared for the geometry to sit on (*See Figure 3.28).*

Figure 3.28: The installing of the finished tapered geometric mockup into the ceiling cavity of the test cell

3. Multi-curvature geometric system (Simplified Version)

The geometric components are made in the workshop and then installed into the ceiling cavity. This assembly uses the self-adhesive silver Durallar as a smoother and easier to install material for a large surface application. The lower plane from the first curvature system is modified to be reused in this system. There are three main components in this design that are prefabricated and installed into the ceiling cavity.

The first component is the inlet ramp made by two layers of corrugated cardboards glued together. Then, a self-adhesive version of the silver Durallar is applied on the top. The prefabricated inlet ramp is then installed on the front lower plane by stapling and taping. Finally, the modified lower plane is inserted into the ceiling cavity of the test cell (*See Figure 3.29*).

Figure 3.29: The reflective inlet ramp

The second component is the reflective ceiling plane. The full-scale drawing line of the ceiling curve is plotted and used as a guide. The sectional curved plane is made of several layers of corrugated cardboards glued together, using the same approach as the louver assembling method. The self-adhesive silver Durallar is applied on the top of each sectional curved plane. Then, all finished sectional curved planes are screwed inside the ceiling cavity. A sloping line is marked along two sides of the internal cavity to allow the tread of the ceiling planes. Each sectional curved ceiling plane is screwed into the side wall by using a series of brackets bending to a given angle (*See Figure 3.30).*

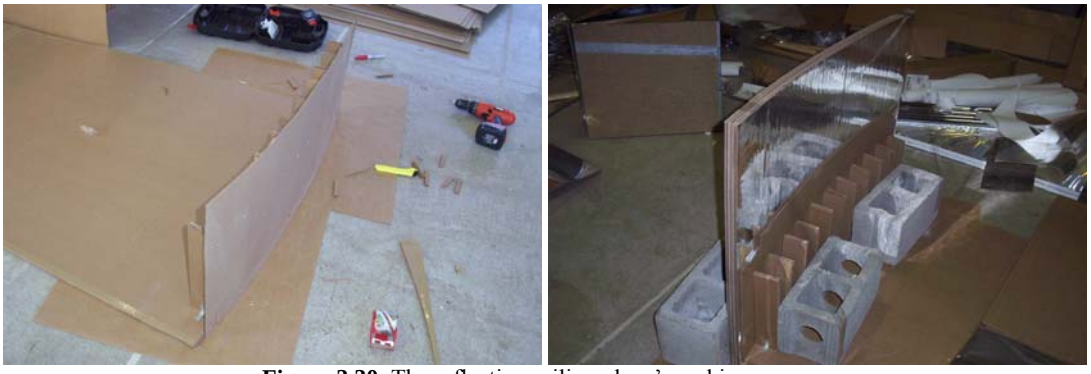

Figure 3.30: The reflective ceiling plane's making process

The third component is the three-piece back reflector. Each piece is made of corrugated cardboard connected with a curved rib cardboard structure to maintain rigidity on its curve line. Then the surface is applied with the self-adhesive silver Durallar. The finished back reflector is installed inside the cavity where a set of brackets is used to affix the component to the back wall (*See Figure 3.31 and 3.32).*

Figure 3.31: The demonstration of the reflection effect on the camera's flash (Left), and the completed assembling of the 3-piece back reflector (Right).

(a)

(b)

Figure 3.32: The images inside the cavity after installing the Multi-Curvature Geometric System ; (a) is the view looking from the diffuser to the inlet aperture, and vise versa (b)

3.2.2.5 Hypothesis Test

The full-scale experimentation is used to verify the following hypothesis:

Hypothesis Three

The multi-curvature system will result in the highest light levels in the rear of the space when compared to the other light transport configurations.

3.3.3 Method of Analysis

The analysis will be carried out based on five sets of comparisons:

1. A comparison between illuminance distribution with daylight systems and illuminance distribution without daylight systems (with a clear window alone).
2. An average daylight factor from each sensor inside the room (sensor 1-6 versus sensor 7)
3. A comparison between scale model and full-scale model performances.
4. An average daylight factor comparison among full-scale model performances.
5. An average daylight factor comparison among scale models.

3.4 Chapter Conclusion

3.4.1 Scale Model Test

Seven geometric prototypes were designed to accommodate the average seasonal solar altitudes of 30, 45, and 60 degree. Each prototype was tested using a scale model of 1.5 inch: 1 foot Ratio. These prototypes are listed:

1. Curvature Geometric System
2. Multi-Curvature Geometric System
3. Multi-Curvature Geometric System (Simplified Version)
4. Cylindrical Geometric System
5. Transforming Geometric System
6. Tapered Geometric System with seasonal louvers
7. Tapered Geometric System

The scale model is composed of a room box, and a ceiling cavity box. The room box is used for measuring horizontal illuminance beneath the ceiling aperture at two levels; at the upper level, analog to the sensor 1 in the test cell, and at the lower level, analog to the sensor 2 in the test cell. The ceiling cavity box is used for housing each of the geometric prototypes whose internal surfaces were covered with a highly specular film.

Measurements were taken under a simple sky simulation by using a 15 degree ramp with five degree increment (0-45 degree) solar azimuth protractor. The ramp was designed to use in either fall or spring to simulate the average seasonal solar altitudes. The solar azimuth protractor was designed to work together with the 36 North Latitude sundials so that a value measured from each scale can be approximated to time of a day. The three most promising prototypes were selected to test for the efficiency in the full-scale experimentation.

The scale model test is used to verify hypothesis test 1 and 2 as follows.

1. Scale models test with simple sky-simulating equipment will represent the full-scale experimental results.
2. Illumination levels measured in the scale models will be proportional to those measured in the full-scale experiments. The proportionality ratio will be estimated.

3.4.2 Full-Scale Experimentation

The simulated room space environment (test cell) was constructed using a wood frame structure with the dimensions of 4 foot in width, 16 foot in depth, and 11 foot in height. The vertical studs were attached alongside the longitudinal floor beams. Each of the longitudinal floor beams was supported by a pair of 1/8-3 inch angle steel plates. The plywood side walls were attached to the array of vertical studs by facing inside the room to leave a smooth surface inside the test cell. Six scaffolding wheels were applied to allow for mobility during the experimentation. A heavy-duty construction plastic sheet was used for rain protection. Each corner of the test cell was tied down to the ground for a moment resistance against wind force loads.

Inside the test cell, equipment was used for data collection. The equipment consisted of six photo cells inside on the workplane level at three feet apart, one photo cell on the top of the roof, a data logger with BNC connectors, and data storage modules.

Three geometric prototypes were built for the full-scale testing, with a test period of one month each. The prototypes are:

1. Curvature Geometric System
2. Tapered Geometric System
3. Multi-Curvature Geometric System (Simplified Version)

Curvature Geometric System

The system was built within the ceiling space by first framing a series of beams to align the geometric shape of the upper surface. The frame was then fixed to the corrugated cardboard layer, and a subsequently covered by the highly specular film and the prismatic sheets for the top layer. The corrugated cardboard curved louvers were then fabricated and installed separately into the inlet opening. A one inch thick insulation board was used for the lower plane because of its light weight and the ability to reduce the heat gain inside the test cell. The lower plane was mounted with the same combination layers as the upper surface. An area of 1.5 x 1.5 sq.ft. was cut at the middle end of the lower plane to provide a space for the diffuser area.

Tapered Geometric System

The Tapered Geometric System was built separately inside the facility lab. The technique of tightening the specular film on the enclosure surfaces was conceived to improve the smoothness of the mockup. An area of 1.5 x 1.5 sq.ft. was cut at the middle end of lower plane to provide a space for the diffuser area. Five enclosures were assembled together using a series of brackets. Seasonal louvers were attached into the inlet opening. The completed mockup was moved to the test site and inserted into the ceiling cavity after the first system was removed.

Multi-Curvature Geometric System (Simplified Version)

To experiment with the manufacturing alternative, the Multi-Curvature Geometric System utilizes the self-adhesive silver Durallar. This system achieves the best possible surface smoothness. The optical elements were made following the same procedure as the previous system.

The full-scale experimentation is used to verify the hypothesis test 3 as follows.

3. The Multi-Curvature System will result in the highest light levels in the rear of the space when compared to the other daylight transport configurations.

Chapter 4. Results

4.1 Introduction

The scale model tests and full-scale experimentation were applied to test the following hypotheses.

Hypothesis 1: Scale models test with simple sky-simulating equipment will represent the full-scale experimental results.

Hypothesis 2: Illumination levels measured in the scale models will be proportional to those measured in the full-scale experiments. The proportionality ratio will be estimated.

Hypothesis 3: The Multi-Curvature System will result in the highest light levels in the rear of the space when compared to the other light transport configurations.

4.2 Scale Model Results

The measured data from the scale model tests are shown and evaluated below:

Curvature Scale Model Test:

Table 4.1: Average illumination levels measured inside the Curvature scale model under a clear sky (raw data)

Average illumination levels (fc.) inside the scale model test at 1.5 inches: 1 ft. ratio under a clear sky condition between 11am and 2pm. in October												
Prototype	**Azimuth / Altitude**		**0˚**	**5˚**	**10˚**	**15˚**	**20˚**	**25˚**	**30˚**	**35˚**	**40˚**	**45˚**
Curvature Geometric System	*8600fc. **30˚** *8610fc.	**Upper**	3603	3690	3160	3037	2787	2137	2040	1830	1883	1480
		Lower	801	484	386	298	262	251	218	202	188	170
	*7550fc. **45˚** *7800fc.	**Upper**	2950	2100	2177	2517	1880	1963	1597	1670	1630	2120
		Lower	1047	443	410	393	320	223	200	180	170	163
	*8870fc. **60˚** *10700fc.	**Upper**	11143	3563	2097	3343	3563	2457	1750	2190	3410	3077
		Lower	504	319	237	238	257	177	169	160	194	185

*Note: the numeric values in footcandle inside the three altitude boxes are the average outside illumination level at the same moment as inside measurements in the same roll.

The numeric values of the outside illuminance are converted to the same scale at 10,000 fc. by using a linear extrapolation. This allows comparison of the Daylight Factor among different seasonal altitudes, and system prototypes.

Table 4.2: Average illumination levels measured inside the Curvature scale model under a clear sky

Average illumination levels (fc.) inside the scale model at 1.5 inches: 1 ft. ratio under a clear sky condition between 11am and 2pm. in October												
Prototype	**Azimuth / Altitude**		**0˚**	**5˚**	**10˚**	**15˚**	**20˚**	**25˚**	**30˚**	**35˚**	**40˚**	**45˚**
Curvature Geometric System	*10000fc. **30˚** 10000fc.	**Upper**	6940	4189	3674	3531	3241	2485	2372	2128	2189	1721
		Lower	930	562	448	346	304	291	253	235	218	197
	10000fc. **45˚** 10000fc.	**Upper**	7456	2782	2883	3326	2601	2490	2212	2116	2159	2808
		Lower	1342	504	525	567	410	286	256	218	230	402
	10000fc. **60˚** 10000fc.	**Upper**	**12562**	4017	2364	3769	3950	2770	1973	2469	3469	3844
		Lower	471	298	175	222	240	221	158	189	213	281

(* Each known outside illuminance is converted to 10,000 fc. by using a linear extrapolation)

Table 4.3: Average illumination levels measured inside the Curvature scale model under a cloudy sky

Average illumination levels (fc.) inside the scale model at 1.5 inches: 1 ft. ratio under a cloudy sky condition between 11am and 2pm. in October												
Prototype	**Azimuth / Altitude**		**0˚**	**5˚**	**10˚**	**15˚**	**20˚**	**25˚**	**30˚**	**35˚**	**40˚**	**45˚**
Curvature Geometric System	*10000fc. **30˚** 10000fc.	**Upper**	2225.9	2200	2166.6	2148.1	2140.7	2114.8	2088.9	2025.9	2003.7	1992.6
		Lower	291	290	285	280	277	272	268	260	257	255.5
	10000fc. **45˚** 10000fc.	**Upper**	2241	2200	2179	2186	2201	2207	2217	2196	2172	2165
		Lower	286	277	270	271	270	269	266	259	252	238
	10000fc. **60˚** 10000fc.	**Upper**	1729	1717	1708	1704	1671	1642	1625	1612	1600	1587
		Lower	161	158	157	153	147	141	136	132	128	119

(*Each known outside illuminance is converted to 10,000 fc. by using a linear extrapolation)

Based on evaluation of the internal illumination levels, the positive slope ceiling (*See Figure 3.2*) seems to work effectively on reducing the number of reflections for the 30 and 45-degree incident rays. The 30-degree louvers work effectively for deflecting 60-degree incident rays deep into the geometric cavity and room, without obstructing the path of the 30 and 45-degree incident rays *(See values hi-lighted in red color)*. The design shows a promising result, and therefore, this prototype was chosen to test further in a full-scale version.

Multi-Curvature Scale Model Test:

Table 4.4: Average illumination levels measured inside the Multi-Curvature scale model under a clear sky

Average illumination levels (fc.) inside the scale model test at 1.5 inches: 1 ft. ratio under a clear sky condition between 11am and 2pm. in October												
Prototype	**Azimuth / Altitude**		**0˚**	**5˚**	**10˚**	**15˚**	**20˚**	**25˚**	**30˚**	**35˚**	**40˚**	**45˚**
Multi-Curvature Geometric System	*10000fc. **30˚** 10000fc.	**Upper**	**Over 20000**	7583	3256	5212	5635	**7997**	4037	2358	1503	1435
		Lower	737.0	338.15	212	246	249	**345**	224	178	156	145
	10000fc. **45˚** 10000fc.	**Upper**	**Over 20000**	4870	4196	3388	3495	3643	**5185**	3517	2486	1776
		Lower	540	227	220	170	175	182	**255**	195	174	161
	10000fc. **60˚** 10000fc.	**Upper**	4848	4124	3859	3585	2887	2135	1780	1423	**2003**	1392
		Lower	342	268	231	251	216	149	121	117	**150**	114

(*Each known outside illuminance is converted to 10,000 fc. by using a linear extrapolation)

Table 4.5: Average illumination levels measured inside the Multi-Curvature scale model under a cloudy sky

Average illumination levels (fc.) inside the scale model test at 1.5 inches: 1 ft. ratio under a cloudy sky condition between 11am and 2pm. in October												
Prototype	**Azimuth / Altitude**		**0˚**	**5˚**	**10˚**	**15˚**	**20˚**	**25˚**	**30˚**	**35˚**	**40˚**	**45˚**
Multi-Curvature Geometric System	*10000fc. **30˚** 10000fc.	**Upper**	1504	1522	1538	1557	1572	1580	1595	1602	**1614**	1591
		Lower	239	243	248	249	248	246	245	243	**242**	231
	10000fc. **45˚** 10000fc.	**Upper**	1250	1286	1361	1364	1346	**1371**	1357	1343	1314	1271
		Lower	160	163	167	167	156	**168**	157	156	139	130
	10000fc. **60˚** 10000fc.	**Upper**	964	971	980	1002	**1024**	1020	982	950	916	890
		Lower	124	125	124	125	**126**	122	116	108	101	93

(*Each known outside illuminance is converted to 10,000 fc. by using a linear extrapolation)

The design works well for transporting and capturing all incident rays from 0-degree to a 45-degree azimuth. The data shows the increasing amount of rays measured in oblique angles by means of a couple of cross reflectors *(See values hi-lighted in red color)*. The design shows a promising result, and therefore, this prototype is chosen to test again in a full-scale version.

Cylindrical Scale Model Test:

Table 4.6: Average illumination levels measured inside the Cylindrical scale model under a clear sky

Average illumination levels (fc.) inside the scale model test at 1.5 inches: 1 ft. ratio under a clear sky condition between 11am and 2pm. in October												
Prototype	**Azimuth / Altitude**		**0˚**	**5˚**	**10˚**	**15˚**	**20˚**	**25˚**	**30˚**	**35˚**	**40˚**	**45˚**
Cylindrical Geometric System (1 ft. diameter)	*10000fc. **30˚** 10000fc.	**Upper**	260	**265**	248	241	229	221	185	179	155	135
		Lower	195	189	181	170	150	142	131	127	122	119
	10000fc. **45˚** 10000fc.	**Upper**	203	199	201	230	162	153	148	134	117	105
		Lower	134	125	130	139	118	116	113	112	111	110
	10000fc. **60˚** 10000fc.	**Upper**	96.5	96.4	95.4	94.2	93	90	88	87	87	86
		Lower	20.8	21.6	19	16.7	16	15.1	14.5	14	14.2	13.5
Cylindrical Geometric System (1.5 ft. diameter)	10000fc. **30˚** 10000fc.	**Upper**	920	1129	1315	1169	1083	**1646**	1046	1042	916	657
		Lower	202	200	205	207	175	169.	160	154	150	145
	10000fc. **45˚** 10000fc.	**Upper**	1136	1183	1205	1029	1046	1147	878	903	663	591
		Lower	198	194	180	172	162	154	149	144	138	134
	10000fc. **60˚** 10000fc.	**Upper**	641	609	600	593	579	534	525	447	419	387
		Lower	97.6	98.4	97.3	96.2	95.4	94.2	94.1	91	90	89.9
Cylindrical Geometric System with Reflector (2 ft. diameter)	10000fc. **30˚** 10000fc.	**Upper**	**3953**	2511	3895	3627	2616	2418	2075	1545	1430	1025
		Lower	396	325	300	268	237	207	176	160	149	137
	10000fc. **45˚** 10000fc.	**Upper**	2514	2450	1883	1602	1508	1473	1368	1112	1040	901
		Lower	189	184	174	166	157	153	148	144	137	132
	10000fc. **60˚** 10000fc.	**Upper**	970	958	931	897	875	820	781	743	692	643
		Lower	141	140	139	139	139	138	138	137	136	135

Cylindrical Geometric System without Reflector (2 ft. diameter)	10000fc. **30˚** 10000fc.	**Upper**	1470	1416	1297	1349	1476	1437	1440	1415	1232	1058
		Lower	236	223	162	183	238	229	230	223	110	104
	10000fc. **45˚** 10000fc.	**Upper**	1318	1536	**1574**	1492	1366	1394	1324	1067	948	838
		Lower	148	157	160.5	154	151	152	149	127	113	97
	10000fc. **60˚** 10000fc.	**Upper**	732	713	698	658	620	599	573	515	454	402
		Lower	94	92.7	90.7	85.5	80.6	77.8	74.5	67	59	52.2

(*Each known outside illuminance is converted to 10,000 fc. by using a linear extrapolation)

Table 4.7: Average illumination levels measured inside the Cylindrical scale model under a cloudy sky

Average illumination levels (fc.) inside the scale model test at 1.5 inches: 1 ft. ratio under a cloudy sky condition between 11am and 2pm. in October												
Prototype	**Azimuth / Altitude**		**0˚**	**5˚**	**10˚**	**15˚**	**20˚**	**25˚**	**30˚**	**35˚**	**40˚**	**45˚**
Cylindrical Geometric System (1 ft. diameter)	*10000fc. **30˚** 10000fc.	**Upper**	**109**	92.8	77	88.4	87.9	62.1	81.5	82.4	80.8	99
		Lower	45.1	37.1	30	33.6	32.5	22.3	28.5	28	26.6	31.7
	10000fc. **45˚** 10000fc.	**Upper**	85.5	69.6	62.4	83	65	42.8	65.2	61.7	61.1	77.2
		Lower	26.5	20.8	18	23.2	17.5	11.1	16.3	14.8	13.4	17.7
	10000fc. **60˚** 10000fc.	**Upper**	62.7	46	40.1	40.8	38.9	33.8	34	37.2	35	38.2
		Lower	15	10.9	9.5	9.54	9.18	8.07	8.13	8.85	8.29	8.98
Cylindrical Geometric System (1.5 ft. diameter)	10000fc. **30˚** 10000fc.	**Upper**	**480**	478	469	462	454	438	423	408	392	384
		Lower	162	160	159	157	155	154	153	152	151	150
	10000fc. **45˚** 10000fc.	**Upper**	387	385.7	381.4	378.6	371.4	357	343	328.6	314.3	300
		Lower	92.8	92.5	91.4	90.7	90	89.3	88.5	87.8	87.1	86.4
	10000fc. **60˚** 10000fc.	**Upper**	173	174	172	170	171	172	172.5	173	173	173
		Lower	29.4	29.6	29.2	28.9	29	29.2	29.3	29	29.1	29.3

Cylindrical Geometric System with Reflector (2 ft. diameter)	10000fc. **30˚** 10000fc.	**Upper**	1630	1600	1405	1470	**1810**	1790	1765	1675	1525	1480
		Lower	192	180	151	160	246	239	228	204	178	164
	10000fc. **45˚** 10000fc.	**Upper**	1014	1003	1032	1061	1118	1139	1100	1011	953	903
		Lower	138	116	151	164	182	187	178	124	109	83
	10000fc. **60˚** 10000fc.	**Upper**	718	741	763	774	748	756	759	770	777	772
		Lower	121	122	123	126	125	126	126	127	128	127
Cylindrical Geometric System without Reflector (2 ft. diameter)	10000fc. **30˚** 10000fc.	**Upper**	760	782	776	788	782	776	770	744	738	710
		Lower	196	240	223	251	240	222	207	189	174	160
	10000fc. **45˚** 10000fc.	**Upper**	664	688	723	753	776	800	**812**	788	770	747
		Lower	109	110	111	112	112	113	114	113	112	110
	10000fc. **60˚** 10000fc.	**Upper**	448	460	472	476	488	492	496	504	512	516
		Lower	88	92	96	98	102	100	102	104	106	107

(*Each known outside illuminance is converted to 10,000 fc. by using a linear extrapolation)

The 2 ft. diameter tube version is the most effective among the three. With its 45-degree back reflector, it reflects the maximum number of rays down into the diffuser *(See values hi-lighted in red color)*. However, its performance is inferior to that of the others. A comparison of the results for the three diameters suggests the larger diameter tube provides the higher illumination levels. This result is not unexpected as the larger tube provides for a larger effective inlet aperture area and consequently larger inlet area to diffuser area ratio. Under a fixed ratio, however, as a design modification by constantly reducing the diameter of the tube from the inlet to create a conical form, more sun light rays penetration may not be expected, according to the diagram in Figure 3.8. As a result, conical geometry is eliminated from the test.

Transforming Scale Model Test:

Table 4.8: Average illumination levels measured inside the Transforming scale model under a clear sky

Average illumination levels (fc.) inside the scale model test at 1.5 inches: 1 ft. ratio under a clear sky condition between 11am and 2pm. in October												
Prototype	**Azimuth / Altitude**		**0˚**	**5˚**	**10˚**	**15˚**	**20˚**	**25˚**	**30˚**	**35˚**	**40˚**	**45˚**
Transforming Geometric System (1 ft. wide x 1 ft. high triangular section)	*10000fc. **30˚** 10000fc.	**Upper**	8618	**10139**	3812	974	608	415	338	298	272	244
		Lower	480	489	384	314	261	213	192	179	170	165
	10000fc. **45˚** 10000fc.	**Upper**	430	472	427	394	359	334	309	285	264	255
		Lower	244	240	222	203	186	173	164	157	15	149
	10000fc. **60˚** 10000fc.	**Upper**	315	333	334	323	307	294	251	266	259	248
		Lower	143	144	143	140	138	136	135	134	131	129
Transforming Geometric System (1.5 ft. wide x 1.5 ft. high triangular section)	10000fc. **30˚** 10000fc.	**Upper**	5099	**13286**	5421	4213	4101	1567	733	573	486	451
		Lower	494	502	487	406	362	284	241	210	196	187
	10000fc. **45˚** 10000fc.	**Upper**	1741	2221	1933	746	621	549	491	457	419	399
		Lower	531	707	430	240	210	186	179	171	166	162
	10000fc. **60˚** 10000fc.	**Upper**	601	621	609	569	533	492	466	435	420	391
		Lower	174	178	177	170	166	163	159	154	153	149
Transforming Geometric System (2 ft. wide x 2 ft. high triangular section)	10000fc. **30˚** 10000fc.	**Upper**	12485	12727	**14424**	12427	11363	2348	1682	942	703	542
		Lower	877	922	1081	752	537	400	291	246	221	213
	10000fc. **45˚** 10000fc.	**Upper**	5281	6756	4213	1916	1605	1148	770	629	562	535
		Lower	402	405	391	311	297	280	217	202	192	189
	10000fc. **60˚** 10000fc.	**Upper**	1024	1086	1070	903	821	779	644	595	549	523
		Lower	185	190	188	175	163	160	154	149	145	140

(*Each known outside illuminance is converted to 10,000 fc. by using a linear extrapolation)

Table 4.9: Average illumination levels measured inside the Transforming scale model under a cloudy sky

Average illumination levels (fc.) inside the scale model test at 1.5 inches: 1 ft. ratio under a cloudy sky condition between 11am and 2pm. in October												
Prototype	**Azimuth / Altitude**		**0˚**	**5˚**	**10˚**	**15˚**	**20˚**	**25˚**	**30˚**	**35˚**	**40˚**	**45˚**
Transforming Geometric System (1 ft. wide x 1 ft. high triangular section)	*10000fc. **30˚** 10000fc.	**Upper**	**3743**	2892	1946	1040	532	300	231	167	139	124
		Lower	493	472	334	293	237	188	156	129	113	105
	10000fc. **45˚** 10000fc.	**Upper**	564	500	369	277	227	182	156	137	126	120
		Lower	220	211	185	165	147	130	114	103	93	87
	10000fc. **60˚** 10000fc.	**Upper**	300	282	245	222	192	167	165	160	152	148
		Lower	128	125	121	115	103	96	90	83	77	71
Transforming Geometric System (1.5 ft. wide x 1.5 ft. high triangular section)	10000fc. **30˚** 10000fc.	**Upper**	**1491**	1436	1409	1318	1191	991	736	627	509	454
		Lower	205	200	197	194	189	187	186	184	184	178
	10000fc. **45˚** 10000fc.	**Upper**	574	528	492	436	403	379	394	400	396	420
		Lower	145	141	137	136	136	135	134	133	126	139
	10000fc. **60˚** 10000fc.	**Upper**	513	498	467	444	413	398	390	388	383	375
		Lower	119	117	113	113	112	110	109	108	107	103
Transforming Geometric System (2 ft. wide x 2 ft. high triangular section)	10000fc. **30˚** 10000fc.	**Upper**	**3887**	3750	3650	3295	2376	1968	1277	1078	841	723
		Lower	653	645	624	612	544	513	468	447	381	362
	10000fc. **45˚** 10000fc.	**Upper**	954	810	624.	581	543	529	504	483	462	448
		Lower	238	233	226	221	214	207	189	173	164	155
	10000fc. **60˚** 10000fc.	**Upper**	802	788	761	753	729	704	686	654	619	583
		Lower	200	187	173	164	158	146	137	128	119	110

(*Each known outside illuminance is converted to 10,000 fc. by using a linear extrapolation)

The results suggest that the Transforming Geometric design is better than the Cylindrical geometric version *(See values hi-lighted in red color)*. However, the twisting side planes make it complicated to build, and therefore, it is simplified for the next design variant.

Tapered Scale Model Test:

Table 4.10: Average illumination levels measured inside the Tapered scale model under a clear sky

Average illumination levels (fc.) inside the scale model test at 1.5 inches: 1 ft. ratio under a clear sky condition between 11am and 2pm. in October												
Prototype	**Azimuth / Altitude**		**0˚**	**5˚**	**10˚**	**15˚**	**20˚**	**25˚**	**30˚**	**35˚**	**40˚**	**45˚**
Tapered Geometric System	*10000fc. **30˚** 10000fc.	**Upper**	**8128**	7119	7089	4445	3337	2282	1141	842	730	667
		Lower	**5923**	482	456	417	354	306	258	221	213	201
	10000fc. **45˚** 10000fc.	**Upper**	**23313**	18716	7209	4060	4697	3189	2347	1403	1085	850
		Lower	**2022**	674	501	448	384	325	282	246	231	226
	10000fc. **60˚** 10000fc.	**Upper**	**6389**	4264	7665	3686	2884	2767	1880	1248	1151	881
		Lower	**329**	284	306	242	224	219	203	194	181	173

(*Each known outside illuminance is converted to 10,000 fc. by using a linear extrapolation)

Table 4.11: Average illumination levels measured inside the Tapered scale model under a cloudy sky

Average illumination levels (fc.) inside the scale model test at 1.5 inches: 1 ft. ratio under a cloudy sky condition between 11am and 2pm. in October												
Prototype	**Azimuth / Altitude**		**0˚**	**5˚**	**10˚**	**15˚**	**20˚**	**25˚**	**30˚**	**35˚**	**40˚**	**45˚**
Tapered Geometric System	*10000fc. **30˚** 10000fc.	**Upper**	1416	1448	1488	1552	1592	1612	1608	1600	1584	1568
		Lower	252	255	256	250	251	242	240	239	237	236
	10000fc. **45˚** 10000fc.	**Upper**	1333	1398	1455	1513	1545	1561	1544	1512	1439	1358
		Lower	194	195	197	198	199	201	199	197	192	186
	10000fc. **60˚** 10000fc.	**Upper**	841	898	962	1013	1051	1064	1070	1057	1025	968
		Lower	164	164.5	165	165.3	166	177	178	164	160	157

(*Each known outside illuminance is converted to 10,000 fc. by using a linear extrapolation)

The Tapered design shows an increase of illuminance at the task level which results from the more vertical passing of the rays along the diffuser plane *(See values hi-lighted in red color)*. Therefore, this prototype was chosen for full-scale testing.

The measured data from the scaled models and full-scaled experiments were analyzed to test the following hypotheses:

4.3 Hypothesis One Results

Scale models tests with simple sky-simulating equipment will represent the full-scale experimental results.

Table 4.12 :Sample data of illumination levels (fc.) with Daylight Factor (%) calculations from a scale model at approximate time intervals of a day by using the Sundial diagram

Prototype	Altitudes	Sensor	7:47AM	8:00AM	8:22AM	8:40AM	9:00AM	9:30AM	10:00AM
curvature geometry (Clear)	30	upper	1721	2189	2128	2372	2485	3241	3531
		lower	197	218	235	253	291	304	346
		DF-lower	1.97	2.18	2.35	2.53	2.91	3.04	3.46
		DF-upper	17.21	21.89	21.28	23.72	24.85	32.41	35.31
	45	upper	2808	2159	2116	2212	2490	2601	3326
		lower	402	230	218	256	286	410	567
		DF-lower	4.02	2.3	2.18	2.56	2.86	4.1	5.67
		DF-upper	28.08	21.59	21.16	22.12	24.9	26.01	33.26
	60	upper	3844	3469	2469	1973	2770	3950	3769
		lower	281	213	189	158	221	240	222
		DF-lower	2.81	2.13	1.89	1.58	2.21	2.4	2.22
		DF-upper	38.44	34.69	24.69	19.73	27.7	39.5	37.69

Prototype	Altitudes	Sensor	10:40AM	11:17AM	12:00PM	12:43PM	1:20PM	2:00PM	2:30PM
curvature geometry (Clear)	30	upper	3674	4189	6940	12562	3674	3531	3241
		lower	448	562	930	471	448	346	304
		DF-lower	4.48	5.62	9.3	4.71	4.48	3.46	3.04
		DF-upper	36.74	41.89	69.4	125.62	36.74	35.31	32.41
	45	upper	2883	2782	7456	2782	2883	3326	2601
		lower	525	504	1342	504	525	567	410
		DF-lower	5.25	5.04	13.42	5.04	5.25	5.67	4.1
		DF-upper	28.83	27.82	74.56	27.82	28.83	33.26	26.01
	60	upper	2364	4017	12562	4017	2364	3769	3950
		lower	175	298	471	298	175	222	240
		DF-lower	1.75	2.98	4.71	2.98	1.75	2.22	2.4
		DF-upper	23.64	40.17	125.62	40.17	23.64	37.69	39.5

As shown in Table 4.12, Curvature Geometric System model was tested with simple sky-simulating equipment; the ramp, and the sundial diagram. Illuminations levels at approximate time intervals were corresponding to those in the full-scale experiment.

The following is the other supporting data showing that there is a corresponding Daylight Factor relationship between the two different scaled models that simulate the winter sky solar altitude condition.

Sensor 1 (in full-scaled) = The Upper Sensor (in scaled)
Sensor 2 (in full-scaled) = The Lower Sensor (in scaled)

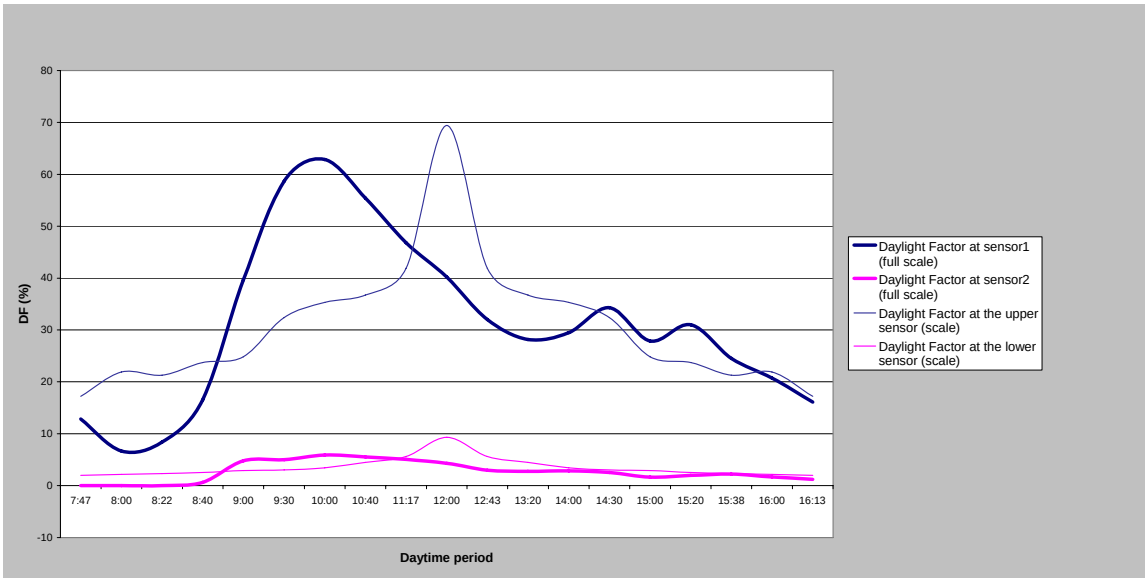

Figure 4.1: Daylight Factor comparison in the Curvature Geometric System at two sensor positions for the full-scale rotated to the East and the 30deg. simulated scale model

Figure 4.1, at sensor 1 and 2, shows Daylight Factor comparisons between the full-scale version of the Curvature Geometric System rotated to the East and its scaled model version under winter sky simulation. Each plot shows a similar range of the Daylight Factor levels throughout a day. The shape difference results from an error of degrees in the test cell rotation. However, the result, still, suggests that performances under the two situations be relevant and therefore it is possible to predict the full-scale system efficiency by using a scale model test with simple sky-simulating equipment. Therefore Hypothesis one is shown to be true.

4.4 Hypothesis Two Results

Illumination levels measured in the scale models will be proportional to those measured in the full-scale experiments. The proportionality ratio will be estimated.

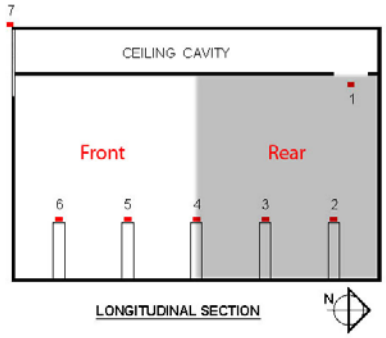

Sensor positioning

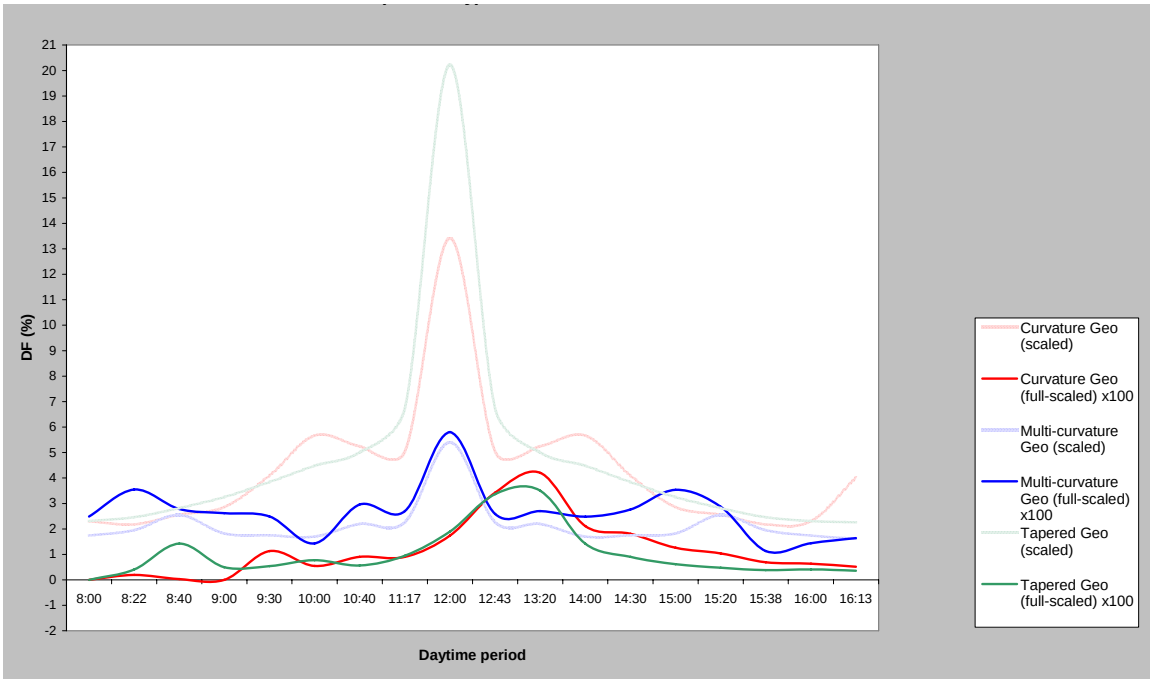

Figure 4.2: Daylight Factor comparison between scale and full-scale models at sensor 2 under clear sky conditions

For each system, the Daylight Factor distributions from the scale and full-scale tests were compared over a typical day. In the Multi-Curvature Geometric System, the Daylight Factor distribution of the full-scale version, after being multiplied by a hundred, shows light levels similar to the scaled model *(See Figure 4.2)*. From the chart, it can be concluded that the scale model performances can estimate the tendency of the full-scale model performances with a scaling multiplier of x100.

Table 4.13: The degree of prediction from the scale model performance to the full-scale measured by the Daylight Factor differences

Daytime	***Multi-curvature*** **(Full-scale)**		***Multi-curvature*** **(Scale)**	***Multi-curvature*** **(Scale – Full-scale)**	
	(A) DF sensor 2	(B) DF sensor 2 (x 100)	(C) DF sensor 2	|(B) - (C)|	% Difference
8:00 am.	0.024879	2.4879	1.74	0.7479	30.06
8:22 am.	0.035523	3.5523	1.95	1.6023	45.11
8:40 am.	0.027851	2.7851	2.55	0.2351	8.44
9:00 am.	0.026165	2.6165	1.82	0.7965	30.44
9:30 am.	0.024871	2.4871	1.75	0.7371	29.64
10:00 am.	0.014284	1.4284	1.70	0.2716	19.01
10:40 am.	0.029605	2.9605	2.20	0.7605	25.69
11:17 am.	0.027026	2.7026	2.27	0.4326	16.01
12:00 pm.	0.058034	5.8034	5.40	0.4034	6.95
12:43 pm.	0.025907	2.5907	2.27	0.3207	12.38
13:20 pm.	0.02703	2.703	2.20	0.5030	18.61
14:00 pm.	0.024834	2.4834	1.70	0.7834	31.55
14:30 pm.	0.027627	2.7627	1.75	1.0127	36.66
15:00 pm.	0.035364	3.5364	1.82	1.7164	48.54
15:20 pm.	0.028689	2.8689	2.55	0.3189	11.12
15:38 pm.	0.011307	1.1307	1.95	0.8193	72.46
16:00 pm.	0.014438	1.4438	1.74	0.2962	20.52
16:13 pm.	0.016435	1.6435	1.61	0.0335	2.04

Table 4.13 shows the Daylight Factor differences between the scale and full-scale (x 100). This may be inferred that the scale model light levels are about 100 times over those in the full-scale test. The percents of difference in the right-most column shows how close the scale model light levels are to a hundred-time full-scale light levels.

$$\%\text{Difference} = \frac{|(B) - (C)|}{(B)} \times 100 \qquad (6)$$

4.5 Hypothesis Three Results

The multi-curvature system will result in the highest light levels in the rear of the space when compared to the other light transport configurations.

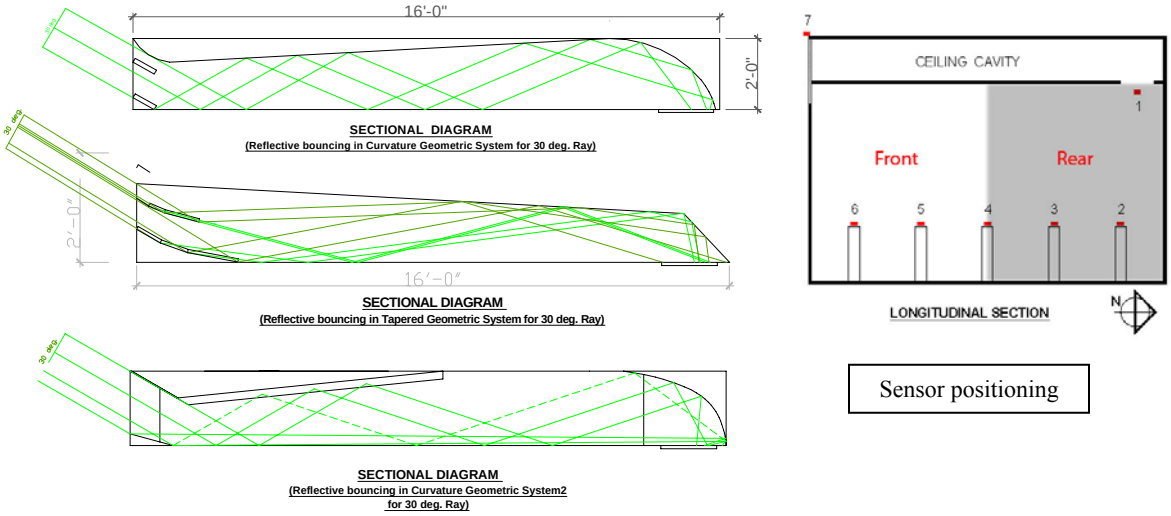

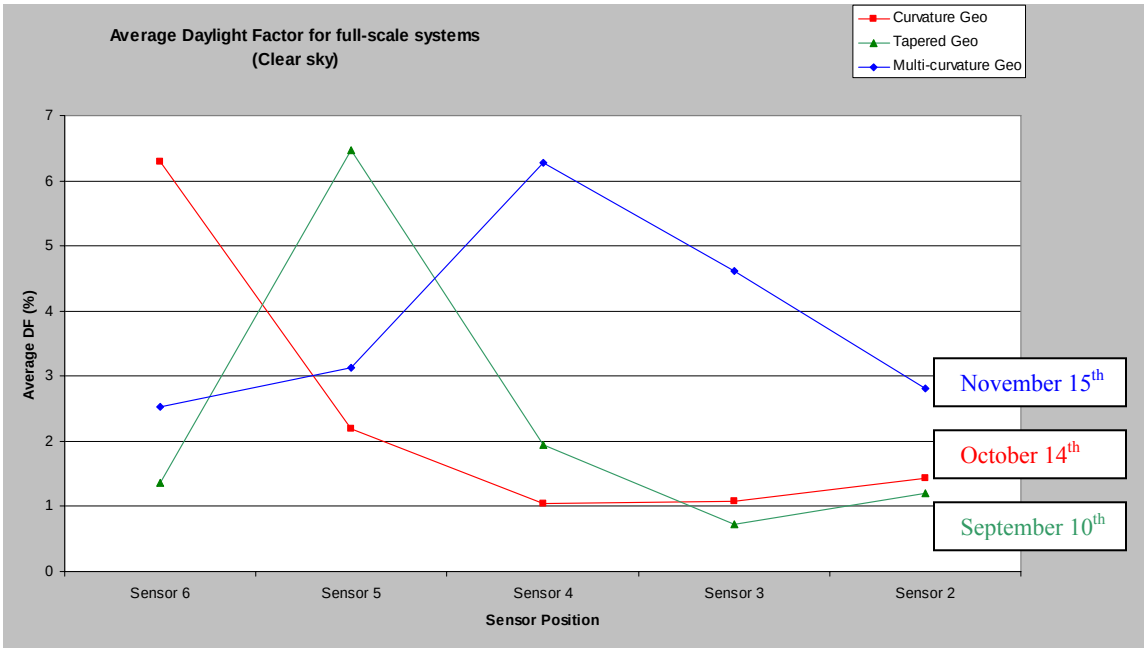

Figure 4.3: Average Daylight Factor for full-scale systems under clear sky conditions

Because the systems were sequentially tested (about a month difference), the peak level of illumination at the front of the test cell for each system appears at a different sensor position, corresponding to direct solar illumination due to the solar altitude. The average Daylight Factor for the Curvature and Tapered Geometric System shows an increased illumination level at sensor 2. The average Daylight Factor for the Multi-Curvature Geometric System at sensor 2 is greater than that of the other two systems. However, this greater illumination might be partially from the direct sun penetration, noticed by the nearby peak level at sensor 4 *(See Figure 4.3)*. Note that, the author realizes that DF is used under cloudy not clear sky

conditions. The reason to be used under clear sky conditions in this case is that the author wants to observe maximal efficiency from these full-scale prototypes.

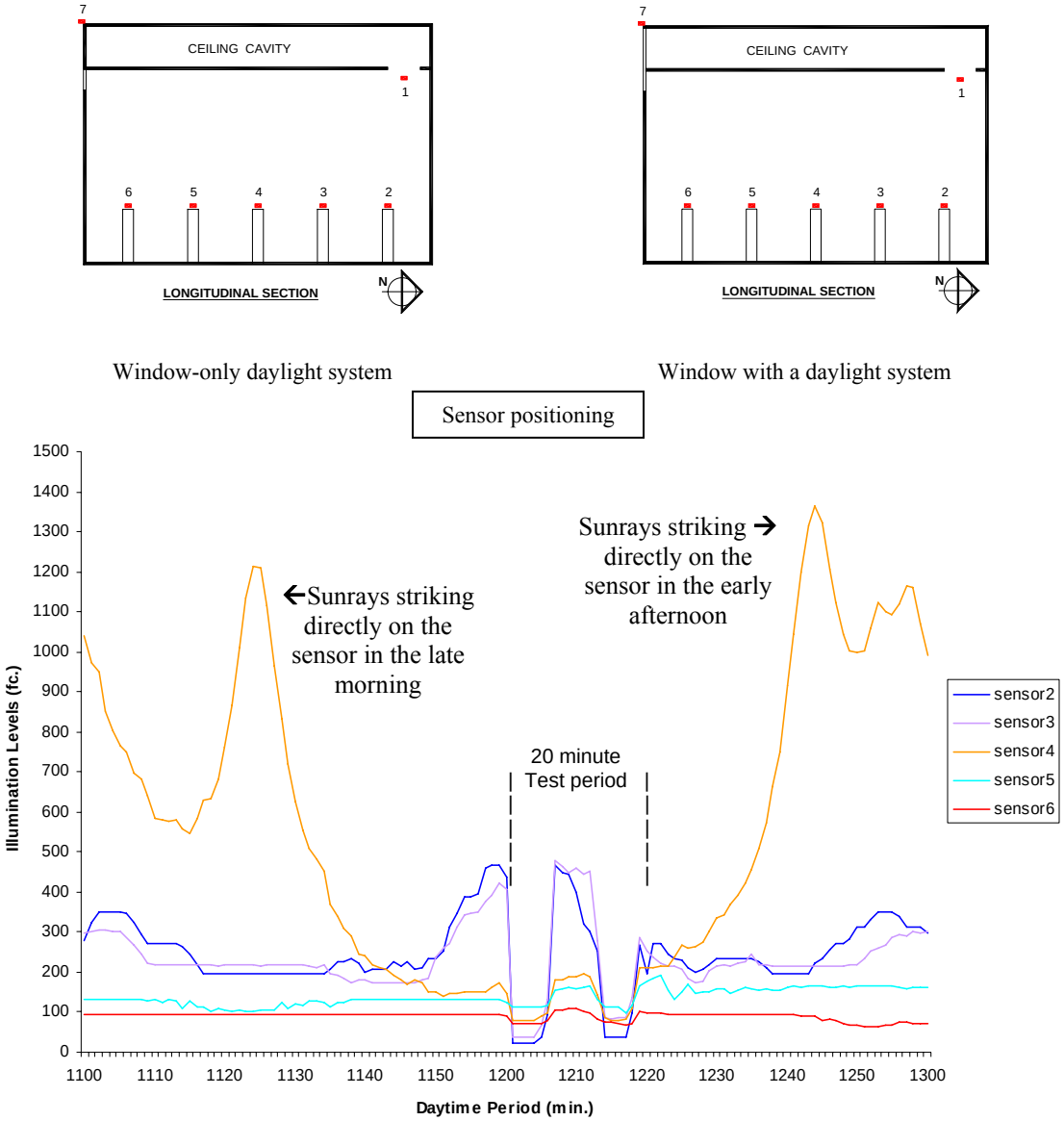

Figure 4.4: Daylight distribution from the Multi-Curvature Geometric System (Window-only daylighting V.S. Window with the system)

To determine the effect of this situation, a second test was undertaken. Here measurements were taken with light only through the window (without daylight transporting system) and then with the daylight transporting system. This allowed the effects of direct sun to be factored out. The results are shown in Figure 4.4.

Figure 4.4 shows illumination levels generated by the Multi-Curvature Geometric System during the midday (11:00am -1:00pm) for mostly sunny conditions. To estimate an average efficiency of the window-only system, the daylight system is blocked intermittently for two 5minute periods each (from 12:00pm to 12:05pm and from 12:15pm to 12:20pm).

The 10-minute range in between is for the unobstructed daylight system. As shown, the illumination level from sensor 2 is lower during the blockage indicating that the illumination level at sensor 2 from Figure 4.4 was generated by the daylight system alone, not by the outside illumination distributing from the nearby peak level. Note that the very high illumination levels from sensor 4, in the late morning and early afternoon, result from direct sun striking the sensor. Since this is a point measurement, such direct illumination should be discarded.

To compare the two systems with the same input energy, the 3 ft. tall inlet window size was maintained in both systems. The window-only system and a transporting system with the same window size are compared:

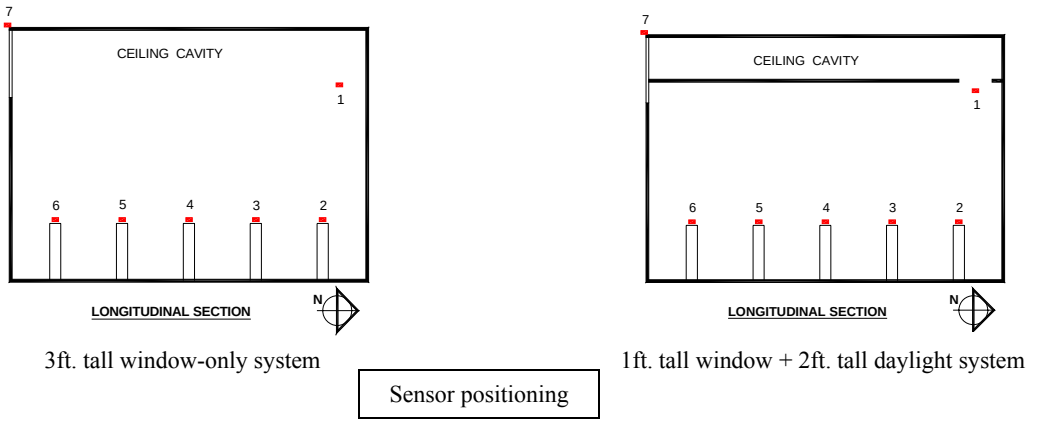

3ft. tall window-only system

1ft. tall window + 2ft. tall daylight system

Sensor positioning

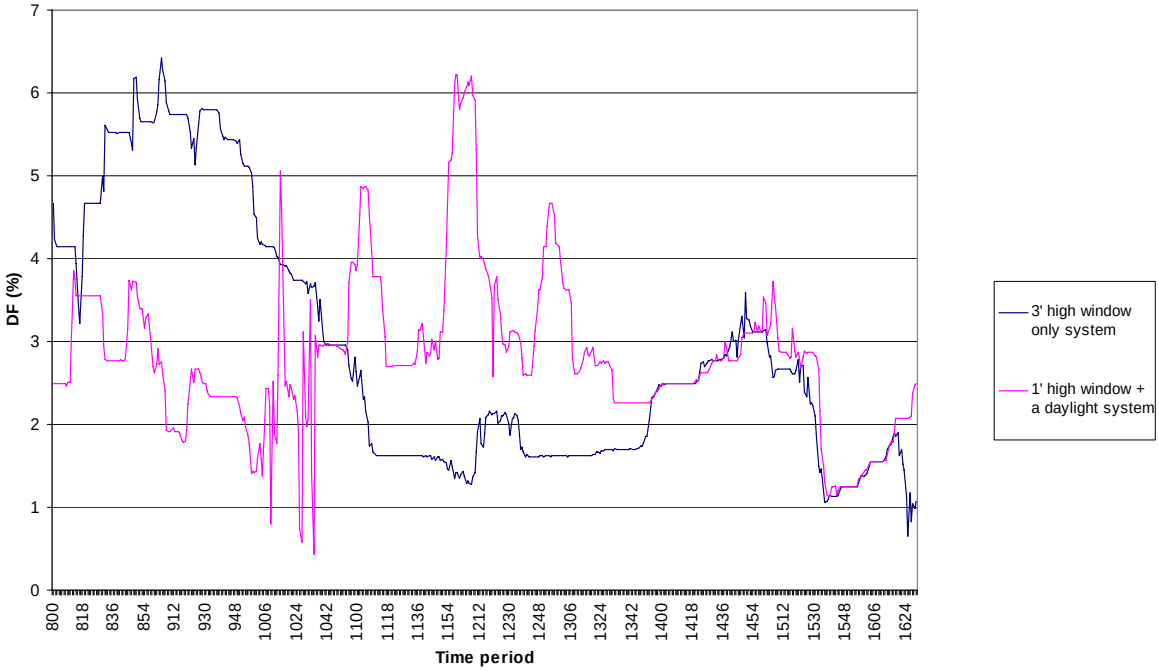

Figure 4.5: Daylight Factor comparison between 3ft. high window and 1ft. high window + a daylight system at sensor 2

From Figure 4.5, the 3ft. high window-only system generates a greater Daylight Factor during the beginning of the day. After 10:45am, it becomes inferior to the window with a daylight system (Multi-Curvature Geometric System).

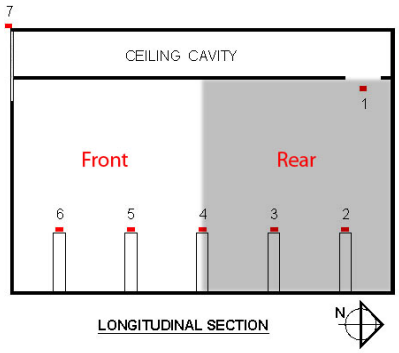

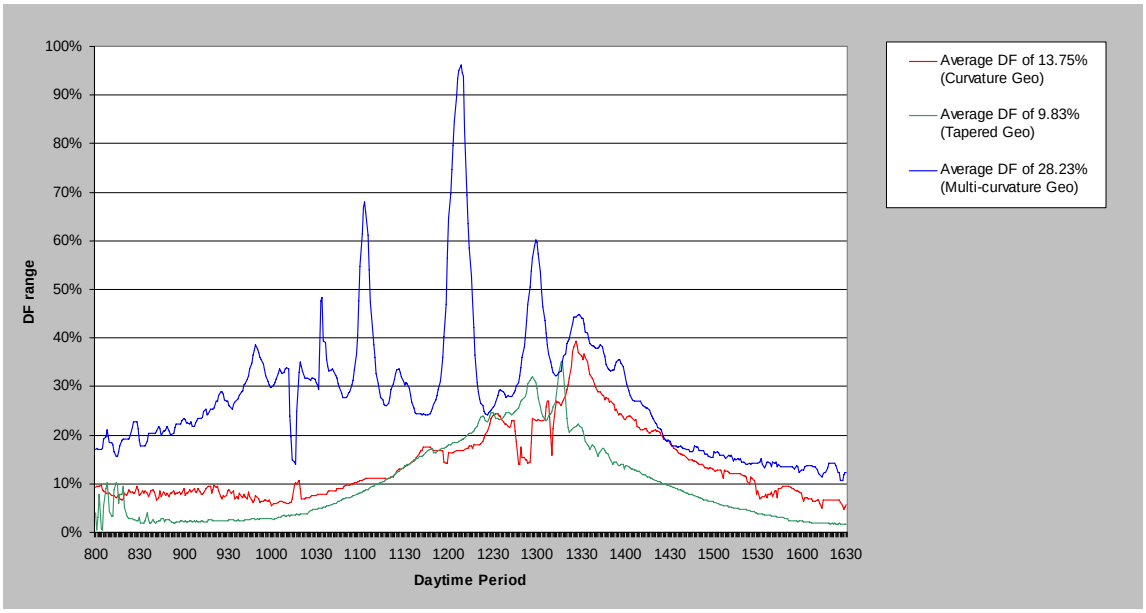

Figure 4.6: Daylight Factor at sensor 1 in full-scale models comparison under a partly cloudy sky condition

The efficiency of each system, evaluated by its Daylight Factor, from Figure 4.6 states that the Multi-Curvature Geometric System produces the highest illumination level overall for the entire daylight period. This is mainly caused by the greater smoothness of the internal surface when compared to the other two systems. Another factor may be from the low altitude condition that allows more transmission through the clear plastic window; angle of incidence is more perpendicular to the clear plastic window.

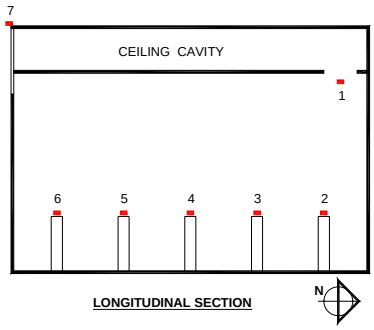

Sensor positioning

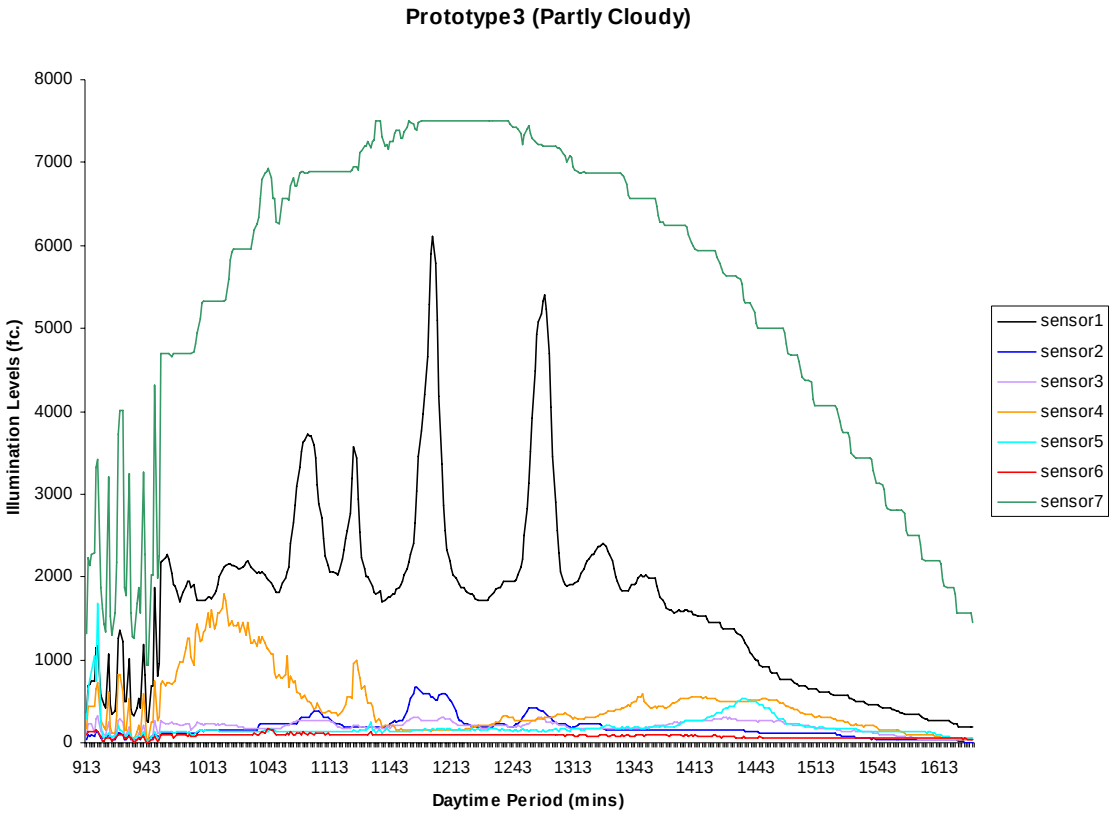

Figure 4.7: The illumination level from each sensor produced by the Multi-Curvature Geometric System for partly cloudy conditions

While under an overcast sky, the efficiency of a daylight system decreases as the DF decreases from 6.5% to 2.4% at the sensor 5, and decreases from 1.2% to 0.45% at the sensor 2, with a slightly increase of illumination at the rear part of the room. Comparison of the Daylight Factor for clear and cloudy sky conditions is provided as follows *(See Figure 4.8)*.

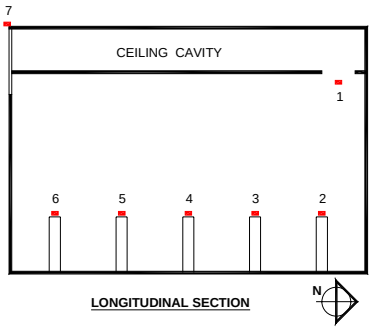

Sensor positioning

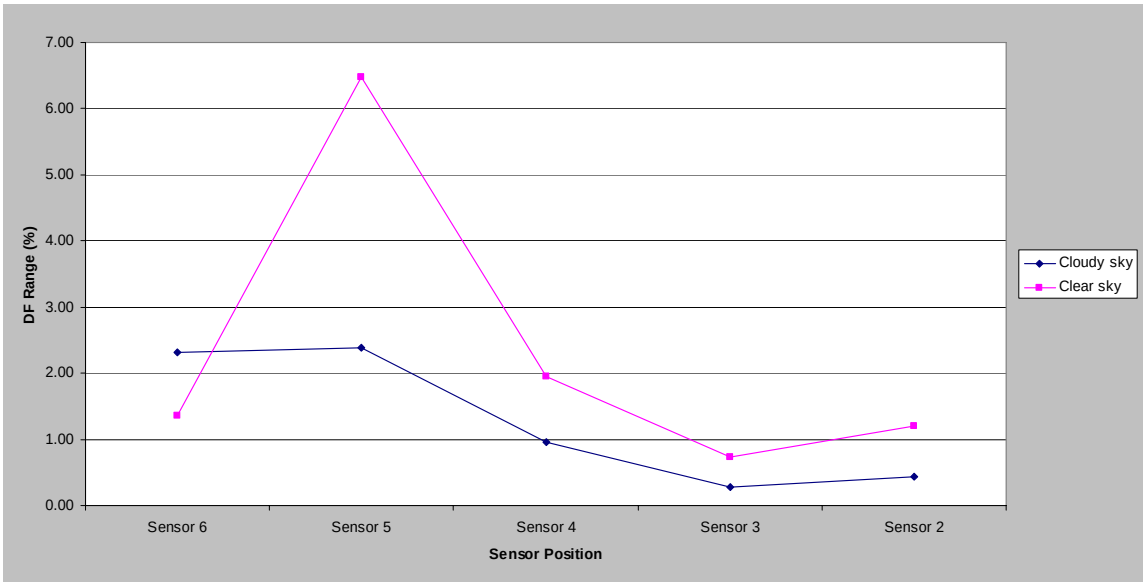

Figure 4.8: Average Daylight Factor for the Tapered Geometric System under clear and cloudy sky conditions.

In the scale model tests, the efficiency of each design reflects its design strategies.

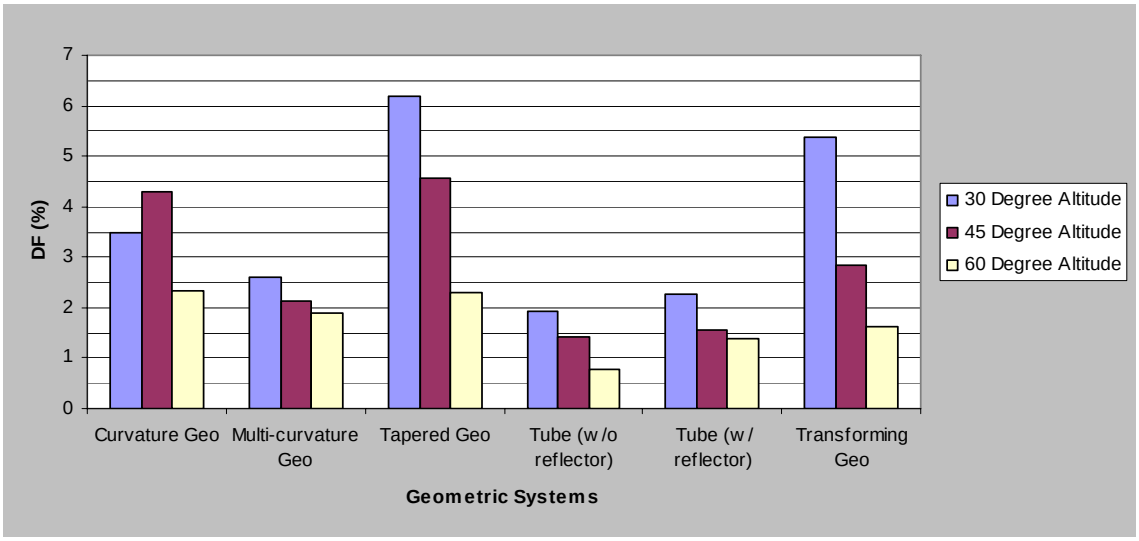

Figure 4.9: Scale model comparison of the average Daylight Factor at the lower sensor, under clear sky conditions

As shown in Figure 4.9, under a clear sky condition, the Tapered Geometric System performs the best overall, followed by the Transforming Geometric System, the Curvature Geometric System, and the Multi-Curvature Geometric System respectively. These scale model measurements are somewhat inconsistent with the full-scale results that suggest the best performer is the Multi-Curvature Geometric System. Accordingly, the author believes that under the same quality of workmanship, the performances will be consistent with those of the scale models.

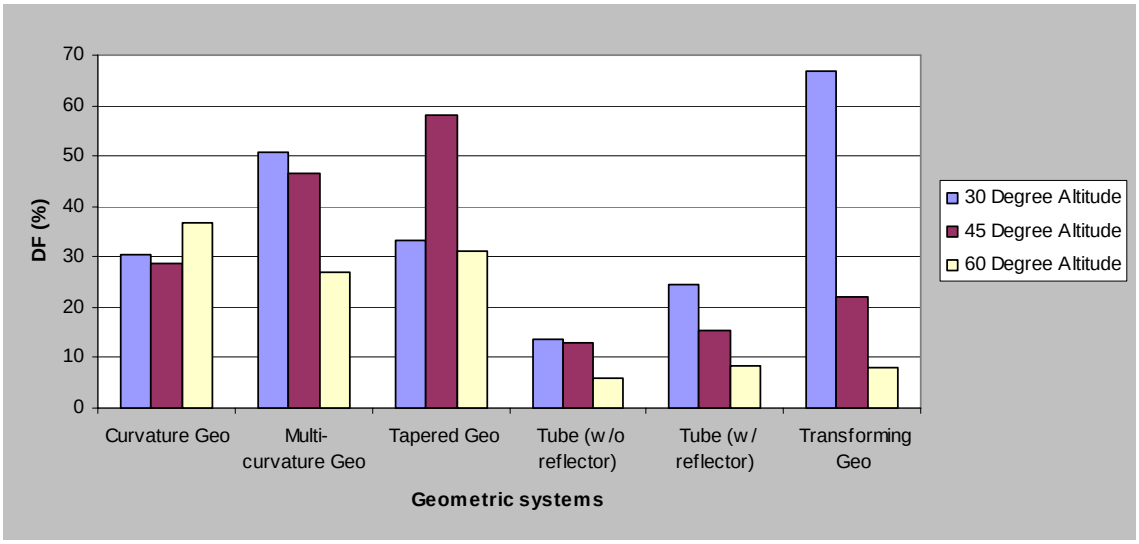

Figure 4.10: Scale model comparison of the average Daylight Factor at the upper sensor, under clear sky conditions

As shown in Figure 4.10, at the upper sensor, sensor 1 in the full-scale model, the Multi-Curvature Geometric System performs much better. It can be inferred that this system actually has a high efficiency with a wide angle illumination distributed to the lower space of the room when compared to the other systems. This causes a large amount of light incident on the upper sensor, but much lower amount of light incident on the lower sensor. For the tube geometric systems, the design with a back reflector also performs much better. The measurements from the upper sensor, not the lower sensor, are desirable to use for evaluating system efficacy because the measurements are taken immediately beneath the output source, the diffuser area.

In the next comparison, the louver design in the Tapered Geometric System is investigated. The seasonal louvers in this system are expected to increase the system efficiency when compared to the system without louvers. The Figure 4.11 shows the Daylight Factor comparison between the system with louvers and the system without louvers.

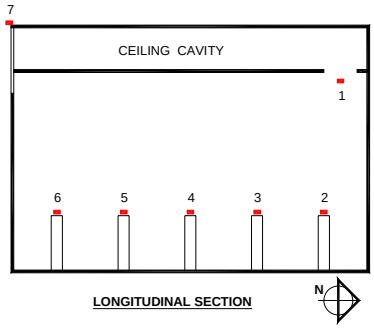

Sensor positioning

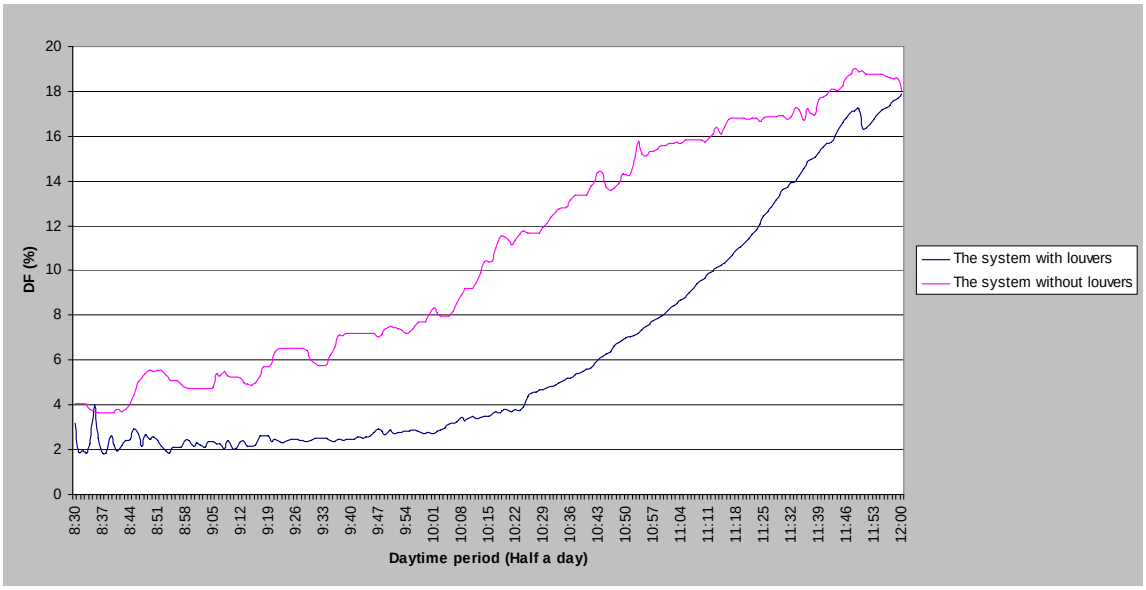

Figure 4.11: Daylight Factor comparison between Tapered Geometric Systems with and without louvers, at sensor 1

The results show a similar efficiency overall between the system with and without louvers. This means the louvers do little to improve the system performance. It was observed that because of the louvers concentration, the Daylight Factor acceleratory increases with the time.

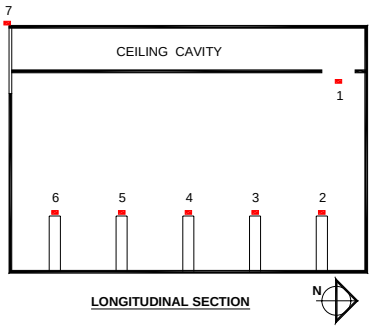

Sensor positioning

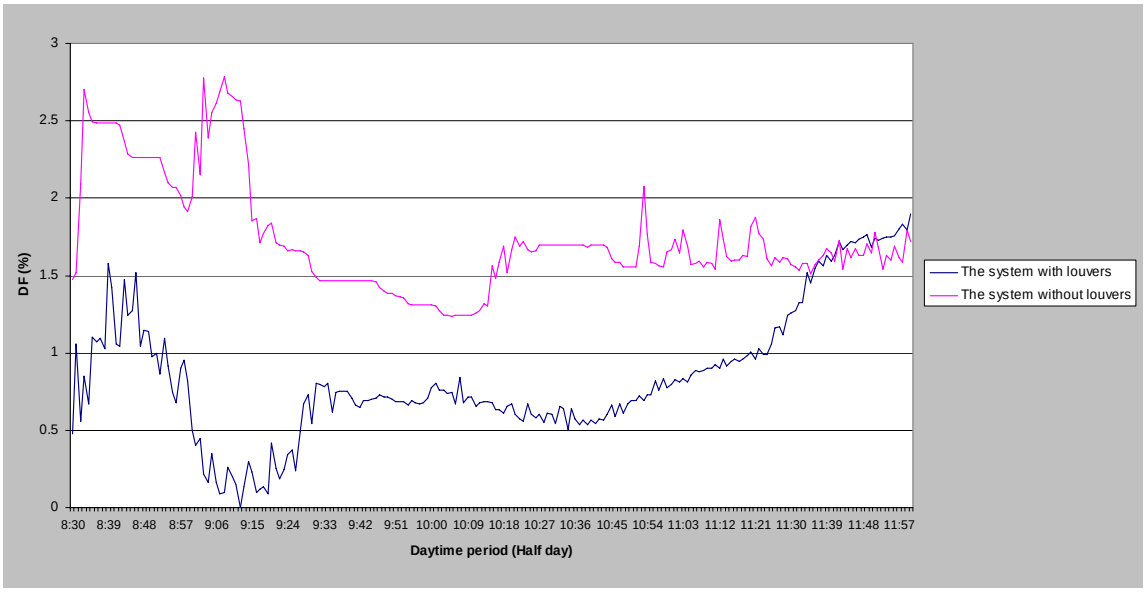

Figure 4.12: Daylight Factor comparison between Tapered Geometric Systems with and without louvers, at sensor 2

Figure 4.12 confirms that without louvers the Tapered Geometric System performs almost as well as without the louvers. The result also indicates that during the early day, the louvers themselves actually block some of the sun beams.

4.6 Chapter Conclusion

Out of the seven geometric prototypes, the best three were selected, based on the illumination level production, to be built for the full-scale testing. These prototypes are:

1. Curvature Geometric System
2. Tapered Geometric System
3. Multi-Curvature Geometric System

A set of comparisons were made to test the hypotheses. They are concluded as follows:

To test Hypothesis One, sample data of illumination levels from a scale model test was used to show that data measured in the scale model can approximate that for the full-scale performance. This was achieved by using simple sky-simulating equipment.

To test Hypothesis Two, the average Daylight Factor was used as a measure for comparison between scale and full-scale models at sensor 2 under clear sky conditions. The average Daylight factor distribution from a scale model test (the Multi-Curvature Geometric System) is proportional to, and with a similar pattern, to that of its full-scale at 100times over-scale. This shows that the scale model tests can approximate their own full-scale experimental results, under the same quality of workmanship with a multiplier of x100.

To test Hypothesis Three, the average Daylight Factors measured from sensors at the workplane (Sensor 2-6) were used for comparison among the three selected prototypes. The direct sun penetration received from the high window was factored out in the Multi-Curvature Geometric System to reveal the system efficiency. The results prove the Multi-Curvature Geometric System performed best.

The Multi-Curvature was used to test the comparisons:

- Average Daylight Factor for full-scale systems under clear sky conditions.
- Daylight distribution between the window-only daylighting and the window with a transporting system.
- Daylight Factor comparison between 3ft. high window and 1ft. high window+ a transporting system, at sensor 2.
- Daylight Factor comparison among three full-scale prototypes at sensor 1.
- The illumination level at each sensor for partly cloudy conditions.

The Scale model systems were used to test the comparisons:

- Scale model comparison of the average Daylight Factor at the lower sensor, under clear sky condition.
- Scale model comparison of the average Daylight Factor at the upper sensor, under clear sky condition.

The other tests are investigated by using the Tapered Geometric System. Those are:

- Daylight Factor comparison from sensors at the workplane (Sensor 2-6) between the system under clear and cloudy sky conditions.
- Daylight Factor comparison between the system with and without louvers, at sensor 1.
- Daylight Factor comparison between the system with and without louvers, at sensor 2.

Chapter 5. Conclusions and Discussion

5.1 Scale Models Performances:

Considered as a standard, each geometric system has a potential average Daylight Factor of 300% (net average DF). This scale derives from the sum of the potential average Daylight Factor productions at solar altitude angles of 30, 45, and 60 degrees (100%+100%+100% = 300%). The system efficiency and system effectiveness in the following were evaluated based on this scale. The system efficiency was evaluated from the upper sensor measurements and the system effectiveness was evaluated from the lower sensor measurements.

5.1.1 System Efficiency

As shown by the Figure 5.1, the average Daylight Factors calculated for the upper sensor measurements, under a clear sky condition, the Multi-Curvature Geometric System produces the highest Daylight Factor overall with the net average DF of 125%, followed by the Tapered Geometric System (net average DF of 122.5%), Transforming Geometric System (net average DF of 97.5%), and Curvature Geometric System (net average DF of 95.5%). In terms of the effect on seasonal altitudes, the Tube Geometric System without a reflector performs the worst overall (net average DF of 33%). At 30-degree altitude, the Transforming Geometric System performs the best with an average DF of 67.5%. At 45-degree altitude, the Tapered Geometric System performs the best with an average DF of 58%. Finally, at 60-degree altitude, the Curvature Geometric System performs the best with an average DF of 37%.

The diagram in Figure 5.1 exhibits the net efficiency of each system. Therefore this diagram does not reflect the effect of the design for each system. The effect of designs on system efficiency can be observed in the system efficiency diagrams shown in the Appendix chapter (page 90-93). These diagrams show illuminance produced from each system progressive toward the peak of a day.

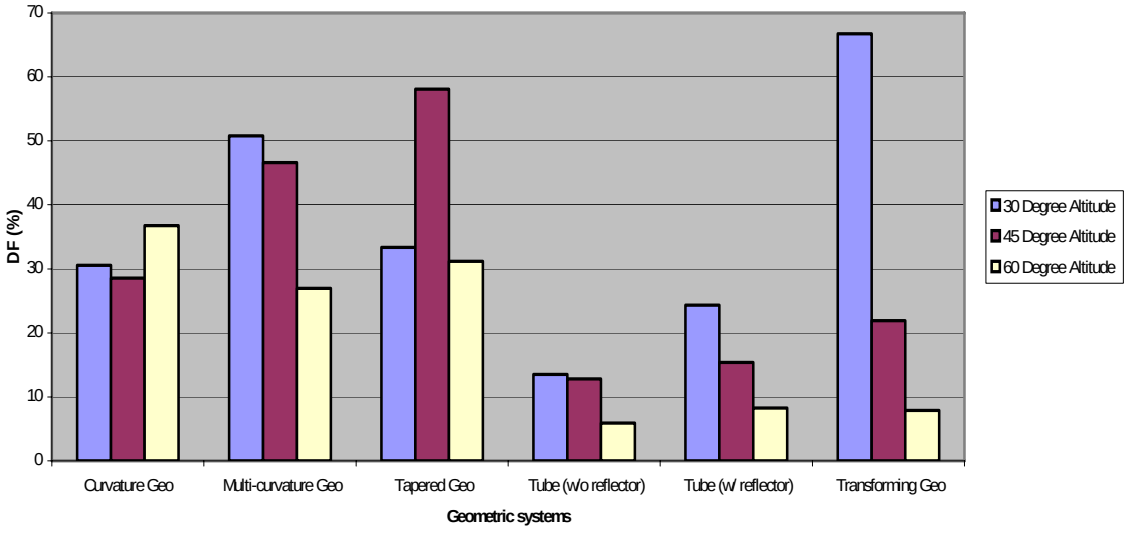

Figure 5.1: Average Daylight Factor comparison among scale model systems measured from the upper sensor under clear sky conditions

5.1.2 System Effectiveness

As shown by the Figure 5.2, the average Daylight Factor calculated for the lower sensor measurements at the workplane level, under a clear sky condition, the Tapered Geometric System produces the highest Daylight Factor overall with the net average DF of 12.8%, followed by the Curvature Geometric System (net average DF of 10.15%), the Transforming Geometric System (net average DF of 9.75%), and the Multi-Curvature Geometric System (net average DF of 6.6%). In terms of the effect of seasonal altitudes, the Tube Geometric System without a reflector performs the worst overall. At solar altitude angles of 30-degree and 45-degree altitude, the Tapered Geometric System performs the best with average DF of 6.2% and 4.55% respectively. At 60-degree solar altitude, the Curvature Geometric System performs the best with an average DF of 2.35%. The effect of designs on system effectiveness can also be observed in the system efficiency diagrams shown in the Appendix chapter (page 90-93).

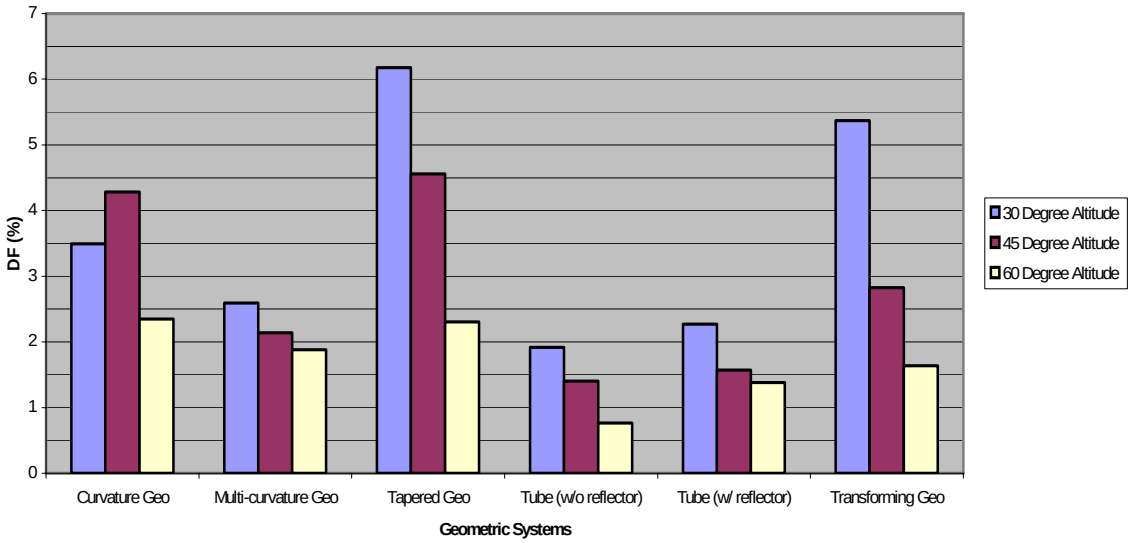

Figure 5.2: Average Daylight Factor comparison among scale model systems measured from the lower sensor under clear sky conditions

5.2 Full-Scale Performances:

The system efficiency in the following was also evaluated based on the same scale system as that of the scale models performance. The system efficiency was evaluated from the sensor 1 measurements analog to the upper sensor in the scale models.

5.2.1 System Efficiency

For a partly cloudy sky day, the Multi-Curvature Geometric System generates the highest atmospheric illumination (average DF of 28.23%) at the rear part of the room. Therefore this system is most efficient overall, followed by the Curvature and then the Tapered Geometric System. However, in terms of investment, the Tapered Geometric System is more desirable since it is inexpensive and simple to construct after eliminating the louver element (*See Figure 5.3*).

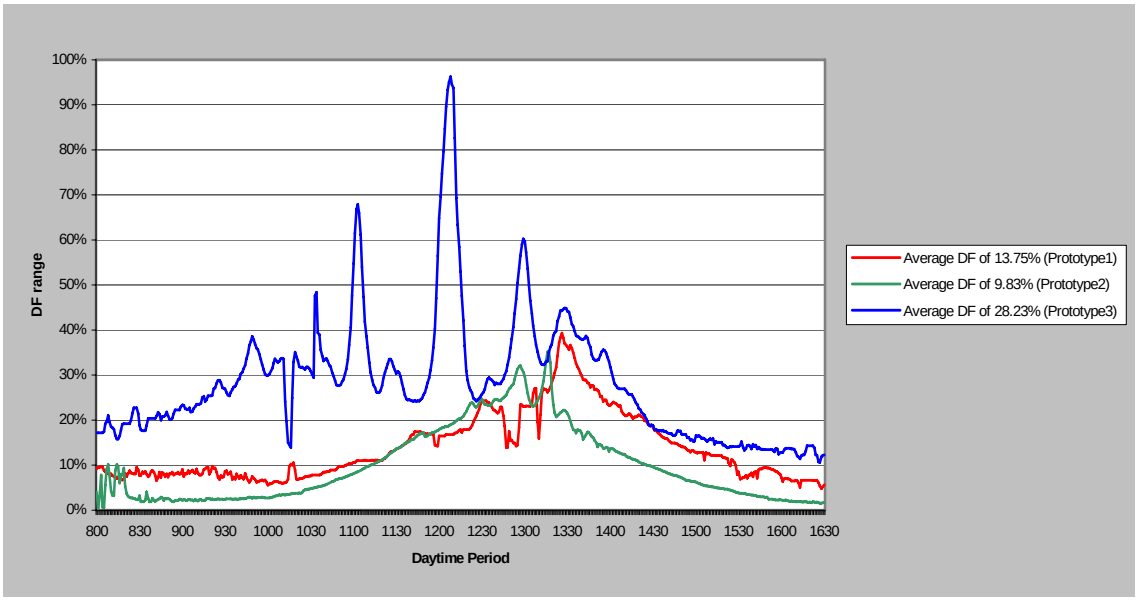

Figure 5.3: Daylight Factor comparison among the three full-scale geometric systems, Curvature (prototype 1), Tapered (prototype 2), and Multi-Curvature (prototype 3) under a partly cloudy sky condition from sensor 1.

5.3 Discussion

State of Imperfection

Due to some technical problems during the data logger programming, the channel 7 of the data logger measuring outside illumination (for the sensor 7) could not display the value beyond 6999 fc. (during the peak daylight hours). As a result, those missing values were estimated by using the precedent Daylight Factor relationship of sensor 1 to sensor 7, and statistics reference of *"Exterior Horizontal Illumination Table"* to find the peak of such days. This could result in some inaccuracy in the analysis.

Techniques used to optimize system performance

Several design techniques can be employed to optimize various performance characteristics of the light tube such as transmitted heat, light output, and reduction of glare.

To minimize the effect of heat gain into the room, the inlet opening area needs to be small and it is preferred to have low-emission glazing.

The use of two types of reflective materials offers a method of controlling the path of the light beam. A prismatic material turns deflected oblique rays to be parallel to the tube, eliminating side reflections; while a specular material employs the theory of reflection to focus the rays, reducing the need for costly reflective surfaces. The key to achieving a high illumination level at the rear space is to control the rays' striking angles; the more perpendicular the rays to the diffuser plane, the greater penetration they get. This supports the idea of focusing and deflecting rays as the characteristic of the proposed daylight systems.

The smoothness of reflective surface is a matter in that it determines the amount of light lost in the travel path, according to a statement from the literature review "Method for Estimating the Efficiency of Prism Light Guide Luminaires" (p.24). Spray gluing the top reflective film is not the way to achieve perfectly smooth surface because a potential of uneven glue distribution creates undesirable wrinkleness and the susceptibility to moisture and heat at the task

environment. To reduce wrinkles on the reflective surface, it is recommended the reflective surface be self-adhesive, rigid, and flexible; otherwise, being silver-coated.

Glare passing through the one foot tall window opening was observed at a certain range of sun path. To eliminate this glare, the window needs to have an internal light shelf integrated; otherwise, be diffusive or translucent.

Prototypes in Practical Use

A number of points need to be considered for the designs to be used effectively in a real building project.

Due to the ever-changing sky conditions, the fluctuating light levels produced from a system need to be made uniform by using a dimming system integration at the output area. To avoid a difficulty of space sharing with ductwork in the room ceiling, the conduits must be located beneath the floor. When no obstructions are present, the width of the systems can be arbitrary; allowing us to maximize the light output efficiency by reducing the proportional amount of oblique rays. In this case, the curvature geometric system is recommended. With obstructions, the tapered geometric system is preferable, due to its smaller space occupancy.

All prototypes were designed to work with a specific ceiling cavity dimensions of 4 ft. in width, 16 ft. in length, and 2 ft. in depth. This depth yields a slight gain of energy saving for the system, but is too large to be invested in a high rise office building due to its expensive space occupying units. Meanwhile, reducing the height of a system in half would reduce its performance and ability to transport daylight as well, with the same geometric configuration. The author found that the concept of geometric optimization for a certain range of solar azimuth degrees is more difficult to achieve as the depth of the system is less. Therefore, when designing a system where sufficient depth is too expensive, it is better to use beam sunlighting by heliostat and light pipes. This system consists of mirrors and light tubes. The system efficiency relies on the reflective surfaces quality and on the ability of reflective planes to collimate light beams*(See Figure 5.4)*.

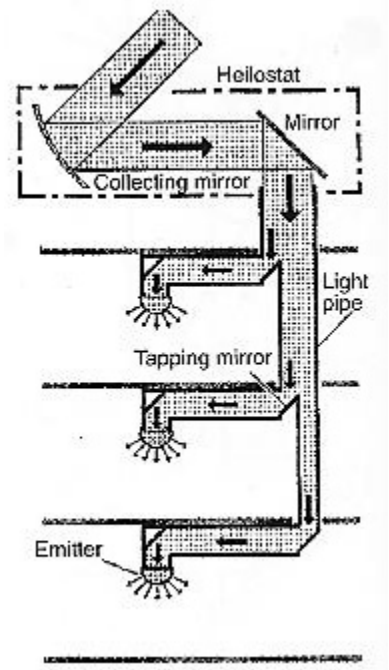

Figure 5.4: Beam Sunlighting by heliostat and light pipes (Szokolay and Steven, 2004)

Appendix

Physics of Light:

Light is defined as radiant energy that activates the eye's receptors to perceive dimension and color brought together in vision. Light is considered a wave phenomenon because it has a frequency (f, in Hz) and a wavelength (λ, in m). The product of these two gives its velocity (C), which equals roughly 3 x 10^8 m/s

$$C = f \times \lambda \quad (7)$$

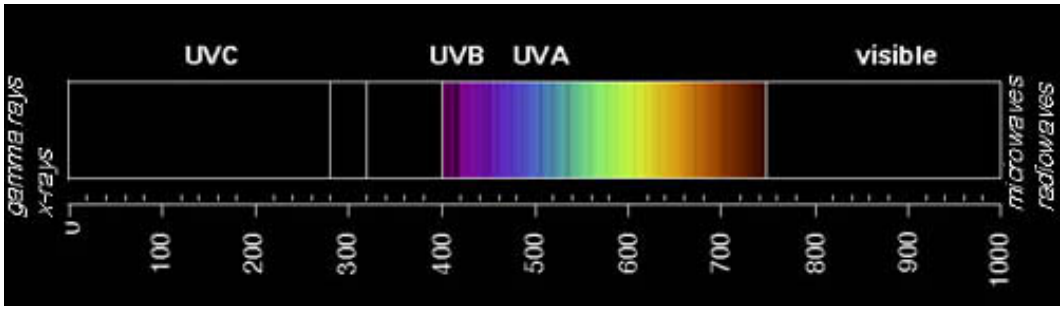

Figure A1: Electromagnetic Spectrum showing the range of visible light whose wavelength lies between 380-780 Nanometers (http://www.accessexcellence.org/BF/bf05/rothschild/roths_imgs/SlideWin15.html)

Human eyes have a limitation on light perception. Light is visible within a range of a wavelength between 380 nm and 780 nm. The wavelength determines the light color which, in the visible spectrum, ranges from red (the longest wavelength light), followed by orange, yellow, green, blue, indigo, and violet (the shortest wavelength light). Beyond this visible spectrum is infrared at the long wavelength and ultra-violet at the short wavelength. If the light source releases energy approximately in equal quantities over the entire visible spectrum, the light will appear "white." Note that when mentioning daylight, its color will be considered "white." (*See Figure A1)*

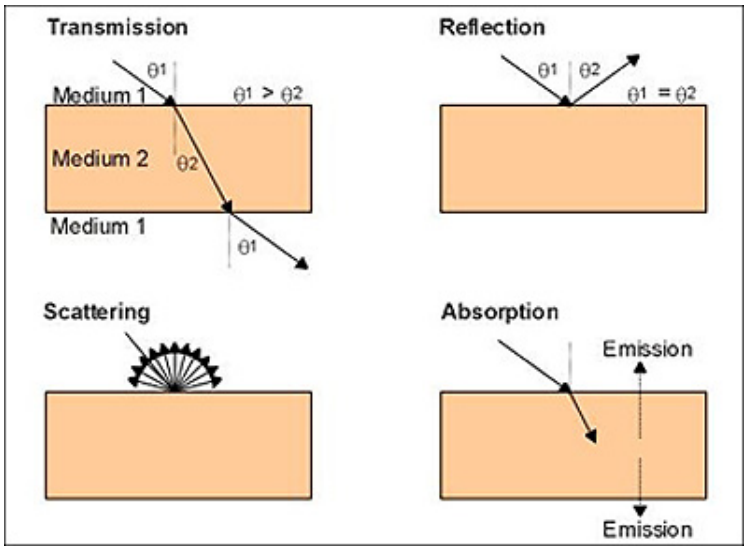

Figure A2: A diagram showing characteristics of light when striking on a surface with a different property (http://www.tpub.com/content/aerographer/14312/css/14312_151.htm)

Light Characteristics

Light has some defining characteristics that make it possible for a lighting designer to control. Those characteristics are reflectance (reflectance coefficient) and transmittance (coefficient of transmission).

Reflectance is the ratio of the total reflected light to the total incident light. This property takes place on any glossy material. The perfect sample would be a silver-coated mirror which displays reflectance close to 100%. There are two types of reflection. The first is referred to as specular reflection which occurs on any smooth surface such as polished marble or glass. The other is referred to as diffuse reflection which occurs on rough surfaces or surfaces with texture (*See Figure A2).*

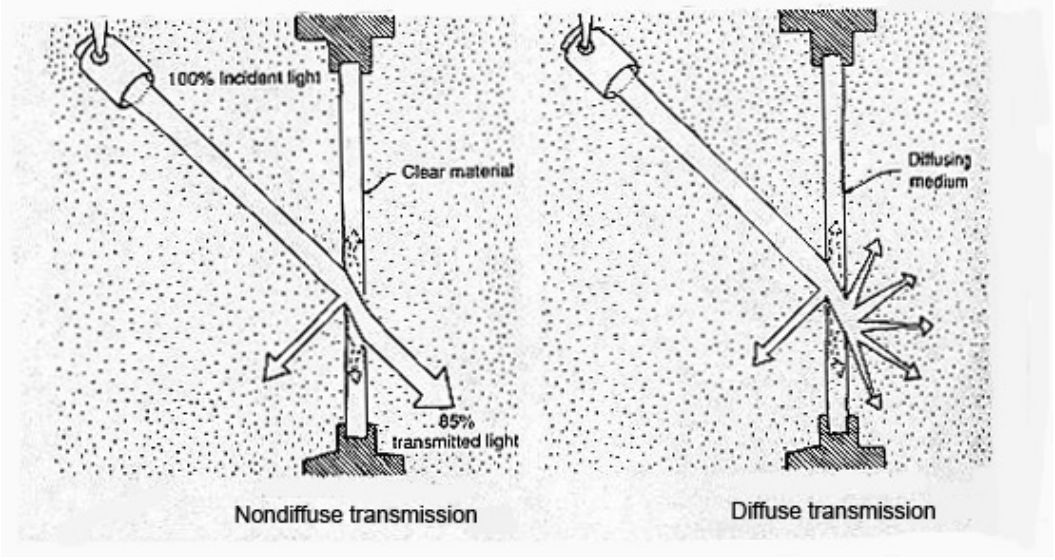

Figure A3: Transmission characteristics (Stein and Reynolds, 2000)

Transmittance is the ratio of the total transmitted light to the total incident light. This property takes place on any material that has a certain degree of transparency, not being completely opaque. A material displaying transmittance at 80% means that 80% of incident light is passing through that material. The remaining 20% can be either reflected or absorbed, or both. There are two types of transmission. Diffuse transmission is demonstrated by translucent materials. Non-diffuse transmission is demonstrated by clear materials (*See Figure A3).*

Note that the amount of absorption depends not only on the type of material itself but also on the angle of light incident. The higher the angle of incidence, the more likely the light is reflected rather than absorbed or transmitted (*See Figure A4).*

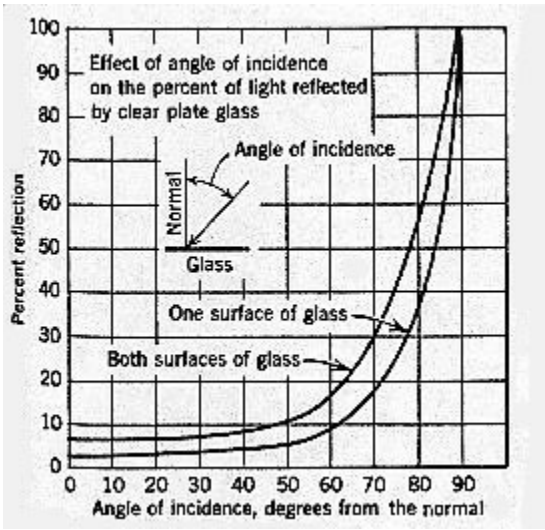

Figure A4: Relation between angle of incidence and percentage reflectance (Stein and Reynolds, 2000)

Photometric Qualities

Luminous intensity (I) is a characteristic of a light source. It represents a force from electromagnetic radiation that generates the light, analogous to pressure in a hydraulic system. A metaphor of this force is a lit single wax candle. The luminous intensity from a wax candle equals to one candela (cd), in SI/Metric units; or one candlepower (cp) in AS units.

Luminous Flux (Φ) is the amount of luminous energy on a spherical surface area of one square meter (one square foot, in AS). The definition exists under the condition that a point source of one candela emanates one meter (foot) radius of luminous intensity equally around the point, creating a spherical force. Its unit is called a "lumen" (lm), for both SI and AS units. Because such a sphere has a surface area of 4¶ square meters (or 4¶ square feet), a 1 cd light source produces 4¶ lumens in total.

Illuminance (E) is a light level of a surface. Illuminance can be described as the density of luminous power (lumens per unit area) or as the amount of uniform luminous flux measured on a unit area. Its unit is, therefore, lm/m^2 or lux in SI units; lm/f^2 or footcandle in AS units. 1 footcandle is produced from 1 lumen distributed over 1 sq.ft. Illuminance varies inversely with the square of the distance from the source (*See Figure 18.15).* Since a difference in scale is from a different unit, here is the relationship.

$$10.764\ (\sim 10)\ \text{lux} = 1\ \text{footcandle} \qquad (8)$$

Luminance (L) is the brightness of a surface measured perpendicularly against a plane surface at an immediate distance away. Luminance is technically the product of illuminance and reflectance. Its unit is luminous intensity per unit area, cd/m^2 (SI) or footlambert (AS).

$$\text{In SI units:} \quad L\ (cd/m^2) = \frac{E\ (\text{lux}) \times RF}{¶} \qquad (9)$$

$$\text{In AS units:} \quad fL = fc \times RF \qquad (10)$$

Where L = luminance, E = illuminance, RF = reflection factor,
fL = luminance in footlambert, fc = luminance in footcandle

Elements in Visual Quality

There are three main variables that determine how accurately a seeing task is being viewed. Each of them has a certain degree of influence on one another.

1. *The Task (visual object)*

1.1 Size

The size of a visual object is actually not the parameter in task acuity because there is no increase in detailed perception with increasing the size of an object. Instead, detailed perception can be increased by bringing the object closer to the eyes. That is the subtended visual angle which is proportional to visibility. Subtended angle is the angle from the eye's center to the size of a seen object (*See Figure A5).*

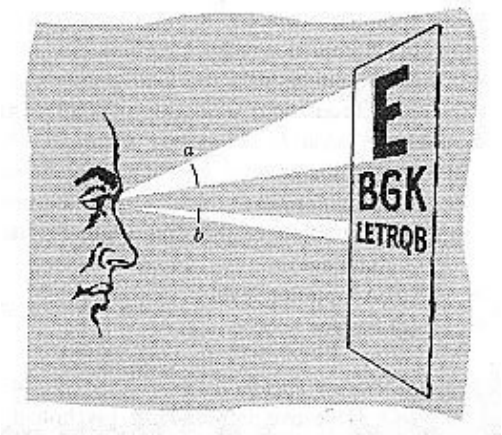

Figure A5: Relationship between object size and visibility
is demonstrated by comparison of subtended angles (a) and (b). (Stein and Reynolds, 2000)

1.2 Brightness

The individual rays that are reflected from a seen object back to the eyes carry different visual information. Such information depends on which part of the object was reflected to the eyes, each of which has a difference in chromaticity and intensity; chromaticity is a quality of a color as determined by its "purity", saturation, and dominant wavelength, according to http://encyclopedia.laborlawtalk.com/chromaticity on June 12, 2005. The intensity of light determines the perceived brightness of the object being viewed. Human eyes detect luminance over a range of 100 million to 1. The lower levels are achieved after a dark adaptation period which takes 2 - 40 minutes. Table A1 shows luminance values for routine visual tasks.

Table A1: Typical Luminance Values (Stein and Reynolds, 2000) p.1069

Object	Luminance	
	Cd/m^2	Footlamberts
Black glove on cloudy night	0.0003	0.0001
Wall brightness in a well-lighted office	100	30
A sheet of paper in an office	120	35
Green electroluminescent lam	150	45
Asphalt paving –overcast day	1,300	380
North sky	3,500	1,000

Moon, candle flame	4,000-5,000	1,300
Fluorescent tube	6,000-8,000	2,200
Kerosene flame	8,500	2,500
Hazy sky or fog	15,000	4,400
Snow in sunlight	25,000	7,300
100-W inside frost incandescent lamp	50,000	14,600
Sun	2.3 E9	0.67 E9

1.3 Contrast and Adaptation

Under "white" light condition, contrast has been recognized as the most influential variable in visual acuity. The eyes use contrast to separate the shapes and details of objects. The degree of contrast is proportional to the difference between luminance of an object and that of its immediate surroundings. Low contrast means there is a small difference between luminance of picture (object) and luminance of background (surroundings). Contrast is expressed as

$$C = \frac{L_T - L_B}{L_B} \quad \text{or} \quad \frac{L_B - L_T}{L_B} \quad \text{or} \quad \left| \frac{L_B - L_T}{L_B} \right| \tag{11}$$

Contrast can also be expressed as

$$C = \left| \frac{R_B - R_T}{R_B} \right| \tag{12}$$

Where L_T and L_B = Luminance of the task and background, respectively

R_T and R_B = Reflectance of the task and background, respectively

C = Contrast (varies from 0 – 10)

1.3 Exposure Time

A visual image requires a certain amount of exposure time when being viewed. Time needed depends on the type of visual task and the other variables that were mentioned previously. Basically, the higher the illumination levels, the shorter time required, incrementally with objects in motion.

2. <u>The Lighting Condition</u>

Lighting condition can be discussed under its two components which designate the condition. Those are quantity and quality of light.

2.1 Quantity of Light

Quantity of light refers to the illumination level. Before 1981, it was very difficult to come up with an exact illumination level needed for a specific visual task. This was the case because each country had a different recommendation level for their specific visual task description, varying as much as a ratio of 1 to 10. There existed no universal standard for all the countries to mutually employ. Recently, American IESNA (Illuminating Engineering Society of North American) recommendations have been modified to establish an average requirement for a task at a given range. IESNA has also rationalized its very influential illumination standards. They include a consideration of task familiarity and fatigue as additional factors in determining illumination levels, as well as lighting power budgets and energy standards, which encourage use of daylight for interior space illumination. Since, as previously stated, luminance is the product of illuminance and reflectance, this relationship can derive a required illuminance from a given

luminance and reflectance value. The visual task studies states that under a condition of good contrast the required luminances for various tasks are as follows:

Table A2: Assuming good contrast, the required luminance, categorized by type of task (Stein and Reynolds, 2000) p.1007

Category of Visual Task	Required Luminance (cd/m^2)
Casual	10 – 20
Ordinary	20 – 100
Moderate	100 – 200
Difficult	200 – 400
Severe	Above 200

And required illuminations on task reflectance (RF) are the following:

Table A3: The illumination requirements in the previous categories for tasks of radically different reflectance. (Stein and Reynolds, 2000) p.1007

Category of Visual Task	Required Illumination (lux)	
	RF = 50%	RF = 10%
Casual	62 – 125	300 – 625
Ordinary	125 – 625	625 – 3,125
Moderate	625 – 1,250	3,125 – 6,250
Difficult	1,250 – 2,500	6,250 – 12,500
Severe	>2,500	>12,500

2.2 Quality of Light

This term deals with psychological perception toward appreciation for lighting design atmosphere in a space. Rooms with the same average illumination level can have a significant difference in visual comfort, depending on the design of light installation. The quality of lighting can be described by its luminances, uniformity, diffusion, and chromaticity.

2.2.1 Disabled Glare is the excessive luminance with a field of vision. If light comes directly from the source, it will be called "direct glare" (discomfort glare). If it comes from a reflection, it will be called "reflected glare" (veiling reflection).

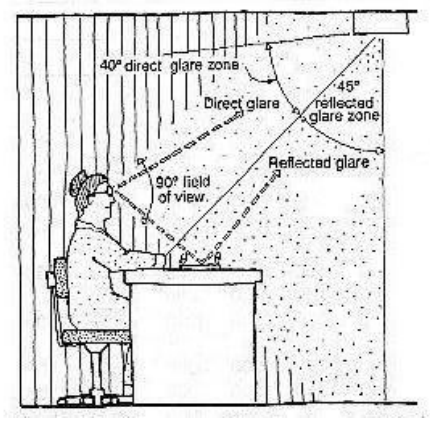

Figure A6: Glare zones. The direct and reflected glare light paths are delineated on the diagram (Stein and Reynolds, 2000)

- *Direct glare* relates to the size, position, and luminance of the light source, as well as the level of eye adaptation. In principle, the eye adapts to an average light level in the scene, followed by the adaptation to details of highly-sparkle brightness in that scene. At the latter adaptation, if we are looking at a task put in the low brightness area, the eye system will be confused, and we will experience visual disturbance caused by the successive fluctuation of eye adaptation (between two different brightnesses), which sooner or later causes eye tensions (*See Figure A6).*

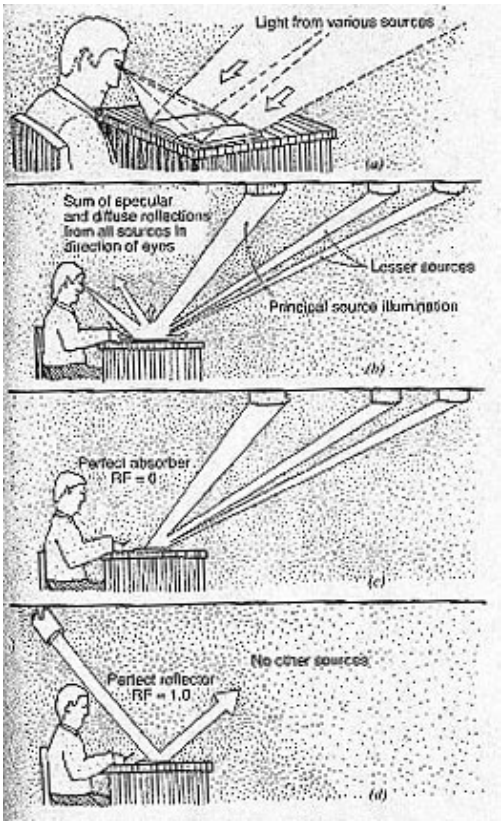

Figure A7: A demonstration of reflected glare from different sources and viewing angles

(a) The nature of the seeing process requires that light from the source(s) be reflected by the task into the eye.
(b) The light entering the eye is the sum of all of the reflected light, specular and diffuse, from all sources, in the direction of the eye. If the task is specular, all of the sources will be seen reflected in the task.
(c) A perfectly absorptive object is jet black because it reflects nothing.
(d) A perfectly reflective object positioned as shown is also black because geometrically it cannot reflect light into the eyes.

- *Reflected glare* is a much more complicated problem because it deals not only with the source, but also with the task and the viewing angle of an observer. The veiling reflection is caused by the mirroring of a source in the task, which is proportional to source luminance, task surface specularity, and object surface diffuseness (*See Figure A7).*

Table A4: Recommended Maximum Luminance Ratios (Stein and Reynolds, 2000) p.1098

1 to one third	Between task and adjacent surroundings
1 to one tenth	Between task and more remote darker surfaces
1 to 10	Between task and more remote lighter surfaces
20 to 1	Between luminaries (or fenestration) and surfaces adjacent to them
40 to 1	Anywhere within the normal field of view

2.3 Luminance Ratio

Luminance Ratio is the difference between a viewed object's luminance and that of immediate surroundings. Like the effect of contrast, luminance ratios can improve the visual ability if they stay in an acceptable proportion. The preferred luminance ratio would be task: surround: background = 1: 0.5: 0.2. Recommendations of maximum luminance ratios for seeing comfort is displayed in Table A4

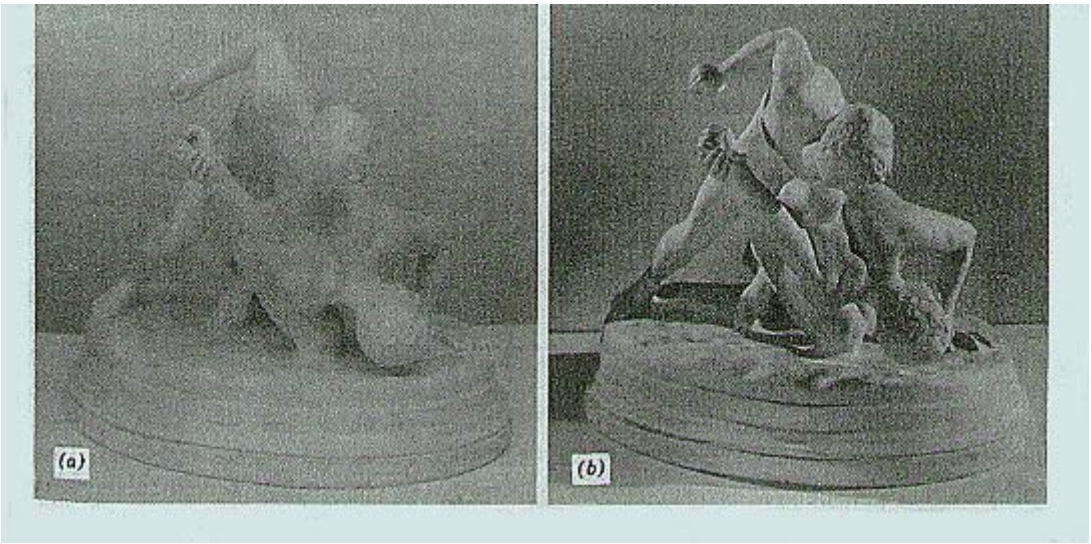

Figure A8: The dimensional effect on an object with total diffuse lighting (a) and that with diffuse and directional lightings (b)
Totally diffuse lighting (a) destroys texture, whereas a combination of diffuse and directional lighting (b) produces the required modeling shadows. (Courtesy of Holophane.), (Stein and Reynolds, 2000)

2.4 Brightness Pattern

Brightness pattern, or pattern of luminances, is the combination of diffuse and directional lighting in the visual field, or in the visual object, that can optimize the visual performance by adding visual interest into the seen object. Directional light reveals the object dimension by creating shade and shadow on the object, thereby maximizing its detail perception. Diffuse light reveals the dimensional relation between the visual task (object being viewed) and its remote surroundings (*See Figure A8).*

Daylighting:

As a necessity to maximize energy conservation, a renewable source, sunlight, is utilized as the most plentiful and magnificent outdoor light source for space illumination in the buildings, supplemented by artificial lights. However, its inherent impact of heat gain and excessive luminance, as well as its variation, are of concern.

The term “daylight”, technically, means only sunlight diffused by particles and clouds in the sky. Daylight has been considered the most desirable light form due to its unique characteristics of continually changing patterns, advantageous for dynamic play on illuminating designed spaces, as well as its excellent efficacy (Its light content as an output is very high compared to the sacrificing heat content as an analogous input represented as Efficacy = Light Output/Energy Input). Such public buildings as museums, schools, and offices are occupied during daylight hours. Therefore, daylight integration becomes ideally beneficial for such buildings. Because the potential of creating glare is overwhelming, providing daylight into an interior must be indirect and controlled.

Daylighting can both lower energy consumption and provide a psychological connection to the outdoors. ASHRAE STANDARD 90, the standard of energy efficient design of nonresidential buildings, allows credit to be taken for daylight utilization. THE LEED RATING SYSTEM by the U.S. Green Building Council also considers the benefits of daylighting.

Exterior Illumination factors

Daylight used to illuminate interior visual tasks varies temporally. There are three factors that determine exterior illumination level availability at a specific area and time:

1. Solar altitude
2. Sky condition
3. Existence of obstructions and their properties

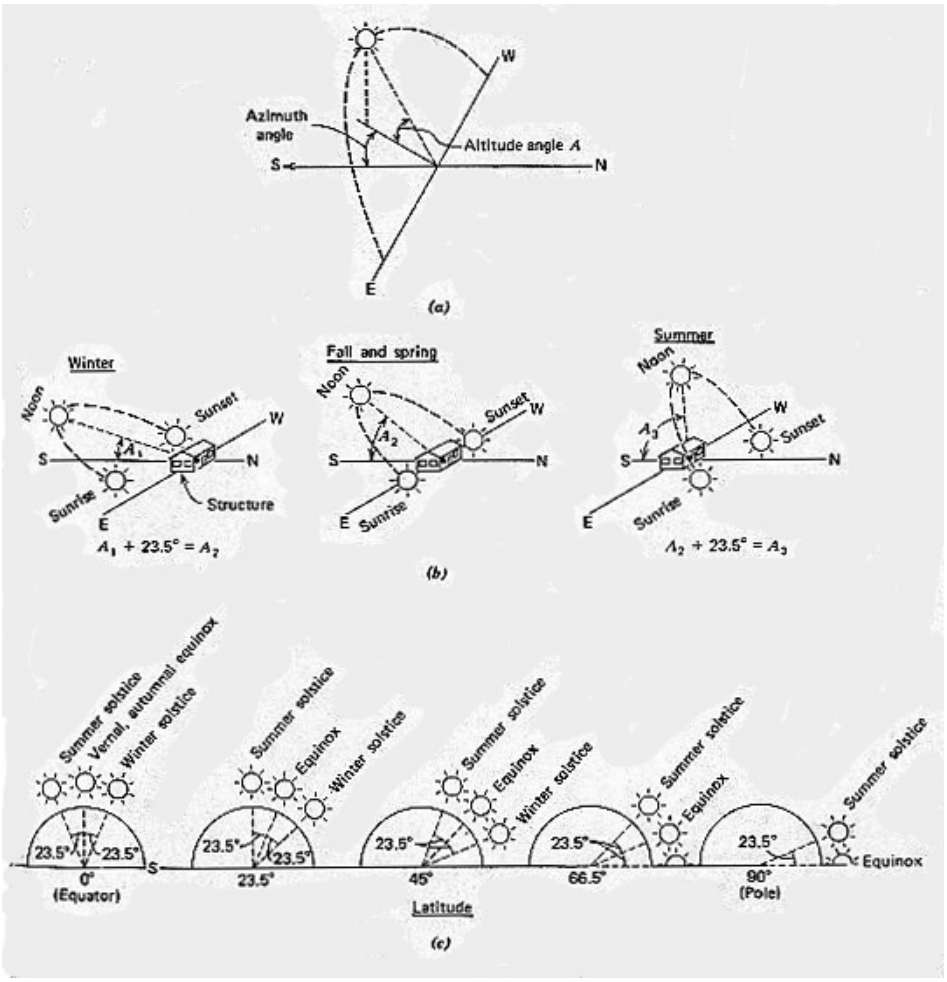

Figure A9: A diagram of the sun positions yearly at various latitudes

(a) The position of the sun is expressed in terms of vertical angle above the horizon (altitude) and horizontal angle (azimuth), measured from the south.
(b) Approximate position of the sun in each of the seasons, at a mid-northern latitude (approximatedly 45º)
(c) Maximum sun altitude at various latitudes for both solstices and equinoxes. Maximum summer sun altitude is 90º minus latitude minus 23.5º. Thus, for all latitudes the yearly difference between maximum and minimum altitudes is twice 23.5º, or 47º, as shown. (Stein and Reynolds, 2000)

1. Solar Altitude:

The position of the sun in the sky hemisphere is detected by measuring interrelated two angles, expressed in degrees. One is the vertical position angle, "altitude", which is the vertical angle measured above the horizontal plane. Another is the horizontal position angle, "azimuth", which is the horizontal angle measured from due south. For all latitudes, the sun's altitude angle is minimum in winter, maximum in summer, and in between in fall and spring. As a location approaches the pole (either north or south), the sun's daily maximum altitude decreases (*See Figure A9*).

2. Sky Condition:

The sky conditions can be categorized below.

- Solid overcast sky (CIE sky)
- Clear sky, without sun
- Clear sky, with sun
- Partly cloudy sky

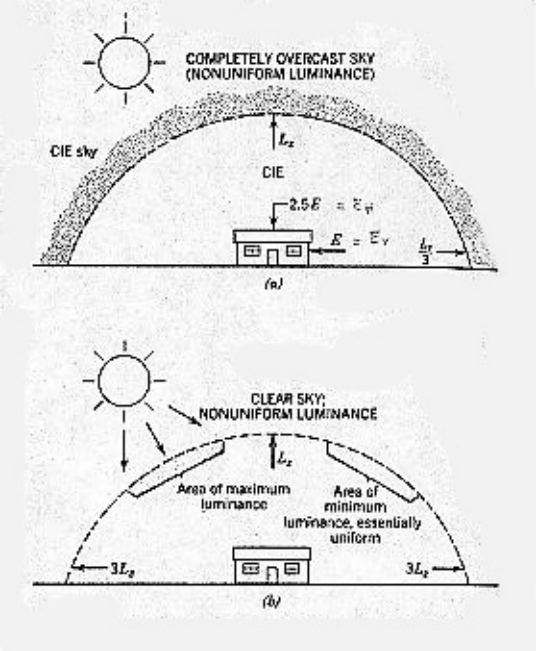

Figure A10: A diagram showing the relationship between zenith and horizon luminance according to the CIE and clear sky formulation

(a) The completely overcast sky has a zenith luminance L_Z , which is three times the horizon Luminance, according to the CIE formulation. With such as sky, illumination on unobstructed exterior horizontal surfaces (E_H) is about 2 ½ times that on a similar vertical surface (E_V).

(b) One widely accepted formulation for clear sky luminance is simply an inversion of the overcast distribution (a); horizon luminance is three times that of the zenith. Obviously, the area around the sun is brightest. The area opposite the sun is darkest and can be considered as essentially uniform at approximately 3500 cd/m^2 (1000 fL). Actual luminance varies arom about 1000 cd/m^2 (300 fL) at the center to 7000 cd/m^2 (2000 fL) at the sides, averaging 3500 cd/m^2 (1000 fL) over the whole area. (Stein and Reynolds, 2000) p.1114

CIE Sky is the standard sky condition for daylight calculations which is defined as a non-uniform brightness distribution sky whose brightness increases from horizon to zenith in approximately the ratio of 1:3 (*See Figure A10).* At any altitude angle, sky luminance is defined as

$$L_A = L_Z \left(\frac{1+2\sin A}{3}\right) \qquad (13)$$

Where L_A = luminance at A˚ above horizon
L_Z = luminance at zenith

Under the distribution, the illuminance (lux) on an unobstructed exterior horizontal to that on vertical surfaces is approximately 2.5:1

Exterior horizontal illumination on a cloudy sky consists of two components which are diffuse illumination from the entire sky and direct sunlight. Regardless of azimuth, with an overcast sky, exterior horizontal illuminance varies directly with the sun's altitude, based on the following formula:

$$E_H = 300 + 21{,}000\sin A \text{ (lux)} \qquad (14)$$

Where E_H = exterior horizontal illuminance
A = the solar altitude, in degrees

Clear Sky is defined as uniform brightness distribution sky. An illuminance of 100,000 lux can be given under clear sky conditions with sun, and 40,000-50,000 lux diffuse illuminance without sun. This varies by climate.

Exterior horizontal illumination on a clear sky, like the previous condition, is the combination of diffuse illumination from the entire sky and direct sunlight. Figure 19.6 shows *sky only* values as a function of solar altitude. The values are used to determine shaded skylight illumination or a north-facing window, based on an unobstructed horizontal exterior surface. However, these values have to be, to some degree, reduced, as a building window is partially obstructed by the building itself.

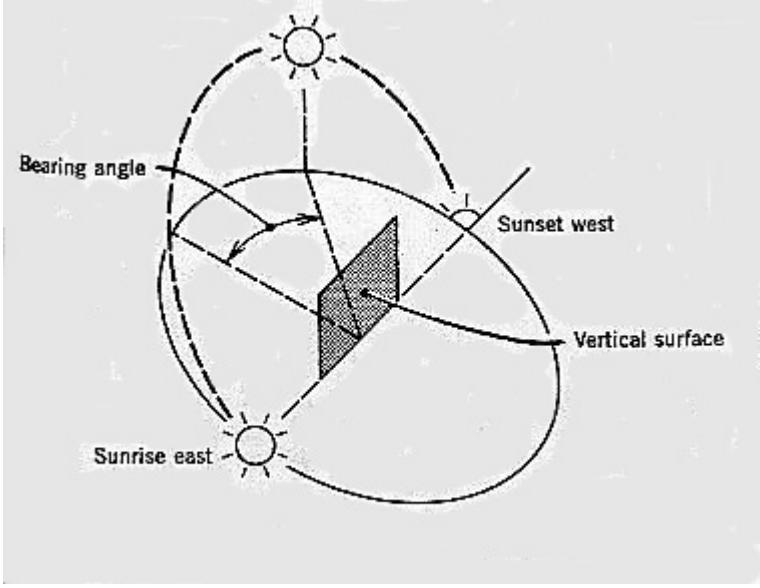

Figure A11: Diagram showing the geometry of a vertical surface in relation to the sun position. The angle between a vertical plane perpendicular to the vertical surface (window) and a vertical plane containing the sun is defined as the bearing angle. (Stein and Reynolds, 2000)

Vertical surface illumination on a clear sky depends on altitude and solar azimuth (more specifically, the bearing angle; window-to-sun azimuth). The *sky only* values are the maximum of the half-sky illumination since a vertical surface can be exposed to only half of the entire sky (*See Figure A11).*

Partly cloudy Sky is used when the illumination from a partly cloudy sky is 10% to 15% higher than that from a clear sky due to the extra reflection from cloud edges.

3. Existence of obstructions and their properties:

The components of terrain also affect the amount of daylight penetration into a building. The existence of trees, rocks, and other man-made objects on the ground obstruct, absorb, and distort daylight rays, into multiple directions, caused by reflection properties and textures on each object *(See Figure A12).*

Daylight Factor

Studies found that no matter how varying illuminance is under overcast sky, the ratio between illuminance at a given point indoors to that of outdoors remains constant. This ratio is called daylight factor, represented by DF

$$D_F\ (\%) = \frac{\text{indoor illuminance, at a given point}}{E_H} \times 100 \qquad (15)$$

Where E_H = unobstructed horizontal illuminance

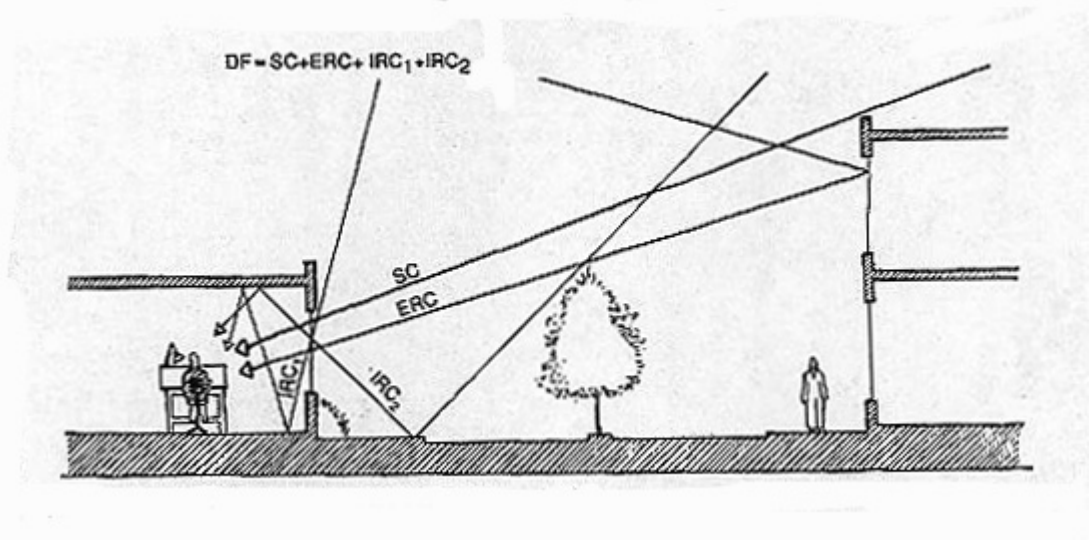

Figure A12: A diagram demonstrates that Daylight Factor is a combination of the three components.

Total daylight factor (DF) is composed of sky component (SC), externally reflected component (ERC), and internally reflected component (IRC). IRC, in turn, is subdivided into reflected skylight and reflected groundlight. Note that surfaces deep in the room are lighted in large measure with reflected light.
(Stein and Reynolds, 2000) p.1121

Daylight factor is used for CIE overcast sky and clear sky, without direct sun. It cannot be used with partly cloudy sky when luminance is constantly changing. As a result, the DF at the point is also continuously unstable.

Daylight obtained at a given point indoor arrives by three different paths.

1. Sky component (SC), the diffused light from the sky reduced by the loss in transmission of the window
2. Externally reflected component (ERC), the reflected light from external surfaces (ground reflection excluded) reduced by their reflectance value.
3. Internally reflected component (IRC), the light reflected by internal surfaces (ground reflection included)

Therefore, DF is a combination of the three components: *See Figure A12*

$$DF = SC + ERC + IRC \qquad (16)$$

Interior Daylighting

Daylight penetrates into building spaces through window openings. Such penetration would be most effective if it is perpendicular to the workplane. As a result, side lighting (e.g. window) is suitable for a vertical workplane; whereas top lighting (e.g. skylight) is for a horizontal workplane. Since most of the tasks are horizontal, windows should be placed as

high as possible for better light condition, yet still provide a visual connection. T-shaped windows may be considered to achieve both benefits.

Several interior daylighting techniques have been developed specifically for tasks that cannot be reached by daylight through side window openings. Those are described below.

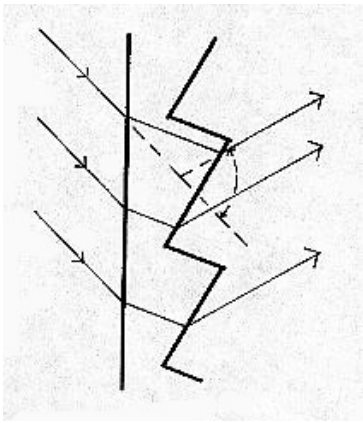

Figure A13
Prismatic glass for beam sunlighting with a deviation angle of 75º.

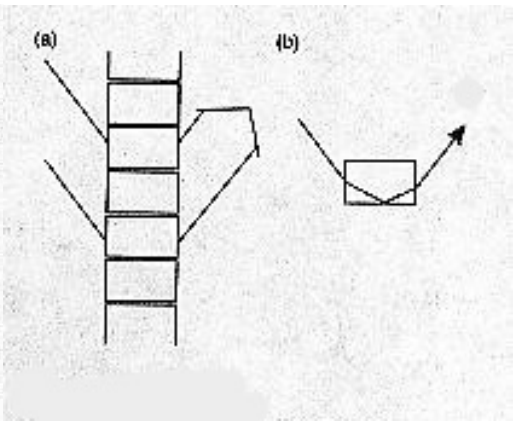

Figure A14
Laser-grooved acrylic sheet

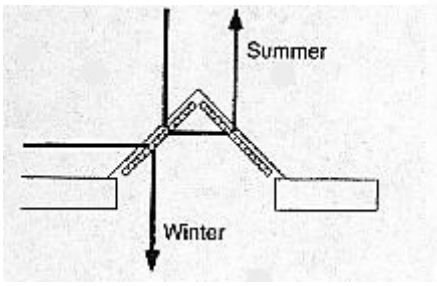

Figure A15
Laser-grooved roof light: at low angle, the sun is admitted, at hight angle, excluded.

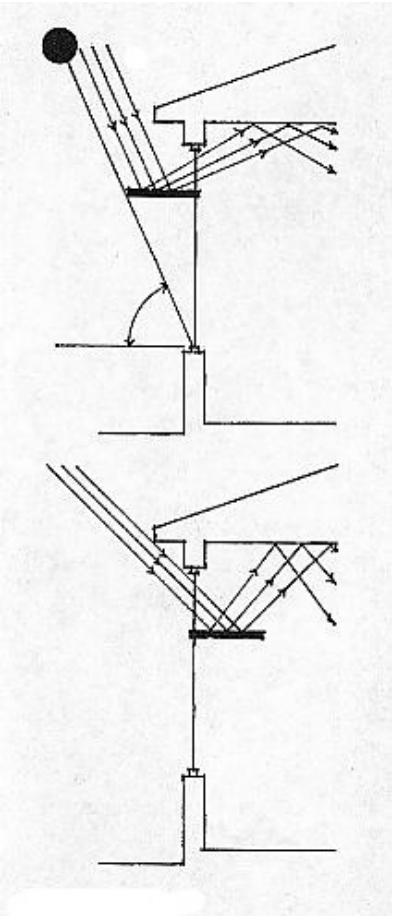

Figure A16
External and internal lightshelves

Prismatic Glass This is designed to divert the incident rays upward to the ceiling diffuser, by means of the refraction principle. It rejects direct sun and also provides a visual connection *(See Figure A13, A14).*

Laser-Grooved Acrylic Sheets This design also utilizes the principle of refraction. It is used effectively as a roof light where high altitude incident rays will be totally refracted back yet allow low altitude incident rays to penetrate in *(See Figure A15).*

Light Shelves Light shelves are often used to achieve daylight penetration; although their actual benefits may be for equalizing light distribution, rather than increasing illumination levels. Its basic form (base case light shelf) is a horizontal platform across the window, with its reflective upper surface. It will bounce the light up to the ceiling, which, in turn, diffuses it to the back room *(See Figure A16).*

Reference for the System Evaluations from the Scale Model Tests

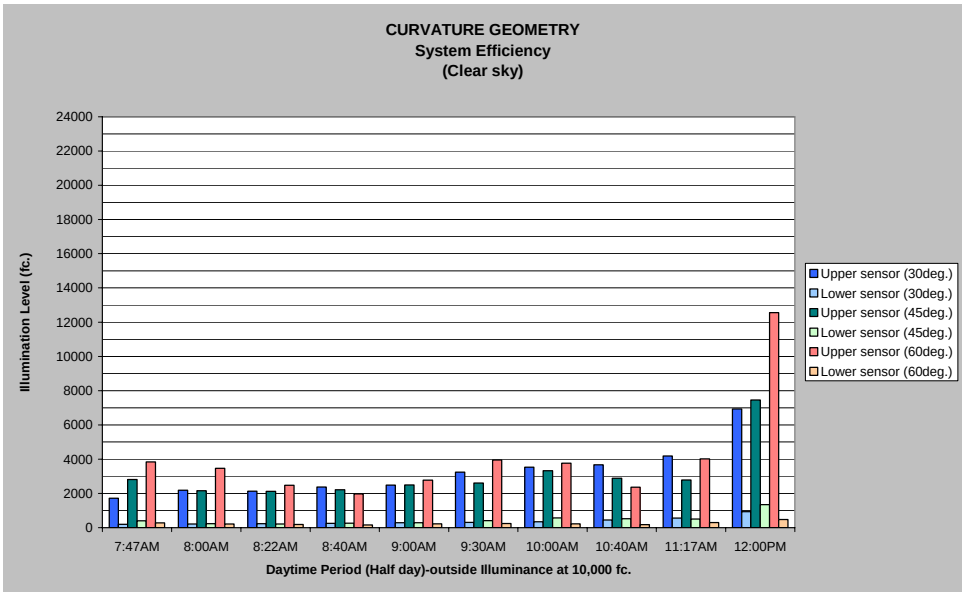

Figure A17: System Efficiency of Curvature Geometric System progressive toward the mid of a clear sky day

Seen from the upper sensor at the incident ray angle of 60 degree (the red bar), the Curvature Geometric System tends to produce a higher illuminance compared to that of the others. This is caused by a more efficient ray redirection technique from the system. At noon, the system efficiency is highest due to its light focusing technique. The side reflective planes add additional illuminance periodically along the day. This is noticed by a fluctuating pattern of data.

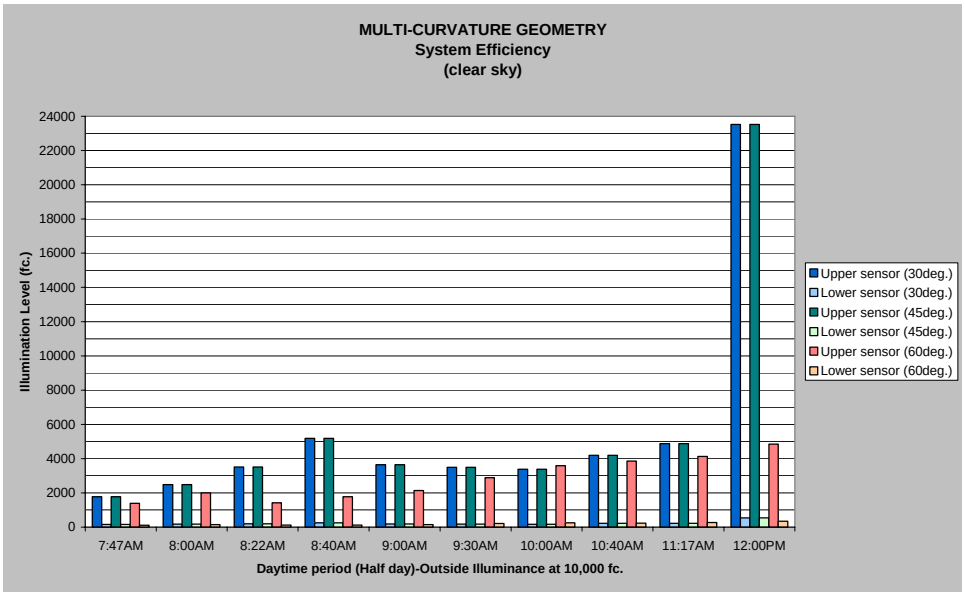

Figure A18: System Efficiency of Multi-Curvature Geometric System progressive toward the mid of a clear sky day

The Multi-Curvature Geometric System has the most efficient ray focusing technique noticed by a much higher illuminance produced at noon. With a perfect modeling, the author believes that the inferior illuminance produced from 60 degree incident ray angle at noon will be improved. The inlet side reflectors add additional illuminance periodically along the day. This is noticed by a fluctuating pattern of data.

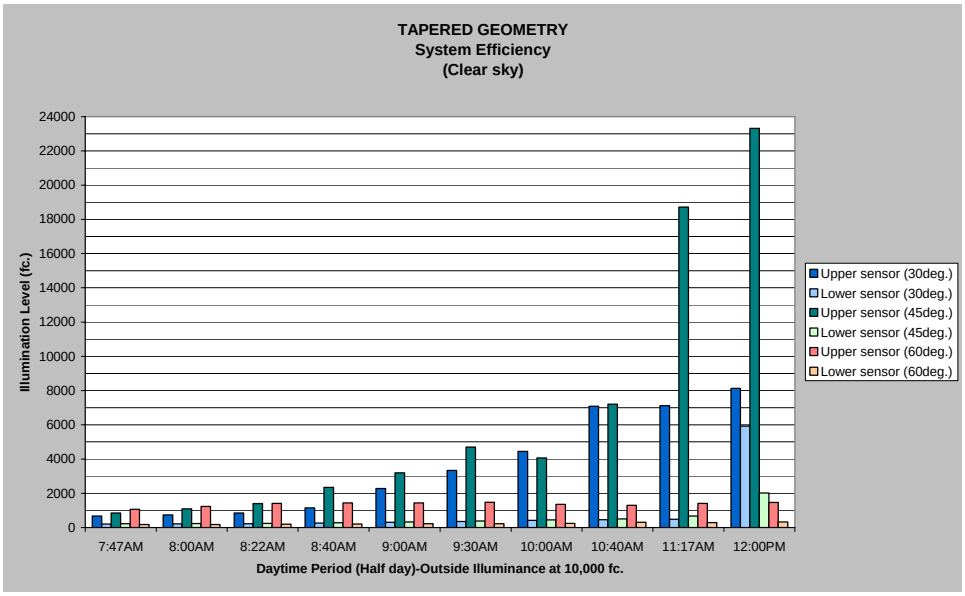

Figure A19: System Efficiency of Tapered Geometric System progressive toward the mid of a clear sky day

The Tapered Geometric System has the most consistency on the efficiency progress due to a careful design of seasonal louvers. However, at the early morning, the louvers themselves block most of the sunrays and make the system efficiency in the early day inferior to the others.

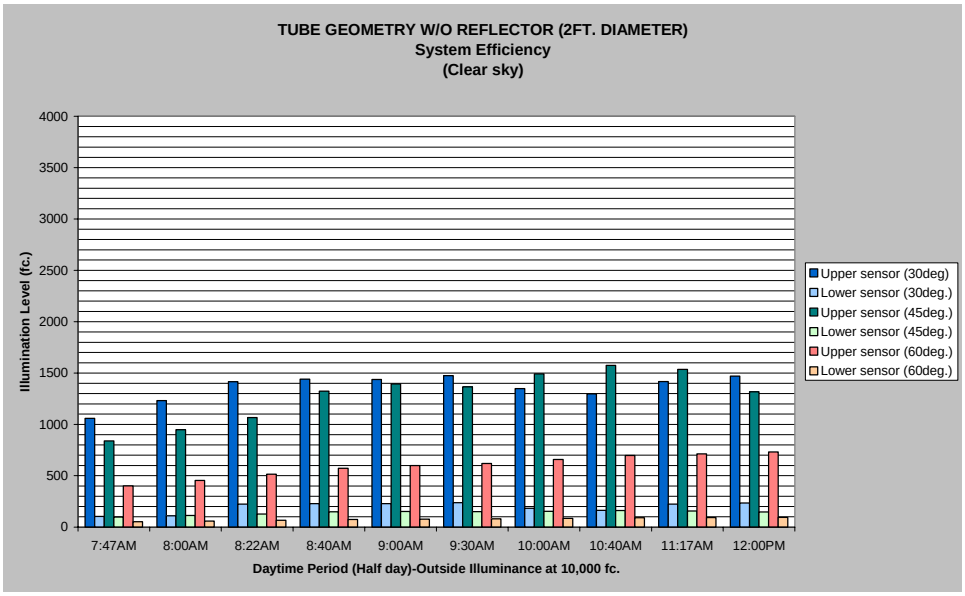

Figure A20: System Efficiency of Cylindrical Geometric System (2ft. diameter) without reflector progressive toward the mid of a clear sky day

The illuminance produced from Cylindrical Geometric System is consistently low toward the peak of the day. This is caused by losses of light energy through a number of reflections. Difference in incident ray source angles does not result in significant difference in illuminance produced.

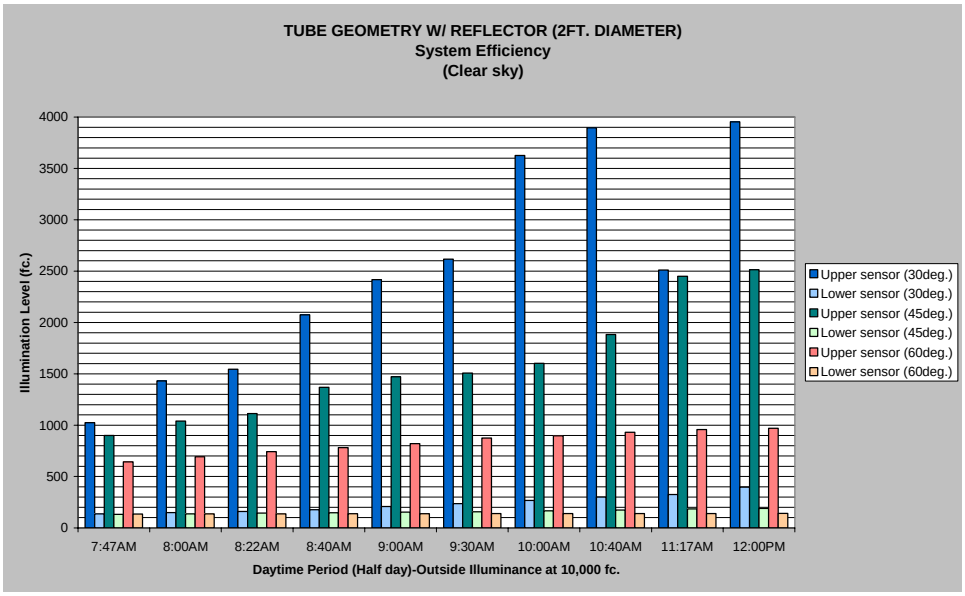

Figure A21: System Efficiency of Cylindrical Geometric System (2ft. diameter) with reflector progressive toward the mid of a clear sky day

Meanwhile, the illuminance produced from such system with 45 degree back reflector is higher and progressive toward the peak of the day. Difference in incident ray source angles result in a significant difference in illuminance produced.

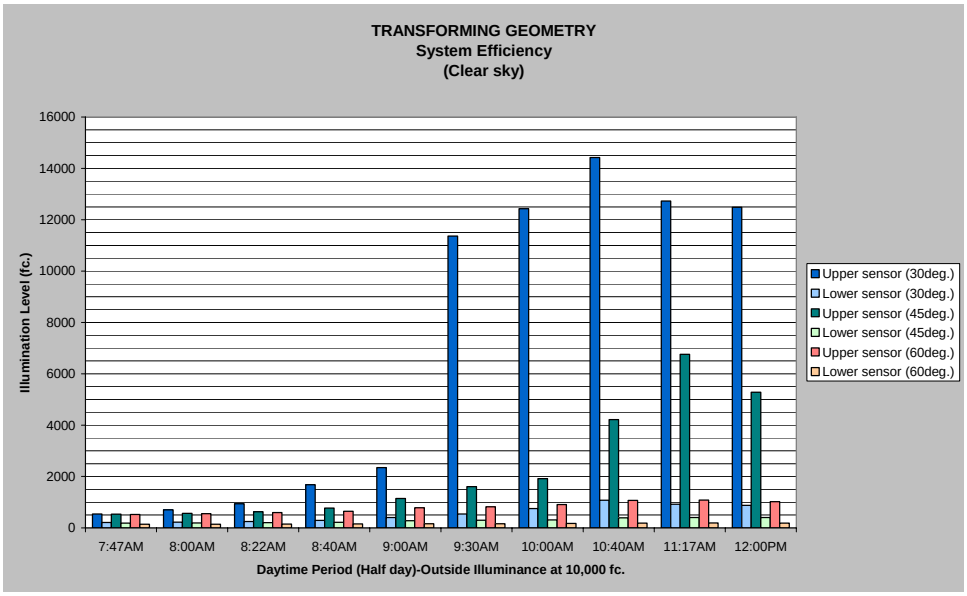

Figure A22: System Efficiency of Transforming Geometric System progressive toward the mid of a clear sky day

The system efficiency from this system is high during the late morning but very low in the early morning. It has a complicate manner of reflection due to its twisting side planes.

Bibliography

- Ben Stein, John S. Reynolds. "Mechanical and Electrical Equipment for Buildings", Ninth Edition. Copyright © 2000
- Brown, G.Z. "Sun, Wind, and Light: Architectural Design Strategies". Copyright © 1985 by John Wiley & Sons, Inc.
- L.O. Beltrán, E.S. Lee, and S.E. Selkowitz. "Advanced Optical Daylighting Systems: Light Shelves and Light Pipes". Journal of the Illuminating Engineering Society. Berkley, CA. Winter 1997
- Lorne A. Whitehead and Kristin Hoffmann. " Method for Estimating the Efficiency of Prism Light Guide Luminaires". Journal of the Illuminating Engineering Society. Vancouver, BC. Summer 1998
- Moeck, M. "On Daylight Quality and Quantity and Its Application to Advanced Daylight Systems". Journal of the Engineering Society. Lawrence, KS. Winter 1998
- Szokolay, V. Steven. "Introduction to Architectural Science: The Basis of Sustainable Design". Copyright © 2004 by Steven Szokolay.
- Whitehead, A. Lorne. "New Simplified Design Procedures for Prism Light Guide Luminaires". Journal of the Illuminating Engineering Society. Vancouver, BC. Summer 1998

Image Credit

- **Figure 1.1** A ceiling duct: “anidolic” ceiling, Szokolay, V. Steven. “Introduction to Architectural Science: The Basis of Sustainable Design”. Burlington, MA, p.126, Figure 2.40
- **Figure 1.2** Transporting sheet, 3M Bulletin: Optical Lighting Film 2001, p.3
- **Figure 1.4** Access to daylight increases as the surface-to-volume ratio increases, Moore. “Environmental Control Systems: heating, cooling, lighting”. The United States, p.305, Figure 23.4
- **Figure 1.5** Farm Credit Bank Building: Typical floor plan, Moore. “Environmental Control Systems: heating, cooling, lighting”. The United States, p.308, Figure 23.10
- **Figure 1.6** The height to depth room ratio of daylight penetration through a clear glass window, Moore. “Environmental Control Systems: heating, cooling, lighting”. The United States, p.324, Figure 24.3
- **Figure 1.8** Longitudinal section of a typical prism light guide system, Whitehead and Hoffmann. “Method for Estimating the Efficiency of Prism Light Guide Luminaires”. Journal of the Illuminating Engineering Society. Vancouver, BC. Summer 1998, p.13, Figure 1
- **Figure 1.9** Losses in a typical light guide system, Whitehead and Hoffmann. “Method for Estimating the Efficiency of Prism Light Guide Luminaires”. Journal of the Illuminating Engineering Society. Vancouver, BC. Summer 1998, p.14, Figure 2
- **Figure 2.1** Base case light shelf. Beltrán, Lee, and Selkowitz. “Advanced Optical Daylighting Systems: Light Shelves and Light Pipes”. Journal of the Illuminating Engineering Society. Berkley, CA. Winter 1997, p.92, Figure 2a
- **Figure 2.2** Single level light shelf with &without side reflectors, Beltrán, Lee, and Selkowitz. “Advanced Optical Daylighting Systems: Light Shelves and Light Pipes”. Journal of the Illuminating Engineering Society. Berkley, CA. Winter 1997, p.92, Figure 2b
- **Figure 2.3** Bi-level light shelf, Beltrán, Lee, and Selkowitz. “Advanced Optical Daylighting Systems: Light Shelves and Light Pipes”. Journal of the Illuminating Engineering Society. Berkley, CA. Winter 1997, p.92, Figure 2c
- **Figure 2.4** Multi-level light shelf, Beltrán, Lee, and Selkowitz. “Advanced Optical Daylighting Systems: Light Shelves and Light Pipes”. Journal of the Illuminating Engineering Society. Berkley, CA. Winter 1997, p.92, Figure 2d
- **Figure 2.5** Section of trapezoidal light pipe C design, Beltrán, Lee, and Selkowitz. “Advanced Optical Daylighting Systems: Light Shelves and Light Pipes”. Journal of the Illuminating Engineering Society. Berkley, CA. Winter 1997, p.93, Figure 3
- **Figure 2.6** Base case light pipe, Beltrán, Lee, and Selkowitz. “Advanced Optical Daylighting Systems: Light Shelves and Light Pipes”. Journal of the Illuminating Engineering Society. Berkley, CA. Winter 1997, p.94, Figure 4
- **Figure 2.7** Light pipe A, Beltrán, Lee, and Selkowitz. “Advanced Optical Daylighting Systems: Light Shelves and Light Pipes”. Journal of the Illuminating Engineering Society. Berkley, CA. Winter 1997, p.94, Figure 4
- **Figure 2.8** Light pipe B, Beltrán, Lee, and Selkowitz. “Advanced Optical Daylighting Systems: Light Shelves and Light Pipes”. Journal of the Illuminating Engineering Society. Berkley, CA. Winter 1997, p.94, Figure 4
- **Figure 2.9** Light pipe C, Beltrán, Lee, and Selkowitz. “Advanced Optical Daylighting Systems: Light Shelves and Light Pipes”. Journal of the Illuminating Engineering Society. Berkley, CA. Winter 1997, p.94, Figure 4

- **Figure 2.10** Prism light guide cross section and isometric view, Whitehead. "New Simplified Design Procedures for Prism Light Guide Luminaires". Journal of the Illuminating Engineering Society. Vancouver, BC. Summer 1998, p.21, Figure 1
- **Figure 2.11** Prism light guide luminaire, Whitehead. "New Simplified Design Procedures for Prism Light Guide Luminaires". Journal of the Illuminating Engineering Society. Vancouver, BC. Summer 1998, p.22, Figure 2
- **Figure 2.12** Fractional extractor width E(x) versus fractional length, x, Whitehead. "New Simplified Design Procedures for Prism Light Guide Luminaires". Journal of the Illuminating Engineering Society. Vancouver, BC. Summer 1998, p.23, Figure 3
- **Figure 2.13** Definition of the profile angle for sun tracking daylight systems, Moeck. "On Daylight Quality and Quantity and Its Application to Advanced Daylight Systems". Journal of the Illuminating Engineering Society. Lawrence, KS. Winter 1998, p.5, Figure 6
- **Figure 2.14** Sun tracking glossy white Venetian blinds (daylight system 2), Moeck. "On Daylight Quality and Quantity and Its Application to Advanced Daylight Systems". Journal of the Illuminating Engineering Society. Lawrence, KS. Winter 1998, p.3, Figure 1
- **Figure 2.15** Stationary daylight system employing sun-rejecting prisms, a mirror, and light redirecting prisms (daylight system 3), Moeck. "On Daylight Quality and Quantity and Its Application to Advanced Daylight Systems". Journal of the Illuminating Engineering Society. Lawrence, KS. Winter 1998, p.3, Figure 2
- **Figure 2.16** Stationary daylight system made out of reflector arrays (daylight system 4), Moeck. "On Daylight Quality and Quantity and Its Application to Advanced Daylight Systems". Journal of the Illuminating Engineering Society. Lawrence, KS. Winter 1998, p.4, Figure 3
- **Figure 2.17** Sun tracking prisms sandwiched into an insulating glass pane (daylight system 5), Moeck. "On Daylight Quality and Quantity and Its Application to Advanced Daylight Systems". Journal of the Illuminating Engineering Society. Lawrence, KS. Winter 1998, p.4, Figure 4
- **Figure 2.18** Sun tracking clear vertical prisms (daylight system 6), Moeck. "On Daylight Quality and Quantity and Its Application to Advanced Daylight Systems". Journal of the Illuminating Engineering Society. Lawrence, KS. Winter 1998, p.4, Figure 5
- **Figure 2.19** Definition of the geometrical parameters of the prism Any face of the prism can be silvered, Moeck. "On Daylight Quality and Quantity and Its Application to Advanced Daylight Systems". Journal of the Illuminating Engineering Society. Lawrence, KS. Winter 1998, p.6, Figure 7
- **Figure 2.20** Longitudinal section of a typical prism light guide system, Whitehead and Hoffmann. "Method for Estimating the Efficiency of Prism Light Guide Luminaires". Journal of the Illuminating Engineering Society. Vancouver, BC. Summer 1998, p.13, Figure 1
- **Figure 2.21** Losses in a typical light guide system, Whitehead and Hoffmann. "Method for Estimating the Efficiency of Prism Light Guide Luminaires". Journal of the Illuminating Engineering Society. Vancouver, BC. Summer 1998, p.14, Figure 2
- **Figure 2.22** Geometrical losses associated with light reflector, Whitehead and Hoffmann. "Method for Estimating the Efficiency of Prism Light Guide Luminaires". Journal of the Illuminating Engineering Society. Vancouver, BC. Summer 1998, p.16, Figure 3
- **Figure 3.13** The sundial for 36 North Latitude, Z. Brown. "Sun, Wind, and Light: Architectural Design Strategies". Canada. p.10

- **Figure 5.1** Beam sunlighting by heliostat and light pipes, Szokolay, V. Steven. "Introduction to Architectural Science: The Basis of Sustainable Design". Burlington, MA., p.126, Figure 2.39

Appendix

- **Figure A1** Electromagnetic Spectrum showing the range of visible light whose wavelength lies between 380-780 Nanometers, http://www.accessexcellence.org/BF/bf05/rothschild/roths_imgs/SlideWin15.html
- **Figure A2** A diagram showing light characteristics, http://www.tpub.com/content/aerographer/14312/css/14312_151.htm
- **Figure A3** Transmission characteristics, Stein and S. Reynolds. "Mechanical and Electrical Equipment for Buildings". Canada, p.1052, Figure 18.4
- **Figure A4** Relation between angle of incidence and percentage reflectance, Stein and S. Reynolds. "Mechanical and Electrical Equipment for Buildings". Canada, p.1051, Figure 18.2
- **Figure A5** Relationship between object size and visibility is demonstrated by comparison of subtended angles (a) and (b), Stein and S. Reynolds. "Mechanical and Electrical Equipment for Buildings". Canada, p.1068, Figure 18.21
- **Figure A6** Glare zones. The direct and reflected glare light paths are delineated on the diagram, Stein and S. Reynolds. "Mechanical and Electrical Equipment for Buildings". Canada, p.1084, Figure 18.25
- **Figure A7** (a) The nature of the seeing process requires that light from the source(s) be reflected by the task into the eye. (b) The light entering the eye is the sum of all of the reflected light, specular and diffuse, from all sources, in the direction of the eye. If the task is specular, all of the sources will be seen reflected in the task. (c) A perfectly absorptive object is jet black because it reflects nothing. (d) A perfectly reflective object positioned as shown is also black because geometrically it cannot reflect light into the eyes. Stein and S. Reynolds. "Mechanical and Electrical Equipment for Buildings". Canada, p.1087, Figure 18.28
- **Figure A8** Totally diffuse lighting (a) destroys texture, whereas a combination of diffuse and directional lighting (b) produces the required modeling shadows. (Courtesy of Holophane.), Stein and S. Reynolds. "Mechanical and Electrical Equipment for Buildings". Canada, p.1099, Figure 18.42
- **Figure A9**
  (a) The position of the sun is expressed in terms of vertical angle above the horizon (altitude) and horizontal angle (azimuth), measured from the south.
  (b) Approximate position of the sun in each of the seasons, at a mid-northern latitude (approximatedly 45º)
  (c) Maximum sun altitude at various latitudes for both solstices and equinoxes. Maximum summer sun altitude is 90º minus latitude minus 23.5º. Thus, for all latitudes the yearly difference between maximum and minimum altitudes is twice 23.5º, or 47º, as shown. Stein and S. Reynolds. "Mechanical and Electrical Equipment for Buildings". Canada, p.1113, Figure 19.3
- **Figure A10**
  (a) The completely overcast sky has a zenith luminance L_z , which is three times the Horizon Luminance, according to the CIE formulation. With such as sky, illumination on unobstructed exterior horizontal surfaces (E_H) is about 2 ½ times that on a similar vertical surface (E_V).
  (b) One widely accepted formulation for clear sky luminance is simply an inversion of the overcast distribution (a); horizon luminance is three times that of the zenith.

Obviously, the area around the sun is brightest. The area opposite the sun is darkest and can be considered as essentially uniform at approximately 3500 cd/m^2 (1000 fL). Actual luminance varies arom about 1000 cd/m^2 (300 fL) at the center to 7000 cd/m^2 (2000 fL) at the sides, averaging 3500 cd/m^2 (1000 fL) over the whole area. Stein and S. Reynolds. "Mechanical and Electrical Equipment for Buildings". Canada, p.1114, Figure 19.4

- **Figure A11** Diagram showing the geometry of a vertical surface in relation to the sun position. The angle between a vertical plane perpendicular to the vertical surface (window) and a vertical plane containing the sun is defined as the bearing angle, Stein and S. Reynolds. "Mechanical and Electrical Equipment for Buildings". Canada, p.1117, Figure 19.7
- **Figure A12** Total daylight factor (DF) is composed of sky component (SC), externally reflected component (ERC), and internally reflected component (IRC). IRC, in turn, is subdivided into reflected skylight and reflected groundlight. Note that surfaces deep in the room are lighted in large measure with reflected light. Stein and S. Reynolds. "Mechanical and Electrical Equipment for Buildings". Canada, p.1121, Figure 19.10
- **Figure A13** Prismatic glass for beam sunlighting with a deviation angle of 75º, V. Szokolay. "Introduction to Architectural Science: The Basis of Sustainable Design". Burlington, MA, p.124, Figure 2.33
- **Figure A14** Laser-grooved acrylic sheet, V. Szokolay. "Introduction to Architectural Science: The Basis of Sustainable Design". Burlington, MA, p.124, Figure 2.34

Figure A15 Laser-grooved roof light: at low angle, the sun is admitted, at hight angle, excluded, V. Szokolay. "Introduction to Architectural Science: The Basis of Sustainable Design". Burlington, MA,p.124, Figure 2.35

- **Figure A16** External and internal lightshelves, V. Szokolay. "Introduction to Architectural Science: The Basis of Sustainable Design". Burlington, MA,p.125, Figure 2.36